

©[2009]
Samuel Straker Henderson
ALL RIGHTS RESERVED

TRACKING DEEP-WATER FLOW ON EIRIK DRIFT OVER THE PAST 160 KYR:
LINKING DEEP-WATER CHANGES TO FRESHWATER FLUXES

by

Samuel Straker Henderson

A Dissertation submitted to the

Graduate School-New Brunswick

Rutgers, The State University of New Jersey

in partial fulfillment of the requirements

for the degree of

Doctor of Philosophy

Graduate Program in Geological Sciences

Written under the direction of

James D. Wright

and approved by

New Brunswick, New Jersey

January, 2009

ABSTRACT OF THE DISSERTATION

TRACKING DEEP-WATER FLOW ON EIRIK DRIFT OVER THE PAST 160 KYR:

LINKING DEEP-WATER CHANGES TO FRESHWATER FLUXES

By Samuel Straker Henderson

Dissertation Director:
James D. Wright

This dissertation uses surface and deep ocean proxies to understand changes in North Atlantic deep-water production associated with periods of increased freshwater input throughout the Late Pleistocene and Holocene. Coring sites on Eirik Drift have long-term sedimentation rates exceeding 15 cm/kyr., allowing for paleoceanographic reconstructions on Milankovitch and millennial time scales.

The transition from glacial North Atlantic Intermediate Water (gNAIW) of marine isotope chron (MIC) 2 to North Atlantic Deep Water (NADW) during the Holocene is examined in Chapter 1. Early Holocene (9000-10,500 ka), sedimentation rates in core 21GGC (3471 m) are >100 cm/kyr., indicating gNAIW winnowed upstream glacial sediments, depositing at 21GGC. Enhanced sediment deposition persisted until ~9ka when long-term rates leveled off at 40 cm/kyr., indicating NADW density had stabilized. From 8.6 to 8.2 ka, catastrophic drainage of glacial Lake Agassiz poured freshwater into the North Atlantic disrupting deep-ocean circulation.

Chapter 2 focuses on the past 160 kyr at Site 1306 (2272 m) on the Eirik Drift where highest sedimentation rates occurred during MIC 2- 5d. Mean sortable silt (SS) and $\delta^{18}\text{O}$ of *N. pachyderma* (s) are inversely related during this interval, indicating that changes in surface conditions above the Eirik Drift are propagated into the deep ocean. During the past 40 kyr., SS decreases are concomitant with instances of surface ocean freshening. These intervals correlate with Heinrich Events, suggesting that massive ice flows released from the continents altered deep ocean circulation.

The final chapter examines deep-ocean response during Terminations 1 and 2. Higher insolation forcing across Termination 2 is postulated to promote rapid melting of continental glaciers, leaving little opportunity for continental storage of freshwater. Conversely, lower insolation across Termination 1 allowed continental ice to linger, allowing for the routing and rapid release of freshwater creating abrupt climate reversals (H1, YD and 8.2 kyr Event). Deep-ocean circulation during MIC 5e loses buoyancy in a fashion similar to the Holocene; however, maximum flow velocities are curtailed for ~7 kyr after the onset of interglacial conditions. This lag is best explained by the melting of Greenland into areas of NCW convection due to increased insolation forcing.

Acknowledgements

During my time at Rutgers several groups of people have been instrumental in the completion of this work including family members, my academic committee and the support of my wife and fellow graduate students (who kept me sane and on track).

Looking back to when I started graduate school, it is easy to see how my graduate committee had steered me on a successful path. Their guidance and advice was freely given when asked, yet they managed to let me find my own path and course of study. For this I am extremely grateful. My major adviser, Jim Wright, has been instrumental in this work and for those who know him, I expect you will see a good deal of him instilled in this work. I will miss our morning runs to the student center for coffee and the half hour of science (or sports) discussed.

My family has also been a great support network throughout this process and a big thank you is in order. Everyone put up with my bad attitude when asking about my dissertation progress and somehow knew when I needed some extra motivation. I would especially like to thank my parents and grandparents for a second chance at higher education after I didn't earn a B.S. the first go around. I hope I have made you all proud.

Finally, I would like to thank my wife Anna. You have put up with late nights, weeks apart, and me being stressed out and grumpy. You always knew when to get me out of the house and when to let me mull things over. I am sorry it took so long and I will forever be in your debt. Thanks for finding a way to make me smile.

Table of Contents

Abstract of the Dissertation.....	ii
Acknowledgements.....	iv
Table of Contents.....	v
List of Illustrations.....	viii
Introduction.....	1
Geologic Setting and Data Collection.....	4
Justification of Study Sites.....	8
Objectives and Overview of Chapters.....	9
Figure Captions.....	12
References.....	19
Chapter 1: Characterizing Early Holocene Establishment of Deep North Atlantic Circulation.....	22
Abstract.....	22
Introduction.....	22
Methods.....	25
Results.....	28
Discussion.....	30
The 8.2 kyr Climate Event.....	32
Conclusions.....	34
Figure Captions.....	37
References.....	43

Chapter 2: Is the last glacial transition a good analogue for prior climate cycles: An examination of abrupt climatic events and establishment of deep water flow across Terminations 1 and 2.....	46
Abstract.....	46
Introduction.....	47
Comparison of North Atlantic Ocean Circulation during abrupt climate change.....	51
Methods.....	53
Results.....	54
Discussion.....	56
Insolation across Terminations 1 and 2.....	56
Circulation MIC 5e vs. MIC 1.....	60
Conclusions.....	61
Figure Captions.....	63
References.....	69
Chapter 3: Surface water forcing of deep-water flow over Milankovitch and millennial time scales as Expedition 303 Site 1306 on the Eirik Drift.....	73
Abstract.....	73
Introduction.....	73
Identification and Provenance H-events.....	76
Methods.....	77
Age Model.....	80
Results.....	81
Discussion.....	84
Conclusions.....	89

Figure Captions.....	92
References.....	98
Conclusions of the Dissertation.....	102
Holocene establishment of deep-water flow.....	102
Comparison of Termination 1 and 2.....	104
Deep-water flow over the past 160 kyr.....	105
Future Work.....	107
Figure Captions.....	110
References.....	117
Appendix A.....	119
Appendix B.....	133
Appendix C.....	148
Curriculum Vitae.....	160

List of illustrations

Figure I.1. Stylized map portraying the “Ocean Conveyor” system from Broecker 1991. Note that Deep-waters are formed in the North Atlantic ocean where and flow southwards and mix into the Indian and Pacific Oceans.....13

Figure I.2. Basemap showing the Eirik Drift (topographic high south of Greenland) and the drilling/coring sites used in this dissertation. Site 1306 sits high on the Eirik drift at a water depth of 2200 m while Site 1305/21GGC can be found at at depth of 3400 m.14

Figure I.3. Base map of the Eirik Drift showing seismic lines collected during KN166-14. Two lines (Lines 19 and 25) pass through Sites 1306 and 1305, respectively and are displayed in Figures I.4 and I.5. Line 19 runs perpendicular to the modern drift crest while Line 25 runs parallel.....15

Figure I.4. Seismic Line 25 with 3.5 kHz inlay collected during KN166-14. Line 25 was collected parallel to the modern drift crest and is vertically exaggerated ~50:1. Site 1305 is was collected in an area where seismic reflectors are expanded suggesting higher sedimentation rates than the surrounding area. The 3.5 kHz record shows a series of weak acoustic reflections ~5 meters below the sediment/water interface indicative of Holocene sedimentation.....16

Figure I.5. Seismic Line 19 with 3.5 kHz inlay collected perpendicular to the modern Eirik Drift crest during KN166-14. Line 19, as reproduced, contains a vertical exaggeration of ~33:1 and shows a series of thickening reflectors from the drift crest down-slope. 3.5 kHz records at Site 1306 show strong acoustic reflectors directly below the sediment/water interface typical of glacial sedimentation.....17

Figure I.6 shows calculated long-term sedimentation rates from Expedition 303 drillcores via paleomagnetic and biostratigraphic datums. Site 1305 (black) is found to contain a long-term average sedimentation rate of 17.5 cm/kyr while Site 1306 yields 15.6 cm/kyr. Both sites contain high enough resolution for the reconstruction of sub Milankovitch variability throughout the North Atlantic (Expedition 303 scientific party).....18

Figure 1.1. Location of 21GGC on Eirik Drift. Also shown are the deep-water currents (dark blue), intermediate water currents (yellow) and surface water currents (light blue) that influence sediments deposited at 21GGC.....38

Figure 1.2. Proxy records generated from 21GGC. All graphs are plotted on a common depth scale from 0 to 500 cm. The blue proxy records are $\delta^{18}\text{O}$ records of *N. pachyderma* (*s*), *G. bulloides* and the difference curve of *N. pachyderma* (*s*) – *G. bulloides*. In all records we find highly variable small amplitude changes down core. Sediment from 342 to 354 cm within 21GGC is barren of all foraminifera. The difference curve suggests that the early Holocene (300-500 cm) more stratified than the mid to late Holocene with divergence rising above 0.8 per mil 5 times.

The two red curves show the %CaCO₃ and SS proxy records. %CaCO₃ increases from ~10 to 40% throughout the Holocene while SS ranges from 16 to 30 microns. Both records show a large negative excursion from 325 to 358 cm with values approaching or exceeding that of earliest Holocene sediment in 21GGC. The green record shows calculated sedimentation rates derived from our age model. Two periods of high sedimentation rates are found in the resulting model, 344-362 and 400 to 482 cm. A longer term Holocene sedimentation rate of ~40 cm/kyr is seen from 0 to 344 and 362 to 400 cm.....39

Figure 1.3. Age model for 21GGC is based on eight AMS ¹⁴C dates using 4-6 milligrams of *N. pachyderma* (*s*) tests run at NOSAMS. Each date (blue triangles) was generated using a 410 yr marine reservoir correction and calculated into calendar ages using the Fairbanks calibration model (Fairbanks et al., 2005). All ages increase with depth however a ¹⁴C plateau occurs from 344 and 362 cm.....40

Figure 1.4. Comparison of SS records from 21GGC and NEAP 15K (Bianchi and McCave, 1999). Both SS records show similar patterns of variability on millennial timescales throughout the Holocene. Both records suggest the early Holocene was dominated by faster flow, with decreasing trend from 9 to 5 kyr. Both records also record similar variability from 5 to 2 kyr suggesting the eastern and western flow regimes act in concert with one other across the time scales.....41

Figure 1.5. The 8.2 kyr event as seen in 21GGC proxy records (top) and SS record of Ellison et al. (2006). Across the 8.2 kyr event %CaCO₃ and %SiO₂ revert to early Holocene values. This suggests that either the sediment supply into the North Atlantic changed across this interval or that the deep current system is remobilizing sediment in a similar area as the early Holocene. SS values indicate a large decrease in flow suggesting that the axis of the current is no longer over the core site and further supports a change in flow regime across this interval. Ellison et al. (2006) show diminished flow across the 8.2 kyr event however the recovery of the SS system is delayed ~250 years from 21GGC. This delay suggests that ISOW may be more susceptible to freshwater input than DSOW during this event.....42

Figure 2.1. Basemap showing the locations of Sites 1306 (2200 m) and 1305/21GGC (3400 m) on the Eirik Drift. Using both the shallow and deep sites on the drift allows for the reconstruction of gross changes in NCW buoyancy as sedimentation rates change between the shallow and deep sites. ODP Site 983 on the Gardar Drift is also identified and is the location used to determine ice volume melt between Termination 1 and Termination 2.....64

Figure 2.2. Figure 2.2 shows SS (blue) and δ¹⁸O (red) records generated over the past 20 kyr at Sites 1306 (top) and 1305/21GGC (bottom). Site 1306 shows winnowing throughout the Holocene while Site 1305/21GGC is expanded indicating NCW is located

deep on Eirik Drift. Likewise, across the last glacial maximum, Site 1306 shows a higher fidelity than Site 1305/21GGC indicating the current is in a gNAIW state.....65

Figure 2.3. SS (blue) and $\delta^{18}\text{O}$ (red) records generated from 110 to 140 kyr at Sites 1305 and 1306. A $\delta^{18}\text{O}$ spike occurs at ~133 kyr which is interpreted as surface freshening due to H11. Interestingly, at Site 1306, we find SS values increasing across H11 which may indicate shoaling of NCW. Site 1305 is expanded throughout MIC 5e indicating a less buoyant NCW however, SS shows an ~7 kyr lag in maximum flow velocity from the onset of interglacial temperatures interpreted as true interglacial flow suppression.....66

Figure 2.4. Comparison of surface and deep ocean records during Termination 1 and 2 through 20 kyr windows. Deep ocean establishment occurs quite differently across the two terminations. After Termination 1, SS measurements indicate deep water flow is quite robust over the deep coring sites on Eirik Drift. However, across Termination 2 deep water velocities are reduced throughout much of MIC 5e, potentially because of Greenland ice melt (deVernal and Hillaire-Marcel 2008).....67

Figure 2.5. Changes in surface (red) and benthic (blue) oxygen isotopes across Terminations 1 and 2 from Site 983 on the Gardar Drift. Across Termination 1 there is a divergence of 0.84 m suggesting that continental glaciers resisted melting in spite of warmer North Atlantic temperatures. Across Termination 2 we find a much smaller divergence of 0.3 m suggesting continental ice melted quickly, probably due to higher insolation forcing during this time.....68

Figure 3.1. Basemap showing the location of Site 1306 on the Eirik Drift. This site is located at a water depth of 2200 m and contains long term sedimentation rates of ~16 cm/kyr. Multi-channel seismic and 3.5 kHz data suggest that this site is ideal for monitoring changes in gNAIW, supporting the idea that NCW buoyancy shifts on glacial/interglacial timescales.....93

Figure 3.2. Figure 3.2 shows the $\delta^{18}\text{O}$, %coarse fraction, % CaCO_3 , % SiO_2 and mean sortable silt proxy records generated at Site 1306 in meter composite depth (mcd). Spikes in coarse fraction, carbonate and silica records at 0-0.5 mcd and 20-21 mcd indicated by the gray bars, are interpreted as winnowed sections, making SS values unreliable. Long term trends down-core show an anti-varying (note the reverse scale on the $\delta^{18}\text{O}$ measurements) relationship between $\delta^{18}\text{O}$ and SS suggesting surface conditions are propagated to the deep-water system at Site 1306. Across the last 7 mcd several instances of strong negative spikes in the $\delta^{18}\text{O}$ record occur. Interpreted as freshwater pulses, these spikes occur during times of SS decreases indicating freshwater is altering deep water circulation on millennial timescales.....94

Figure 3.3. Figure 3.3 shows the data used in order to construct the age model for Site 1306 using a combination of stable isotopic correlation (blue dots), AMS ^{14}C dates (red) and identification of paleomagnetic LaChamp event (orange). MIC transitions, especially during MIC 5 substages, were not always transparent in the stable isotope record due to

changing sedimentation rates so %coarse fraction and %CaCO₃ proxies were used to better constrain our age model. The resulting picks show MIC 5a, 5c and 5e intervals containing high %CaCO₃ values as expected because these substages are warm. Calculated sedimentation rates show that the colder intermediate climate states of MIC 3, 5b and 5d preferentially deposit sediments at Site 1306 relative to full glacial or interglacial settings.....95

Figure 3.4. Figure 3.4 shows $\delta^{18}\text{O}$ (blue) and SS (red) smoothed by a 7 pt Gaussian filter. The top panel shows the complete record over the past 160 kyr while the bottom two panels show 0-80 kyr and 80-160 kyr, respectively. Across the 80-160 kyr a strong anti-varying relationship exists between the SS and $\delta^{18}\text{O}$ suggesting surface temperature is controlling the rates of deep ocean circulation. Conversely, from 40 kyr to present strong negative spikes in $\delta^{18}\text{O}$ are seen with decreases in the SS record interpreted as freshwater capping of the surface oceans that slow deep ocean circulation.....96

Figure3.5 Magnetic Susceptibility (green) and SS (red) variability during the last 50 kyrs. MS and SS show decreases during Heinrich event periods, suggesting that deep ocean circulation over Site 1306 diminished.....97

Figure C.1. Basemap showing the locations of Sites 1306 (2200 m) and 1305/21GGC (3400 m) on the Eirik Drift. Using both the shallow and deep sites on the drift allows for the reconstruction of gross changes in NCW buoyancy as sedimentation rates change between the shallow and deep sites. ODP Site 983 on the Gardar Drift is also identified and is the location used to determine ice volume melt between Termination 1 and Termination 2.....112

Figure C.2. Proxy records generated from 21GGC. All graphs are plotted on a common depth scale from 0 to 500 cm. The blue proxy records are $\delta^{18}\text{O}$ records of *N. pachyderma* (*s*), *G. bulloides* and the difference curve of *N. pachyderma* (*s*) – *G. bulloides*. In all records we find highly variable small amplitude changes down core. Sediment from 342 to 354 cm within 21GGC is barren of all foraminifera. The difference curve suggests that the early Holocene (300-500 cm) more stratified than the mid to late Holocene with divergence rising above 0.8 per mil 5 times. The two red curves show the %CaCO₃ and SS proxy records. %CaCO₃ increases from ~10 to 40% throughout the Holocene while SS ranges from 16 to 30 microns. Both records show a large negative excursion from 325 to 358 cm with values approaching or exceeding that of earliest Holocene sediment in 21GGC. The green record shows calculated sedimentation rates derived from our age model. Two periods of high sedimentation rates are found in the resulting model, 344-362 and 400 to 482 cm. A longer term Holocene sedimentation rate of ~40 cm/kyr is seen from 0 to 344 and 362 to 400 cm..113

Figure C.3. Changes in surface (red) and benthic (blue) oxygen isotopes across Terminations 1 and 2 from Site 983 on the Gardar Drift. Across Termination 1 there is a divergence of 0.84 m suggesting that continental glaciers resisted melting in spite of warmer North Atlantic temperatures. Across Termination 2 we find a much smaller divergence of 0.3 m suggesting continental ice melted quickly, probably due to higher insolation forcing during this time.....114

Figure C.4. Data used in order to construct the age model for Site 1306 using a combination of stable isotopic correlation (blue dots), AMS ^{14}C dates (red) and identification of paleomagnetic LaChamp event (orange). MIC transitions, especially during MIC 5 substages, were not always transparent in the stable isotope record due to changing sedimentation rates so %coarse fraction and % CaCO_3 proxies were used to better constrain the age model. The resulting picks show MIC 5a, 5c and 5e intervals containing high % CaCO_3 values as expected because these substages are warm. Calculated sedimentation rates show that the colder intermediate climate states of MIC 3, 5b and 5d preferentially deposit sediments at Site 1306 relative to full glacial or interglacial settings.....115

Figure C.5. $\delta^{18}\text{O}$ (blue) and SS (red) data smoothed by a 7 pt Gaussian filter. The top panel shows the complete record over the past 160 kyr while the bottom two panels show 0-80 kyr and 80-160 kyr, respectively. Across the 80-160 kyr a strong anti-varying relationship exists between the SS and $\delta^{18}\text{O}$ suggesting surface temperature is controlling the rates of deep ocean circulation. Conversely, from 40 kyr to present strong negative spikes in $\delta^{18}\text{O}$ are seen with decreases in the SS record interpreted as freshwater capping of the surface oceans that slow deep ocean circulation.....116

Introduction

Perilous warnings about the effects of future climate change have been and continue to be a major driving force of paleoceanographic and paleoclimatic research and have been highly reported on in the popular press (e.g., IPCC, 1990; 1995; 2001; 2007; Time Magazine, 2006). One direct consequence, the melting of the world's glaciers, is a future concern for several reasons. The most obvious is the melting of glacial ice that finds its way into the oceans, therefore raising sea level. While this process is “slow” on human time scales and people are not likely to wake up one day living in the ocean, the costs associated with coastal flooding and property damage due to heightened storm surge coupled with potential inland migration of populations living in coastal areas may prove to be immense.

A second consequence, less appreciated by the general population, arises when the flux of freshwater into the saline oceans increases. This process can abruptly disrupt the prevailing climate state by altering ocean circulation and distribution of heat around the globe. Hollywood popularized this idea for the general public in making “The Day After Tomorrow,” a film in which glaciers across the world rapidly break up and fall into the ocean, ceasing ocean circulation, and therefore initiating the next ice age. While the movie has some entertainment value, it falls short on the science with one notable exception—introducing the public to the concept of global thermohaline circulation (THC).

The concept of thermo (heat) and haline (salt) driven currents is not new. Evidence of

cold deepwaters in the tropics was collected in the mid 1700s and interpreted as originating in polar regions by Benjamin Thompson (Thompson, 1797). Johan Sandstrom (1908) conducted some of the first modeling studies using physical tank models to differentiate thermal and wind driven ocean circulation. The salinity component was added at a later date with the term ‘thermohaline circulation’ appearing in textbooks in the late 1920s (Defant, 1929).

The idea that freshwater can disrupt oceanic circulation is also not a new concept. Early examples include Chamberlin’s (1906) examination of the links between freshwater input and ocean circulation and postulation that changes in the deep-ocean system may be responsible for glacial climates. Wust (1935) built upon the work of early oceanographic pioneers and largely developed the theory of global thermohaline circulation as we know it today. Over the years, continued study and the advent of new technologies have shaped these early ideas of the ocean system, refining them into what we understand today.

In order to comprehend the impacts of freshwater input on global THC, it is essential to understand how THC works and why it is vital in regards to past, present, and future climate states. As hinted above, thermohaline currents are driven by differential fluxes in heat and/or salt. These currents link together forming a global “conveyor belt” in which heat and salt travel throughout the world’s oceans (Broecker, 1991) (Figure I.1). We can trace the path of the conveyor in the Atlantic Ocean where warm salty surface currents head north via the Gulf Stream. South of Iceland and Greenland, a branch of the Gulf

Stream called the North Atlantic Current flows northward into the Norwegian and Greenland Seas transporting warm salty water to the high latitudes. As the water travels north, heat is lost from the ocean to the atmosphere in the mid to high latitudes, moderating the climate across northern Europe. Eventually, the salty surface water loses enough heat to sink, thus causing downward convection in the Labrador, Greenland and Norwegian Seas. Each of these water masses mixes and entrains ambient intermediate and deepwaters to form North Atlantic Deepwater (NADW) today.

In the northernmost North Atlantic, seafloor topography and the Coriolis force cause NADW to take a circuitous route before heading south along the western boundaries of the Atlantic ocean basins. NADW flows to $\sim 40^\circ$ S where it encounters the circum-polar current (CPC). NADW shoals and vigorous surface-to-bottom circulation of the CPC mixes NADW with outflows from the Pacific and Indian Oceans (Oppo and Fairbanks, 1987; Broecker, 1991). From the Antarctic, the majority of deepwater flows northward into the Pacific and Indian Oceans where it upwells slowly. Surface and thermocline waters make their way back into the Atlantic Ocean primarily through the Drake Passage in the Antarctic as well as around Cape Horn in Africa through inter-ocean exchange of thermocline and surface water masses (Gordon, 1986; Schmitz and McCartney, 1993). Once in the Atlantic, these surface waters warm in the tropics and increase in salinity due to higher evaporation versus precipitation. The warm, salty water flows to the North Atlantic, thus completing the “conveyor belt” of ocean transport (Broecker, 1991).

Along the conveyor, there are only a few areas where surface temperatures and salinities

are appropriate for the formation of deepwater, these areas include the Greenland-Norwegian Seas, the Labrador Sea, the Mediterranean Sea in the Northern Hemisphere and the Ross and Weddell Seas in the Southern Hemisphere (e.g., Worthington, 1970). Two striking observations can be made about the deep convection sites: 1) they generally occur at sub-polar/polar latitudes (except the Mediterranean Sea which forms an ultra-saline water mass through extreme evaporation and limited open-ocean water exchange). Continental ice sheet growth also is largely confined to the high latitudes therefore putting large stores of freshwater proximal to the deep-ocean convection sites. These ideally-located large freshwater reservoirs are unstable and often release their freshwater directly into areas of deep-ocean convection, thus altering THC and redistributing heat across the globe. This unique balance between the flux of freshwater and creation of a viable deepwater mass suggests that 2) changes within geographically small areas of the high latitudes may cause significant shifts in the global oceanic and climatic systems.

Geologic Setting and Data Collection

The North Atlantic is often cited as the “smoking gun” when trying to understand the mechanisms controlling abrupt climate events (e.g., Broecker et al., 1989; Alley et al., 1997; Barber et al., 1999). This area is an excellent candidate as an initiator of abrupt climatic events because over the past 15 Myr and especially during the last 2.5 Myrs, the Northern Hemisphere has undergone the most dynamic ice sheet fluctuations on Earth (e.g., Jansen and Sjolholm, 1991; Wolf and Thiede, 1990). Several studies have hypothesized that the waxing and waning of the Laurentide and Fenno-Scandinavian ice sheets and the associated release of freshwater must interact with global ocean circulation

over Milankovitch and shorter time scales (e.g., Manabe and Stouffer, 1988; Manabe and Stouffer, 1999; Broecker, 1994).

This dissertation attempts to understand the relationship between freshwater and thermohaline circulation by examining sediment cores collected from the Eirik Drift. This North Atlantic sediment drift is located off southern Greenland and occupies water depths of 1000-4000 m (Figure I.2). Eirik Drift is formed as deep currents are pushed westward around the tip of Greenland, via the Coriolis force. As the current heads north into the Labrador Sea, it loses speed, as well as the ability to carry sediments, which fall to the ocean floor creating the sediment drift. This particular type of deposition has been classified as detached drift accumulation and generally forms elongate drift morphologies (McCave and Tucholke, 1986; Faugeres et al., 1999).

The data used in this dissertation are derived largely from two North Atlantic cruises targeting the Eirik and Gardar Drifts: KN166-14 and IODP Expedition 303. KN166-14 had several objectives including: 1) constraining long-term drift dynamics through the collection of high-resolution multi-channel seismic (MCS) data (Figure I.3); 2) coring mud wave fields to understand modern drift building processes and Northern Component Water (NCW) paleo-flow directions; and 3) the collection of cores in high sedimentation rate areas in order to reconstruct centennial to millennial scale changes in surface and deep-ocean processes over the past 100 kyrs. KN166-14 sailed under the supervision of CO-PI's Patricia Manley, Gregory Mountain and James Wright and also served as a site survey for IODP Expeditions 303 and 306.

Two areas with thick sedimentary sections, Plio-Pleistocene in age, were identified on Eirik Drift by shipboard 3.5 kHz and high-resolution MCS profiles. A shallow water site (~2200 m) and a deepwater site (~3400m) were targeted as coring opportunities (Figure I.2). Previous work in the Eirik Drift area suggested that the deep current system underwent changes in density over glacial/interglacial cycles (e.g., Stoner et al., 1998). Shipboard 3.5 kHz records from KN166-14 identified potential areas of enhanced deposition over the last glacial/interglacial cycle. The high resolution seismic imaging indicates that this depositional pattern has developed during the late Pliocene (Figures I4,I5).

The deepwater site was identified as a suitable interglacial site because the 3.5 kHz record showed an interval of ~5m with relatively weak acoustic reflectors interpreted as an expanded Holocene section. Likewise, our shallow water site was thought to be dominated by glacial sedimentation because it showed strong reflectors directly below the sediment/water interface in the 3.5 kHz record indicative of deposition during glacial periods. The MCS and Seabeam data showed that these areas were gently sloping with no nearby topographic anomalies which may alter the deep sea currents. Furthermore, the R1 reflector (a regional North Atlantic seismic reflector, coincident with the initiation of Northern Hemisphere glaciation during the middle late Pliocene) was identified at both the deep and shallow sites suggesting sedimentation rates have been high at these areas on the Eirik Drift since the Pliocene (Earley, 2006).

IODP Expedition 303 continued the work laid out from KN 166-14 by drilling several coreholes in areas of high sedimentation across the North Atlantic including Orphan Knoll, Eirik Drift, Gardar Drift and a re-drill of Deep Sea Drilling Project (DSDP) Site 609. The Expedition's primary objective was to couple high-resolution paleointensity (measurement of changes in the Earth's magnetic field through time) with stable isotopic $\delta^{18}\text{O}$ stratigraphies to form "paleointensity assisted chronologies" (PACs). The combination of these proxy records provides new age constraints for marine cores collected in the North Atlantic, thereby facilitating better site-to-site correlation. A secondary objective for Expedition 303, and the concentration of this dissertation, was the generation of high-resolution records of surface and deep-ocean circulation over the past ~3 million years.

This dissertation sampled two Expedition 303 drilling locations, Sites 1305 and 1306, raised on Eirik Drift (Figure I2). Shipboard magneto- and biostratigraphy show long-term sedimentation rates at Sites 1305 and 1306 are 17.5 and 15.6 cm/kyr, respectively, and are therefore suitable for this study (Figure I.6). Several collaborators have contributed to this goal, notably my advisor James Wright who has overseen the generation stable isotopic records at Site 1306 and Anne de Vernal/Claude Hillaire-Marcel who generated stable isotopic records at Site 1305. I performed %CaCO₃, %SiO₂ and mean sortable silt (SS) measurements at both sites and contributed some of the isotopic analysis for Site 1306. The generation of both surface and deepwater proxy records will allow 1) monitoring the surface water influence on deep-ocean circulation; and 2) examination of NCW buoyancy states across glacial terminations

Justification of Study Sites

When conducting a paleoceanographic study, it is essential to ensure that a 3 to 4 inch core from the seafloor is representative of regional sedimentation. Large-scale depositional processes were determined by geophysical methods conducted during cruise KN166-14, including Seabeam, 3.5 kHz, and MCS data, showing changes in surface topography, depositional patterns just below the ocean floor, and long-term sedimentation histories, respectively.

The reconstruction of deepwater flow histories can be distorted in regions where seafloor bathymetry deflects deep-ocean currents. Thus, KN166-14 traversed Eirik Drift with a series of seismic transects designed to reveal gross morphological features and sediment depositional patterns (Figure I.3). Seismic lines 19 (perpendicular to the modern drift crest) and 25 (parallel to the modern drift crest) show gently sloping surfaces free of topographic features which would disrupt the deep currents and locally enhance or decrease sedimentation. Along these transects, localized topographic variability is minimal, ensuring interpreted changes in deepwater flow regimes must be derived from changes in formation strength or density rather than shoaling from localized effects.

High sedimentation rates make sediment drift systems attractive areas for research, however, localized sediment recycling and other depositional processes may influence areas on the drift raising concerns about what information can be garnered from a particular location. Sites 1305 and 1306 have thick sedimentary sections indicating

enhanced deposition in these areas. Furthermore, the reflectors contained at both sites can be traced across a large area of the Eirik Drift, indicating that the sediment deposition at the coring sites is representative of sediment processes on the drift.

Objectives and Overview of Chapters

Freshwater control of North Atlantic circulation is a common theme for the research presented herein. This dissertation attempts to understand the role of freshwater forcing across different temporal scales and climatological base states by determining if changes in surface conditions are propagated to the deep-ocean basins. This research attempts to constrain known problems, such as the lack of a deepwater response to the 8.2 kyr event (e.g., Alley and Augstsottir, 2005; Keigwin and Boyle, 2000) as well as generating new data of surface and deep-ocean interaction from the relatively under sampled Eirik Drift. Much of this research compliments pre-existing work from the Gardar Drift (eastern North Atlantic) and helps to clarify those results because topography and localized depositional effects on Eirik Drift are much smaller than they are on Gardar Drift, thus allowing for more robust reconstructions to be developed.

Chapter 1 is an expansion of my Master's research and examines how deepwater transitioned from the gNAIW state of the last glacial maximum to the NADW state of the Holocene. This chapter contains measurements from gravity core 21GGC, which was collected at a depth of 3471 m on the Eirik Drift and was chosen for this study because the Holocene section was greatly expanded. A significant part of this chapter is dedicated to defining a deep-ocean response to the 8.2 kyr event as identified by other

researchers (Alley et al., 1997; Ellison et al., 2006; Kleiven et al., 2007). This chapter utilizes both surface and deepwater proxies to quantify: 1) the presence of freshwater in the surface ocean above our coring site; and 2) determine what, if any, changes occurred in the deep-ocean at this time. Core 21GGC is ideally located because it is in the heart of the modern deep flow axis while overlying surface waters should be influenced by freshwater inputs resulting from catastrophic North American lake drainage (LeGrande et al., 2008). Furthermore, because this study uses surface and deepwater proxies in a single core, we may be able to develop lead-lag relationships between changes in surface-ocean properties above and their effects on the deep-ocean system below.

Chapter 2 compares and contrasts deepwater flow at the Termination 1/Holocene transition with the transition of Termination 2/MIC 5e. The last glacial cycle is often thought to be a good analogue for previous terminations. However abrupt climate events such as the YD and 8.2 kyr Event are not widely seen during Termination 2, implying that Termination 1 to Holocene transition may be a unique climate state. This chapter identifies two potential differences in the insolation forcing 1) rate of change and, 2) total insolation forcing, which may account for the abrupt climate changes seen across Termination 1 relative to Termination 2. Furthermore, the excesses insolation during Termination 2 may have produced excess melting of Greenland ice into the North Atlantic. This chapter explores whether these factors contributed to circulation suppression throughout a large portion MIC 5e and may provide useful insights as to how deep-ocean circulation will respond to increased Greenland ice melt due to the influences of global warming.

Chapter 3 examines surface and deepwater conditions over the past 160 kyr at Site 1306 on the Eirik Drift. Of particular interest is the deep-ocean response to large-scale North Atlantic ice rafting events coined ‘Heinrich Events’ in honor of Hartmut Heinrich who identified layers of lithic fragments in marine cores and concluded they were deposits from icebergs (Heinrich, 1988). Few events have garnered more attention in paleoclimate community than H-events; however, the duration of each event and deep-ocean response are still not well constrained (Hemming, 2004). The down core $\delta^{18}\text{O}$ stratigraphy at Site 1306 shows expanded sedimentation across intermediate climate states making this location ideal for the examination of H-events. In particular, MIC 3 which contains 4 of the 6 “classic” H-events, has sedimentation rates that average 30 cm/kyr. This study also monitors the change in deepwater circulation across glacial/interglacial time frames and finds a strong correlation between deepwater production and insolation at 65° North, confirming that deep-ocean circulation to the first order is driven by Milankovitch forcing.

Figure Captions

Figure I.1: Stylized map portraying the “Ocean Conveyor” system from Broecker 1991. Note that deepwaters are formed in the North Atlantic Ocean where and flow southwards and mix into the Indian and Pacific Oceans.

Figure I.2: Base map showing relevant features throughout the North Atlantic discussed in this dissertation. Names in black signify sediment drifts, items in orange represent surface ocean seas and, areas marked in light blue represent regionally important topography on the sea floor. Of particular note is Eirik Drift (topographic high south of Greenland) and the drilling/coring sites used in this dissertation. Site 1306 sits high on the Eirik drift at a water depth of 2240 m while Site 1305/21GGC can be found at a depth of 3470 m.

Figure I.3: Base map of the Eirik Drift showing seismic lines collected during KN166-14. Two lines (Lines 19 and 25) pass through Sites 1306 and 1305, respectively and are displayed in Figures I.4 and I.5. Line 19 runs perpendicular to the modern drift crest while Line 25 runs parallel.

Figure I.4: Seismic Line 25 with 3.5 kHz inlay collected during KN166-14. Line 25 was collected parallel to the modern drift crest and is vertically exaggerated ~50:1. Site 1305 is located in an area where seismic reflectors are expanded suggesting higher sedimentation rates than the surrounding area. The 3.5 kHz record shows a series of weak acoustic reflections ~5 meters below the sediment/water interface indicative of Holocene sedimentation.

Figure I.5: Seismic Line 19 with 3.5 kHz inlay collected perpendicular to the modern Eirik Drift crest during KN166-14. Line 19, as reproduced, contains a vertical exaggeration of ~33:1 and shows a series of thickening reflectors from the drift crest down-slope. 3.5 kHz records at Site 1306 show strong acoustic reflectors directly below the sediment/water interface typical of glacial sedimentation.

Figure I.6 shows calculated long-term sedimentation rates from Expedition 303 drillcores via paleomagnetic and biostratigraphic datums. Site 1305 (black) is found to contain a long-term average sedimentation rate of 17.5 cm/kyr while Site 1306 yields 15.6 cm/kyr. Both sites contain high enough resolution for the reconstruction of sub Milankovitch variability throughout the North Atlantic (Expedition 303 scientific party).

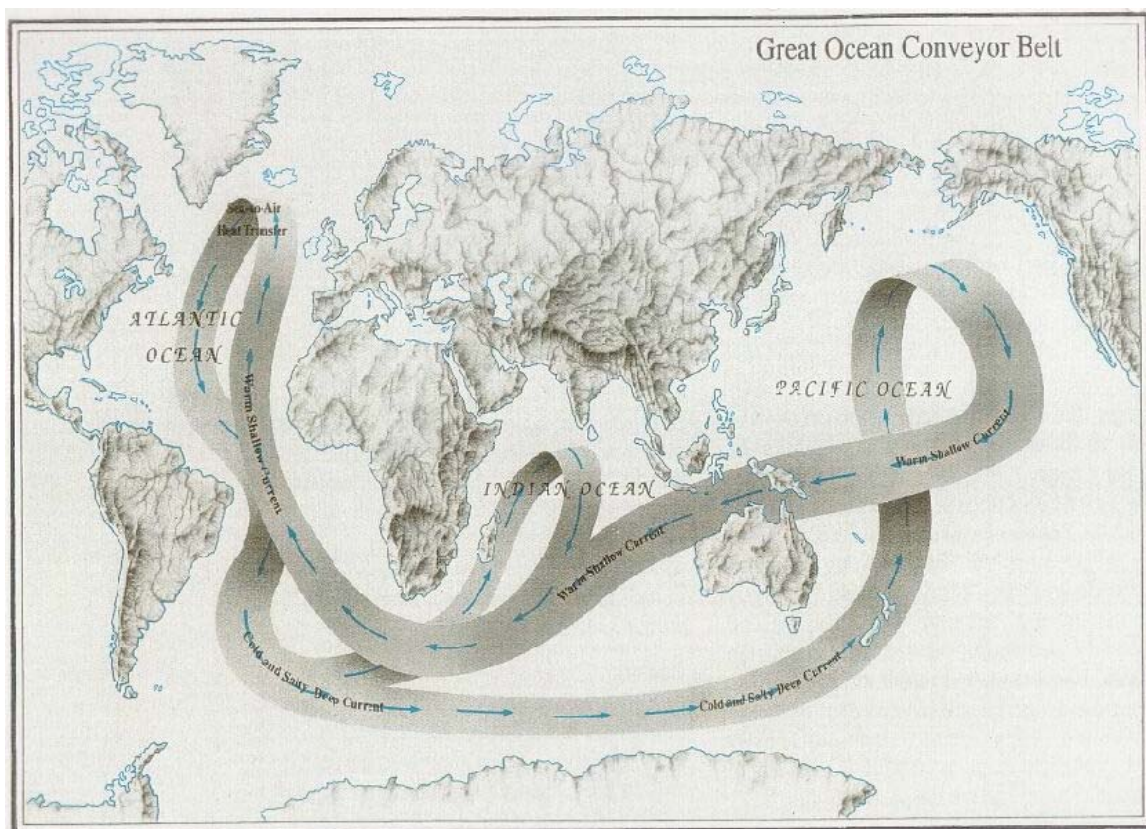
Figure I.1

Figure I.2

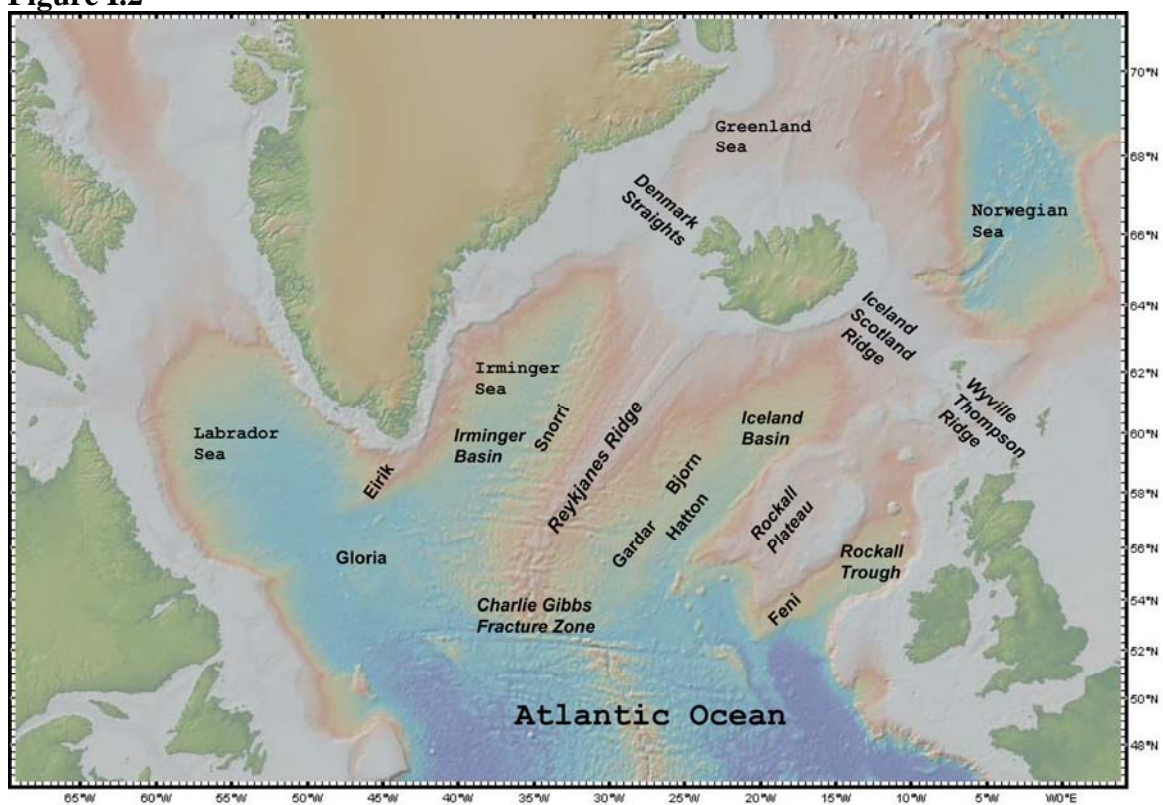


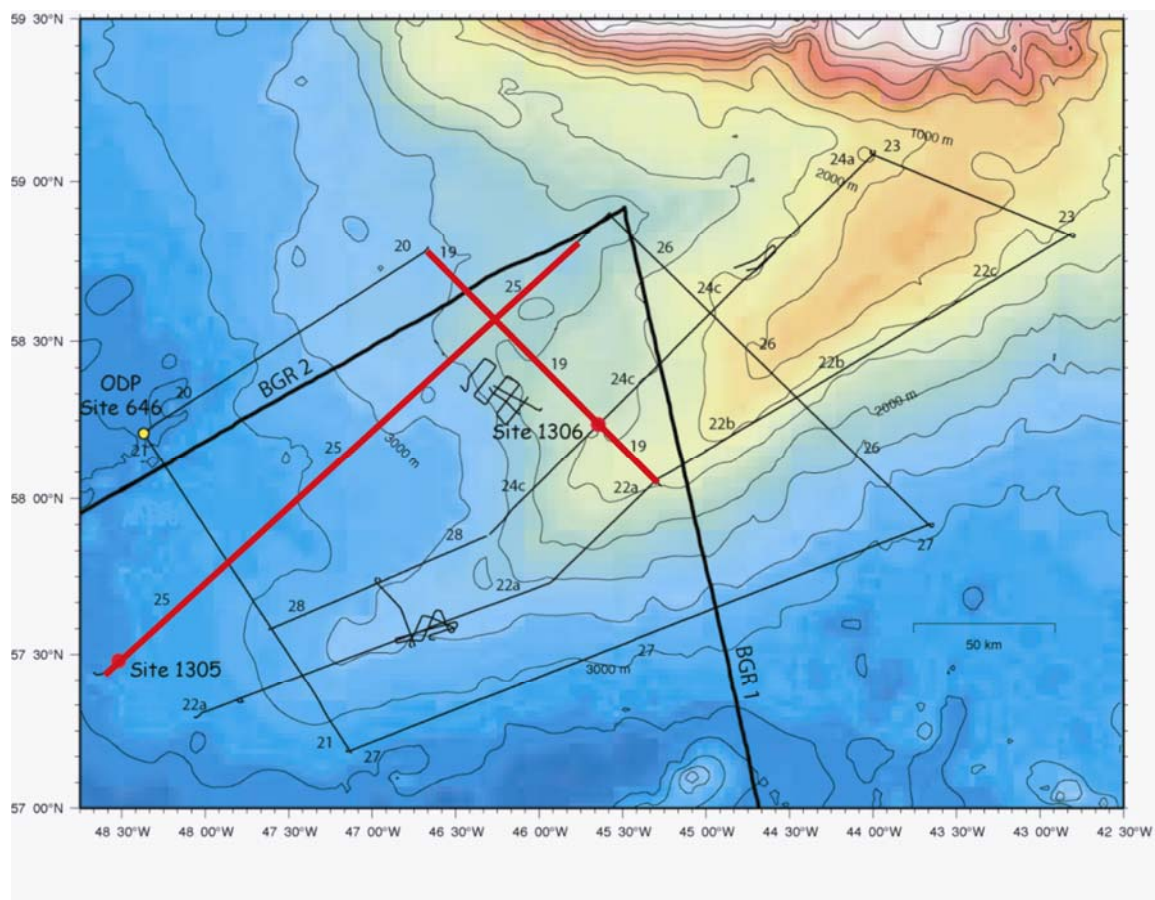
Figure I.3

Figure I.4

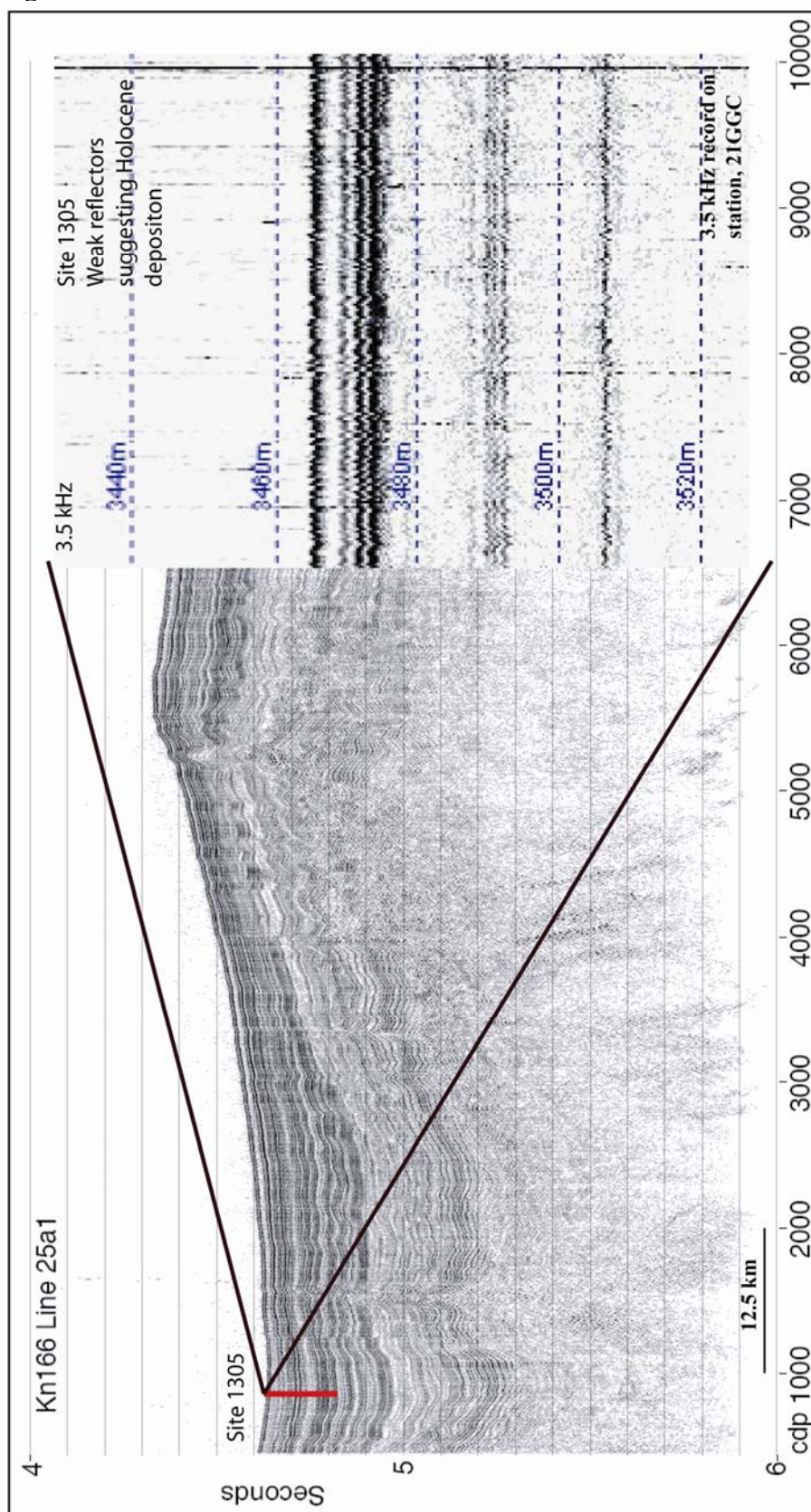


Figure I.5

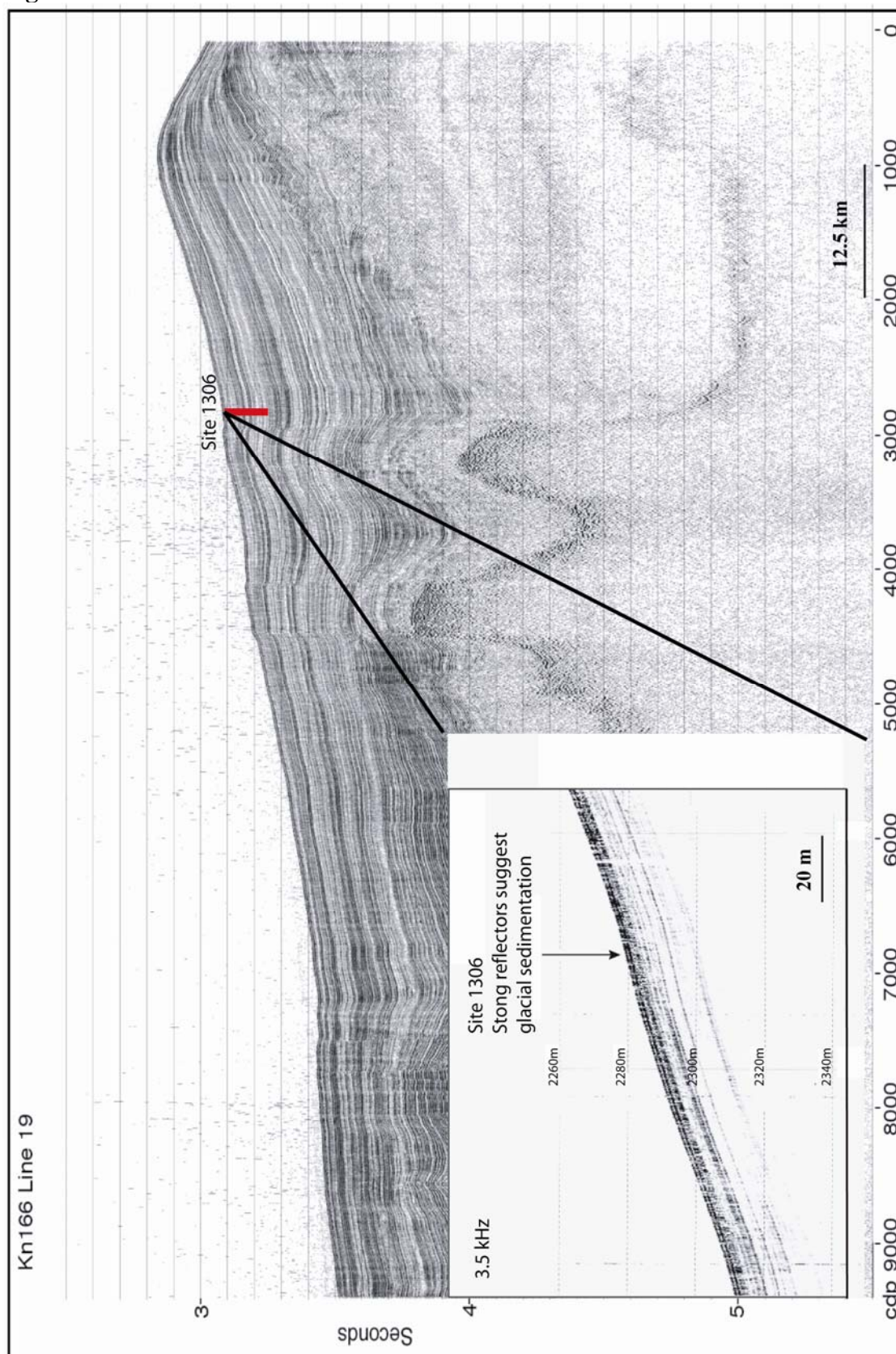
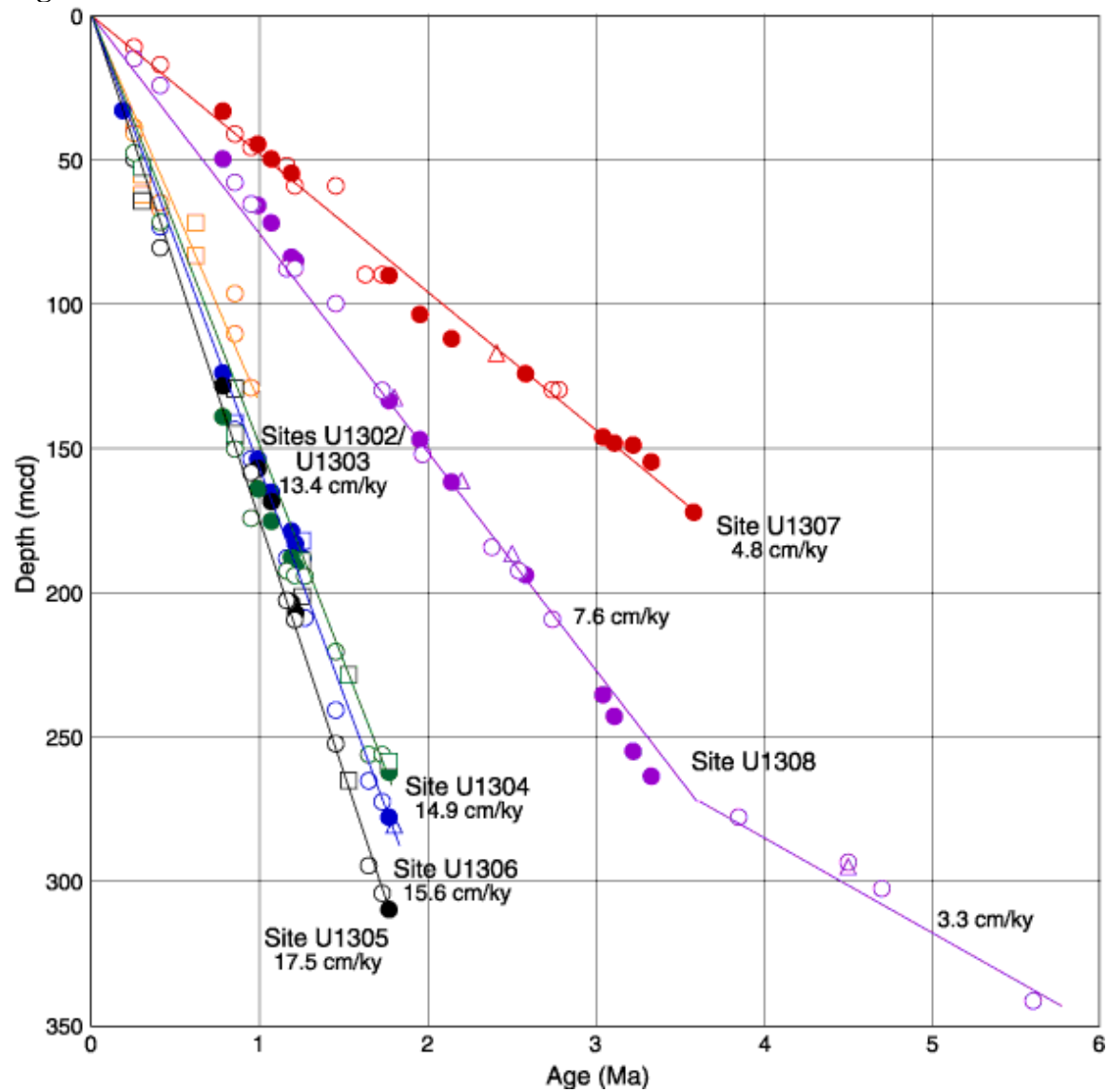


Figure I.6



References

- Alley, R.B., Mayewski, P.A., Sowers, T., Stuiver, M., Taylor, K.C., Clark, P.U. (1997). Holocene climatic instability: A prominent, widespread event 8200 yr ago. *Geology*, 25, 483-486.
- Alley, R. B., and A. M. Agustsdottir (2005), The 8k event: cause and consequences of a major Holocene abrupt climate change, *Quaternary Science Reviews*, 24(10-11), 1123-1149.
- Barber, D. C., et al. (1999), Forcing of the cold event of 8,200 years ago by catastrophic drainage of Laurentide lakes, *Nature*, 400(6742), 344-348.
- Broecker, W. S., et al. (1989). Routing of meltwater from the Laurentide ice-sheet during the Younger Dryas cold episode, *Nature*, 341(6240), 318-321.
- Broecker, W. S., (1991). The great ocean conveyor. *Oceanography*, 4, 79-89.
- Broecker, W.S. (1994). Ocean circulation – An unstable superconveyor. *Nature*, 367(6462), 414-415.
- Chamberlain, T.C., (1906). On a possible reversal of deep-sea circulation and its influence on geologic climates. *Jour. Geol.* 363-373.
- Defant, A. (1929), *Dynamische Ozeanographie*, J. Springer, Berlin.
- Ellison, C.R.W., et al., (2006), Surface and deep-ocean interactions during the cold climate event 8200 years ago. *Science*, 312(5782): 1929-1932.
- Faugeres, J. C., et al. (1999), Seismic features diagnostic of contourite drifts, *Marine Geology*, 162(1), 1-38.
- Gordon, A., (1986). Interocean exchange of thermocline water: *J. Geophys. Res.*, 91 (C4), 5037-5046.
- Heinrich, H. (1988). Origin and consequences of cyclic ice rafting in the Northeast Atlantic-Ocean during the past 130,000 Years. *Quaternary Research*, 29(2), 142-152.
- Hemming, S. R. (2004), Heinrich events: Massive late Pleistocene detritus layers of the North Atlantic and their global climate imprint, *Reviews of Geophysics*, 42(1).
- IPCC. (1990). *Scientific Assessment of Climate Change – Report of Working Group 1*. Cambridge Univ. Press, Oxford.
- IPCC. (1995). *Climate Change 1995: a report of the Intergovernmental Panel on Climate Change / Intergovernmental Panel on Climate Change*. World Meteorological

Association, Geneva.

IPCC. (2001). *Climate Change*. Cambridge Univ. Press, Oxford

IPCC (2007) *Climate Change 2007: The Physical Science Basis. Contribution of Working Group I to the Fourth Assessment Report of the Intergovernmental Panel on Climate Change* [Solomon, S., D. Qin, M. Manning, Z. Chen, M. Marquis, K.B. Averyt, M. Tignor and H.L. Miller (eds.)]. Cambridge University Press, Cambridge, United Kingdom and New York, NY, USA.

Jansen, E., and J. Sjöholm (1991), Reconstruction of glaciations over the past 6 Myr from ice-borne deposits in the Norwegian Sea, *Nature*, 349(6310), 600-603.

Keigwin, L. D., and E. A. Boyle (2000), Detecting Holocene changes in thermohaline circulation, *Proceedings of the National Academy of Sciences of the United States of America*, 97(4), 1343-1346.

Kleiven, H.F. et al., (2008), Reduced North Atlantic Deepwater coeval with the glacial Lake Agassiz freshwater outburst. *Science*, 319(5859): 60-64.

Kluger, J. (2006), Global Warming Heats Up. *Time Magazine*, March, 26th

LeGrande, A.N., and Schmidt, G.A. (2008). Ensemble, Water-Isotope Enabled, Coupled General Circulation Modeling Insights into the 8.2-kyr Event. *Paleoceanography*. Vol 23 (3207).

Manabe, S., and Stouffer, R.J. (1988). Two Stable Equilibria of a Coupled Ocean-Atmosphere Model: *Journal of Climate*. 1(9), p. 841-866.

Manabe, S., and R. J. Stouffer (1999), The role of thermohaline circulation in climate.

McCave, I.N., Tucholke, B.E., (1986), *Deep current-controlled sedimentation in the western North Atlantic*. In: Vogt, P.R., Tucholke, B.E. (Eds.), *The Geology of North America*, Vol. M, The Western North Atlantic Region. Geological Society of America, Boulder, CO, 451–468.

Oppo, D.W., and R. G. Fairbanks (1987), Variability in the deep and intermediate water circulation of the Atlantic-Ocean during the past 25,000 years – Northern-Hemisphere modulation of the Southern-Ocean, *Earth and Planetary Science Letters*, 86(1), 1-15.

Sandström, J. W. (1908), Dynamische Versuche mit Meerwasser, *Ann. Hydrogr. Marit. Meteorol.*, 36, 6-23.

Schmitz, W. J., Jr., and McCartney, M.S. (1993). On the North Atlantic circulation, *Rev. Geophys.*, 31(1), 29–50.

Stoner, J. S., et al. (1998), A 200 ka geomagnetic chronostratigraphy for the Labrador Sea: Indirect correlation of the sediment record to SPECMAP, *Earth and Planetary Science Letters*, 159(3-4), 165-181.

Wolf TCW, Thiede J. (1991) History of terrigenous sedimentation during the past 10 m.y. in the North Atlantic (ODP Legs 104, 105, and DSDP 81). *Mar Geol* 101: 83–102

Worthington, L.V. (1970). The Norwegian Sea as a Mediterranean basin. *Deep-Sea Research*, 17, 84.

Wust, G. (1935): Die stratosphäre. *Wissenschaftliche Ergebnisse der Deutschen Atlantischen Expedition "Meteor"*. 6, 109-288.

Chapter 1: Characterizing Early Holocene Establishment of deep North Atlantic Circulation

Abstract

Several proxy records, including mean sortable silt (SS), percent CaCO_3 and stable isotopes of two planktonic species of foraminifera, were generated from a gravity core located on the southern terminus of Eirik Drift. Calculated sedimentation rates coupled with these proxy records enable us to identify two major flow regimes operating in the North Atlantic during the Holocene. The early Holocene (10 to 9 ka) was best characterized by a strong flow with variable buoyancy causing the winnowing and transport of large volumes of sediment to our core site. After 9 kyr, the axis of the deep current lost buoyancy and flowed along the base of Eirik Drift for the remainder of the Holocene. One exception to this pattern occurred at 8.6 kyr where circulation reverted back to its early Holocene state for ~250 years. This relatively brief change in flow was likely caused by the catastrophic outburst of glacial Lake Agassiz during the 8.2 kyr event and suggests changes in thermohaline circulation of the North Atlantic are responsible for surface cooling seen across the Northern Hemisphere during this time.

Introduction

North Atlantic deepwater formation and circulation is often portrayed as bi-modal with 1) a more deeply penetrating current during times of Northern Hemisphere warmth, and 2) a more buoyant, shallow flowing current associated with cooler Northern Hemisphere temperatures (e.g. Curry et al., 1988; Duplessy et al., 1988; Oppo and Lehman 1995). This climate-deepwater relationship has been a fundamental part of the climate system

for the past 2.5 Myr (Raymo et al., 1990; 2004; Oppo et al., 1995; deMenocal, 1995; Haug and Tiedemann, 1998). North Atlantic deepwater circulation during the most recent glacial-interglacial cycle operated in intermediate flow states associated with the quasi-interglacial climates of Marine Isotope Chron (MIC) 3 and MIC 5a, 5c (Raymo et al., 2004; Hoogakker et al., 2007). The transition from MIC 2 to 1 indicates that additional forcings operated at higher frequencies and overprinted the longer-term cycles attributed to orbital variations.

The positive climate feedbacks associated with heat transport related to variations in Northern Component Water (NCW) formation are considered by some to be instrumental in climate change (e.g., Broecker and Denton, 1990). Benthic foraminiferal $\delta^{13}\text{C}$ records indicate that the North Atlantic contribution to the Southern Ocean increased during the Bolling-Allerod, well before the Holocene (e.g., Charles and Fairbanks, 1992). Likewise, several geochemical/lithological studies (e.g., Fagel et al., 2004 and refs. contained therein) have suggested that the establishment of deepwater flow across the last transition was more complex than a single response to prevailing Holocene temperatures. The present study aims to help clarify the timing and position of the deep current system in the North Atlantic by using several proxy records including mean sortable silt (SS, the mean of the 10 to 63 μm grain size fraction), to better understand the establishment of Northern Component Water (NCW, analogous to the modern NADW) during the last deglaciation and throughout the early Holocene.

Changes of SS are highly sensitive to perturbations of deepwater currents throughout the North Atlantic and Pacific Oceans (McCave et al., 1995; Hall et al., 2001). This proxy is useful because it monitors variations in relative paleocurrent across the core site.

Sortable silt records compliment $\delta^{13}\text{C}$ studies, because the latter only show the degree of mixing of deepwater mass end members, while the former identify finer scale relative velocity variations that may occur while an area maintains a similar $\delta^{13}\text{C}$ composition.

This study presents a high-resolution reconstruction of North Atlantic surface and deepwater variability throughout the Holocene by using the planktonic foraminifera $\delta^{18}\text{O}$, $\%\text{CaCO}_3$, SiO_2 , sedimentation rates and SS proxies from core 21GGC located at the southern terminus of Eirik Drift (Figure 1.1). AMS ^{14}C dates indicate that Holocene sedimentation rates at this location on Eirik Drift have generally exceeded 40 cm/kyr over the past 10 kyrs, affording the opportunity to reconstruct surface-ocean conditions and deep-ocean circulation changes through short-lived climate events over the entire Holocene.

North Atlantic sediment drifts are deep-ocean systems formed by the interaction of bottom currents, topography, and submarine down slope sediment transport and provide valuable records of how these processes have interacted in the past. Drift formation is controlled primarily by density-driven water masses flowing along sea-floor contours, eroding sediments in some areas and depositing sediments in others (e.g., Heezen et al., 1966; McCave and Tucholke, 1986). The sediments comprising Eirik Drift, shaped by NADW, are composed of terrigenous material from Greenland, Iceland, and Canada as

well as a biogenic component of diatoms, radiolarians, foraminifera and nannofossils (McCave and Tucholke, 1986; Fagel et al., 1996). Eirik Drift sediments are also influenced by Labrador Intermediate Water (LIW), Denmark Straights Overflow Water (DSOW), and Iceland-Scotland Ridge Overflow Water (ISOW), and are therefore ideally situated to monitor the variations in NADW (Hillaire-Marcel et al., 1994; McManus et al., 2004). Finally, Eirik Drift is adjacent to the Greenland ice sheet which has recorded many smaller climate events during the Holocene allowing for the comparison of atmospheric and deep-ocean conditions over decadal time scales.

The reworking and focusing of sediments in drift systems can cause sedimentation rates to vary greatly over short distances and through time (Hunter et al, 2007). In areas of high sedimentation rate on Eirik Drift, we are able to resolve sub-Milankovitch climate variability. Knorr cruise 166-14 collected a 4.87 m gravity core (21 GGC) from the southern terminus of the Eirik Drift (57° 26.3' by 48° 36.4') in a water depth of 3471 m (Figure 1.1). This core location was selected because the locally subdued seafloor morphology suggested limited complications from topographic changes common to other drift settings (for example, mud wave fields). Furthermore, the 3.5 kHz record showed a thick (~5m) acoustically transparent layer below the sea floor, suggesting an expanded Holocene section (Figure 1.1).

Methods

Approximately 5 cc of sediment was collected at 2 cm intervals throughout the core.

Samples were weighed wet and dry to obtain wet and dry bulk densities and then were

washed in a 63 μ m sieve. The remaining fraction was then dried and weighed again to obtain coarse fraction measurements. Two species of planktonic foraminifera were picked for stable isotopic analysis, *Neogloboquadrina pachyderma* (sinistral) and *Globigerina bulloides*. *N. pachyderma* (s) dominated the foraminiferal assemblage and was picked for isotopic analysis in the 150-212 μ m size fraction. *G. bulloides* was much less abundant than *N. pachyderma* (s) and was picked from the greater than 212 μ m size fraction.

Stable isotopic values ($\delta^{13}\text{C}$ and $\delta^{18}\text{O}$) were measured at Rutgers University on a Micromass Optima mass spectrometer with a Multiprep peripheral for the automated analysis of carbonate samples at Rutgers University. For each analysis, 8-12 individual foraminifera were picked from each sample. Special effort was made to take samples that visibly looked similar, were clean and not broken or deformed in any way. The samples were generally run in groups of 24 or 32 with an accompanying eight standards. Data are reported versus V-PDB through the analysis of an in-house standard (J.D. Wright, unpublished). This standard was routinely run against NBS-19 to ensure its accuracy; 1-sigma errors are 0.05‰ and 0.08‰ for $\delta^{13}\text{C}$ and $\delta^{18}\text{O}$, respectively

Approximately 3cc of sediment was sampled at a 2 cm downcore interval for sortable silt, %CaCO₃ and SiO₂ measurements. Biogenic carbonate and silica were removed by dissolution following the process outlined in McCave et al. (1995) using a series of acetic acid and sodium hydroxide treatments, respectively. By rinsing and drying the samples between each procedure we were able to calculate %CaCO₃ and %SiO₂. Mean sortable

silt measurements were conducted at Middlebury College on a Horiba LA-920. This machine uses a Helium-Neon Laser and a Tungsten lamp for calculating grain size measurements between 0.02 and 2000 microns with a precision of 0.6% per measurement (NIST-traceable standard particle, Horiba). The samples were pre-soaked in a 3% Sodium metaphosphate solution, stirred, and placed in a sonic bath for 4 minutes in order to deflocculate all silt and clay particles prior to analysis. After the samples were agitated they were placed into the Horiba auto sampler with 30 samples comprising a run. Each sample was re-stirred by the Horibia autosampler and a small sub-sample was taken for measurement. Upon entering the machine the sample was subjected to a sonic bath to ensure deflocculation of all particles while the measurement was performed. Several duplicates were run to ensure the preparation process was standardized and to determine the level of machine reproducibility. Mean SS duplicates varied within 1.5 μm from the original sample, indicating a maximum measurement error of ~12%, with an average measurement error of ~7.5%. Results are shown in Figure 1.2 and may be found in Appendix A.

Age control for this study is based on eight radiocarbon dates conducted at the National Ocean Sciences Accelerator Mass Spectrometer (NOSAMS) facility at Woods Hole Oceanographic Institution (Table 1). All eight dates were obtained by picking between 4 and 6 mg of *N. pachyderma* (s) tests and sonicating the material in distilled water, followed by rinsing in distilled water and drying. A reservoir correction of 410 years has been applied to all dates and converted into calendar ages using the Fairbanks calibration model (Fairbanks et al., 2005). All dates increase with depth, though there is an age

plateau of 8.5 kyr between 344 and 362 cm. (Figure 1.3)

Results

Stable isotopic records from the two surface dwelling foraminifera *N. pachyderma* (s) and *G. bulloides* are useful in determining changes in surface water hydrography.

Abundances of subpolar to polar planktonic foraminifera in both the surface water and sediment assemblages follow oceanographic and climate patterns (Bé, 1977; Bé and Tolderlund, 1971). However, information about the hydrographic structure in the surface can be inferred from their stable isotopic values when found together. *N. pachyderma* (s) is a polar species that lives in the uppermost surface water during the first part of its life cycle, but later descends into the thermocline. Kohfeld et al. (1996) showed that >80% of the calcite in *N. pachyderma* (s) is added within the thermocline which reflects winter surface conditions. *G. bulloides* is a subpolar species, but is found in low abundances in polar environments. Paired $\delta^{18}\text{O}$ analyses of these two species show that *G. bulloides* $\delta^{18}\text{O}$ values are similar to or lower than *N. pachyderma* (s), indicating that test chemistry of *G. bulloides* records conditions in the upper surface waters (e.g., Lagerklint et al., 1999). Therefore, based on patterns of paired $\delta^{18}\text{O}$ values I conclude that nearly similar isotopic values indicate a well-mixed water column, and dissimilar values indicate a strongly stratified upper water column. The isotopic difference between the two species may indicate times of increased surface water freshening (strong halocline stratification with some warming) and, therefore, may be useful in linking changes in Holocene deepwater production to overlying surface water conditions.

The $\delta^{18}\text{O}$ record from *N. pachyderma* (s) shows high-frequency variability, with values ranging from 2.1‰ to 2.8‰ (mean 2.5‰) (Figure 1.2). One prolonged interval from 358 to 440 cm shows higher values averaging 2.60 ‰. The interval from 342 to 354 cm is barren of all foraminifera. Oxygen isotope values collected for *G. bulloides* range from 1.4‰ to 2.8‰ with a mean of 2.0‰. The *G. bulloides* record contains higher variability than *N. pachyderma* (s) throughout the Holocene (Figure 1.2). There are two intervals (37-45 cm and 342-354 cm) that contain no *G. bulloides* tests.

The $\delta^{18}\text{O}$ difference curve of (*N. pachyderma* (s) - *G. bulloides*) shows a highly variable relationship throughout the entire core (Figure 1.2). Large divergences are recorded between the two species (>0.8 per mil) throughout the entire core, however; most of these events are generally constrained to the early Holocene. Several events greater than 0.8 per mil occur throughout the core at 22, 241, 253, 293, 321, 373, 403 cm with the largest divergence (1.78 ‰) occurring at 417cm.

Mean sortable silt measurements range from 16.8 to 31.8 μm with a mean value of 25.9 μm (Figure 1.2). A saw tooth pattern of slowly increasing/rapidly decreasing SS values is superimposed on this record (Figure 1.4). Three cycles can be seen from 0 to 80, 100 to 180 and 190 to 320 cm. A strong negative excursion in the SS record occurs from 325 to 358 cm with SS values approaching 16 μm . This interval also coincides with a change from homogeneous gray sediment found throughout 21GGC to a finely laminated dark gray interval which contains the foraminiferal barren zones and decrease in % CaCO_3 noted above. A fourth cycle may be present from 325 to 480 cm, however the event

noted above may or may not be anomalous with regards to the typical cyclical variability of the preceding cycles.

A down core sedimentation rate history for 21GGC was constructed using AMS ^{14}C dates converted to calendar year ages (Figure 1.2). The highest sedimentation rate at the toe of Eirik Drift occurred between 10 and 9.5 kyr with values approaching 170 cm/kyr. High sedimentation rates (~ 140 cm/kyr) are also recorded from 8.5 to 8.0 kyr. From ~ 7.5 kyr to present, sedimentation rates remained relatively constant at ~ 40 cm/kyr.

Discussion

High early Holocene sedimentation rates have been noted in several North Atlantic studies and are attributed to the reworking of glacial sediments as NCW increased in density from a gNAIW to NADW flow state (e.g., Keigwin and Jones, 1994; Bianchi and McCave, 1999). Core 21GGC corroborates these findings on the deep Eirik Drift, where sedimentation rates diminish from an early Holocene high of 170 cm/kyr to ~ 40 cm/kyr after 9 ka. SS values reach a pinnacle at 9.1 kyr suggesting an early Holocene pulse in the strength of NCW over Eirik Drift. This finding is consistent with Fagel et al. (1997) who inferred maximum WBUC flow at ~ 9 ka based on changes in clay assemblages from cores raised from the Labrador Sea, and Irminger/Iceland basins.

After 9ka, sedimentation rates across Eirik Drift stabilized at ~ 40 cm/kyr indicating NCW has developed density characteristics analogous to modern NADW and is no longer winnowing glacial sediments. An interruption in this flow state occurs between

8.6-8.2 ka, where sedimentation rates return to the early Holocene values suggesting NCW briefly returned to gNAIW flow state. This reduction in flow is concurrent with the outburst of glacial Lake Agassiz and provides strong support that oceanic circulation was curtailed due to a rapid freshwater pulse into the North Atlantic (Alley et al., 1997; Barber et al., 1999). From 8 ka to present, SS values indicate variable current intensities throughout the Holocene while sedimentation rates remain constant suggesting on millennial scales deepwater density and production rate may become decoupled or that topography across Eirik Drift is acting as a density “floor” (topography on Eirik Drift causes NCW to flow higher than if there was ocean floor). For example at 2.2 and 4.6 kyr we see paleoflow at a relative maximum at 21GGC while calculated sedimentation rates remain constant, suggesting that changes in the axis of the current are occurring at deeper depths in the ocean.

Similar patterns in flow history from both sides of the Atlantic are revealed in comparing the Gardar Drift SS record from Bianchi and McCave (1999) and the SS record from 21GGC (Figure 1.4). For example, both Eirik and Gardar Drifts show faster flows from 10.5 to 9.5 kyr and similar long-term decreases in SS from 9 kyr to 5 kyr and from 5 kyr to 2 kyr, respectively. Superimposed on this variability are higher frequency cycles such as increased flow during the Medieval Warm Period (MWP) and a weakening of flow during the Little Ice Age (LIA). This agreement between the two records suggests that while North East Atlantic Bottom Water (NEABW, the eastern component of NCW) can bypass Eirik Drift over short time periods (Hunter et al., 2007), long-term deposition across the drift must be controlled by both DSOW and ISOW.

The 8.2 kyr Climate Event

The 8.2 kyr event has been described as a freshwater perturbation of global THC that resulted in cooling across the Northern Hemisphere (see Alley and Agustsdottir, 2005 for a review). However, until recently, no direct evidence existed to indicate that deep-ocean circulation was altered at this time. Ellison et al. (2006) showed diminished deepwater flow across the 8.2 kyr time interval on Gardar Drift using the sortable silt proxy (Figure 1.5). This work was closely followed by Kleiven et al. (2008) that interpreted a decrease in benthic foraminiferal $\delta^{13}\text{C}$ values as a reduction in NADW flow on Eirik Drift.

The SS record in 21GGC, which is 1 km from MD 2664 core of Kleiven et al. (2008), indicates that change in deep circulation on Eirik Drift preceded the cooling seen in Greenland ice cores and was concurrent with initial outburst of glacial Lake Agassiz (Barber et al., 1999). In Core 21GGC, this interval is a 12 cm unit of un-fossiliferous clay from 342 to 354 cm, and shows rapid decreases in the $\%\text{CaCO}_3$, $\%\text{SiO}_2$, and SS values (Figure 1.5). According to the age model calculated at 21GGC, the decrease in SS commenced at ~ 8.6 kyr, suggesting that the initial outburst rapidly curtailed ocean circulation. Evidence of surface-ocean cooling also exists at 14 cm above the clay layer, as indicated by increases in $\delta^{18}\text{O}$ values of both *N. pachyderma* (s) and *G. bulloides*. Likely changes in the atmospheric carbon reservoir associated with the disruption of North Atlantic overturning increase uncertainty in our age model throughout this interval (age plateau Figure 1.3). Therefore, we only make the observation that surface ocean freshening preceded a slowing in circulation in support of the 8.2 kyr Event hypothesis.

In both 21GGC and MD2664 of Kleiven et al. (2008), a strong decrease in %CaCO₃ marks the onset of the “8.2 kyr” interval (345 cm in MD2664 and 355 cm in 21GGC). However, the age models from both studies, based on AMS ¹⁴C dating, yield a large (250 to 300 year) discrepancy in the ages for this low CaCO₃ zone with the younger age reported by Kleiven et al. (2008). The AMS ¹⁴C dating for this study was based exclusively on *N. pachyderma* (s) which is the dominant species during this interval. In contrast, Kleiven et al. (2008) used the less abundant *G. bulloides* and often mixed species (*G. bulloides*, *N. pachyderma* (s) and *N. pachyderma* (d)). I argue that the ages for this interval are more robust in this study because there is less possibility of contamination from reworking/bioturbation when exclusively selecting the dominant species for AMS dating (Bard et al., 1987).

Comparing SS records of Ellison et al. (2006) and this study paint a very different picture of how circulation changed during the 8.2 kyr event. On Gardar Drift, SS initially decreases at 8.49 ka reaching minimum flow at 8.2 ka. It takes another 200 years for circulation patterns to recover indicating circulation was depressed for ~500 years at this site on Gardar Drift. On Eirik Drift, circulation changes at ~8.6 ka, which is ~100 years prior to the initial decrease on Gardar Drift based on the age models. The decrease on Eirik Drift was shorter in duration than on Gardar with circulation remaining depressed for 400 years and fully recovered by 8.2 ka. We postulate that the discrepancy between the eastern and western Atlantic may in part be related to the establishment of DSOW which began to flow around 8.5 ka (Innocent et al., 1997). The east to west comparison

suggests that DSOW lessened the duration and/or overall climate response to the 8.2 kyr event by providing an avenue to deep convection not available during the Younger Dryas or H1. This notion may explain why circulation over Gardar Drift stays depressed over the entire 8.2 kyr event while circulation changes over Eirik Drift are recorded as very rapid.

Conclusions

Comparison of SS and sedimentation rates on Eirik Drift show deepwater formation on Eirik Drift operated in two modes during the Holocene. During the early Holocene (10-9 ka), production of NADW was vigorous with large changes in density as indicated by high SS values and high sedimentation rates on Eirik Drift. NCW during this time was in a transitional state from glacial to interglacial flow regimes and suggests that changes in deepwater flow on glacial to interglacial time scales are best described as changes in water mass density, not production rate. At 9 ka, NCW reached the “true” interglacial flow regime indicating a ~1.5 kyr lag between the onset of warmer Holocene temperatures and equilibrium in the deepwater system. This suggests that at least on glacial to interglacial time scales, the buoyancy and flow rates of NADW, and therefore overall ocean ventilation respond to changes in the surface freshwater budget controlled largely by climatic change.

The deepwater response to the 8.2 kyr event still remains a matter of debate. At 21GGC, SS shows strong evidence of NCW disruption between 8.6-8.2 ka and is coeval glacial outburst of Lake Agassiz. However, when compared with other records, discrepancies

arise. The presence of newly formed DSOW may be responsible for contributing to the discrepancy in the SS records in the eastern and western North Atlantic. Likewise, the inception of DSOW flow may be responsible for reducing the impact and duration of the 8.2 kyr event as compared to other events such as the YD and H1 when a DSOW flow regime was not present.

Table 1

Depth (cm)	Reservoir Corrected ^{14}C Age	Measurement error	Calander Age (ka)	Standard Deviation
0	269	35	307	71
100	2659	25	2762	12
200	4489	35	5156	94
300	6919	40	7739	50
340	7679	45	8455	47
365	7869	35	8638	48
400	8419	40	9460	32
475	9069	50	10229	25

Table 1 contains the depth horizons and corresponding ^{14}C ages used in the creation of the 21GGC age model.

Figure Captions:

Figure 1.1: Location of 21GGC on Eirik Drift. Also shown are the deepwater currents (dark blue), intermediate water currents (yellow) and surface water currents (light blue) that influence sediments deposited at 21GGC.

Figure 1.2: Several Proxy records generated from 21GGC. All graphs are plotted on a common depth scale from 0 to 500 cm. The blue proxy records are $\delta^{18}\text{O}$ records of *N. pachyderma* (*s*), *G. bulloides* and the difference curve of *N. pachyderma* (*s*) – *G. bulloides*. All records show highly variable small amplitude changes down core. Sediment from 342 to 354 cm within 21GGC is barren of all foraminifera. The difference curve suggests that the early Holocene (300-500 cm) more stratified than the mid to late Holocene with divergence rising above 0.8 per mil 5 times. The two red curves show the %CaCO₃ and SS proxy records. %CaCO₃ increases from ~10 to 40% throughout the Holocene while SS ranges from 16 to 30 microns. Both records show a large negative excursion from 325 to 358 cm with values approaching or exceeding that of earliest Holocene sediment in 21GGC. The green record shows calculated sedimentation rates derived from our age model. Two periods of high sedimentation rates are found in the resulting model, 344-362 and 400 to 482 cm. A longer term Holocene sedimentation rate of ~40 cm/kyr is seen from 0 to 344 and 362 to 400 cm.

Figure 1.3: Eight AMS ^{14}C dates were calculated by using 4-6 milligrams of *N. pachyderma* (*s*) tests run at NOSAMS. Each date (blue triangles) was generated using a 410 yr marine reservoir correction and calculated into calendar ages using the Fairbanks calibration model (Fairbanks et al., 2005). All ages increase with depth however a ^{14}C plateau occurs from 344 and 362 cm.

Figure 1.4: Comparison of SS records from 21GGC and NEAP 15K (Bianchi and McCave, 1999). Both SS records show similar patterns of variability on millennial timescales throughout the Holocene. Both records suggest the early Holocene was dominated by faster flow, with decreasing trend from 9 to 5 kyr. Both records also record similar variability from 5 to 2 kyr suggesting the eastern and western flow regimes act in concert with one other across the time scales.

Figure 1.5: The 8.2 kyr event as seen in 21GGC proxy records (top) and SS record of Ellison et al. (2006). Across the 8.2 kyr event %CaCO₃ and %SiO₂ revert to early Holocene values. This suggests that either the sediment supply into the North Atlantic changed across this interval or that the deep current system is remobilizing sediment in a similar area as the early Holocene. SS values indicate a large decrease in flow suggesting that the axis of the current is no longer over the core site and further supports a change in flow regime across this interval. Ellison et al. (2006) show diminished flow across the 8.2 kyr event however the recovery of the SS system is delayed ~250 years from 21GGC. This delay suggests that ISOW may be more susceptible to freshwater input than DSOW during this event.

Figure 1.1

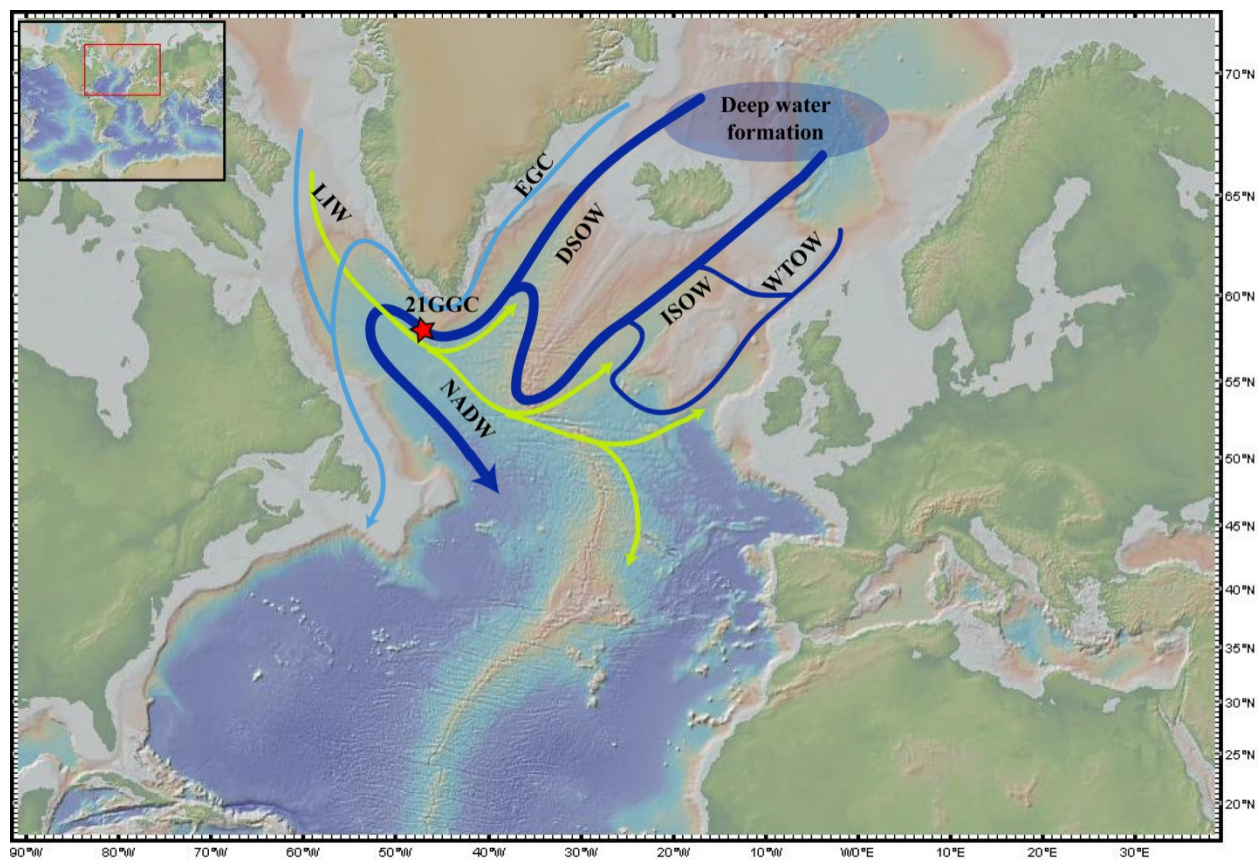


Figure 1.2

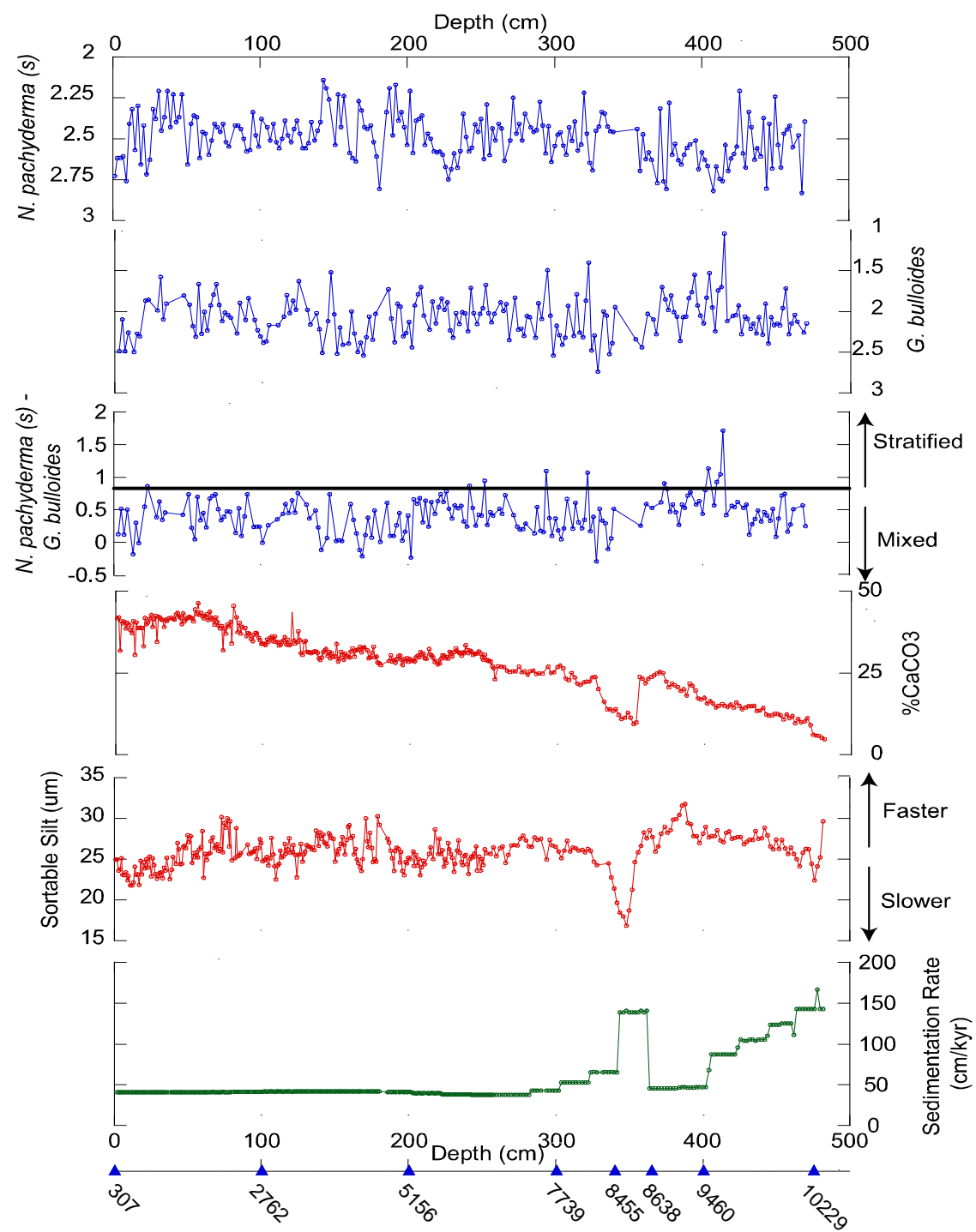


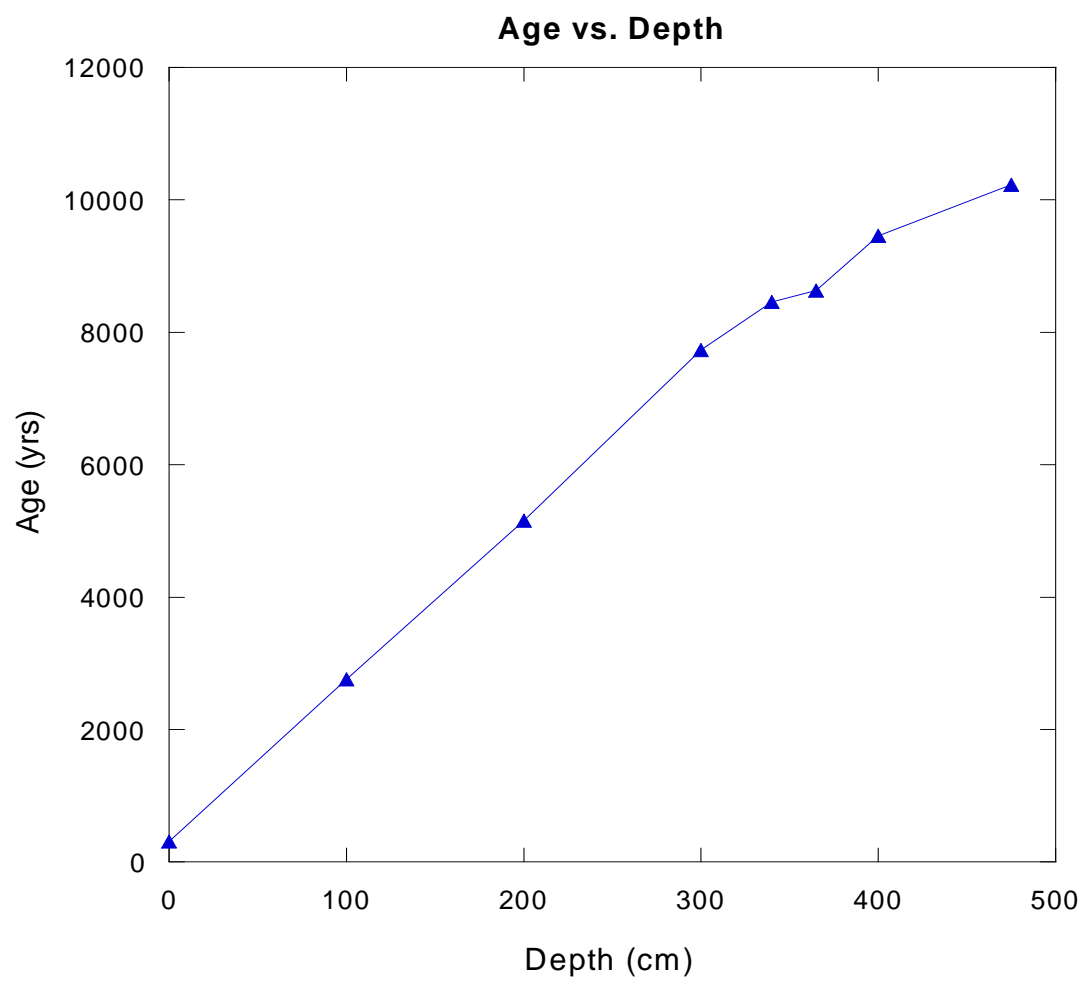
Figure 1.3

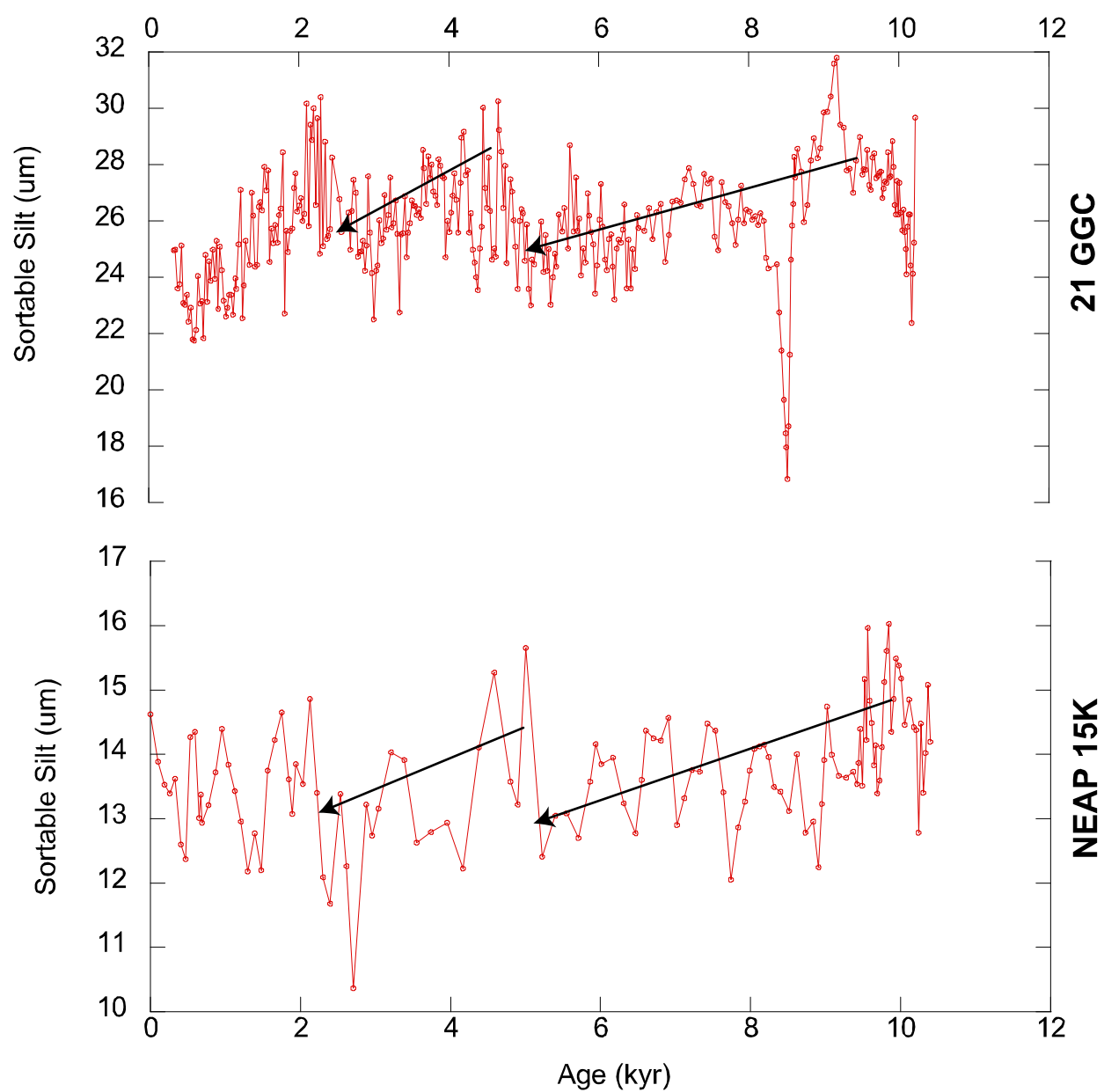
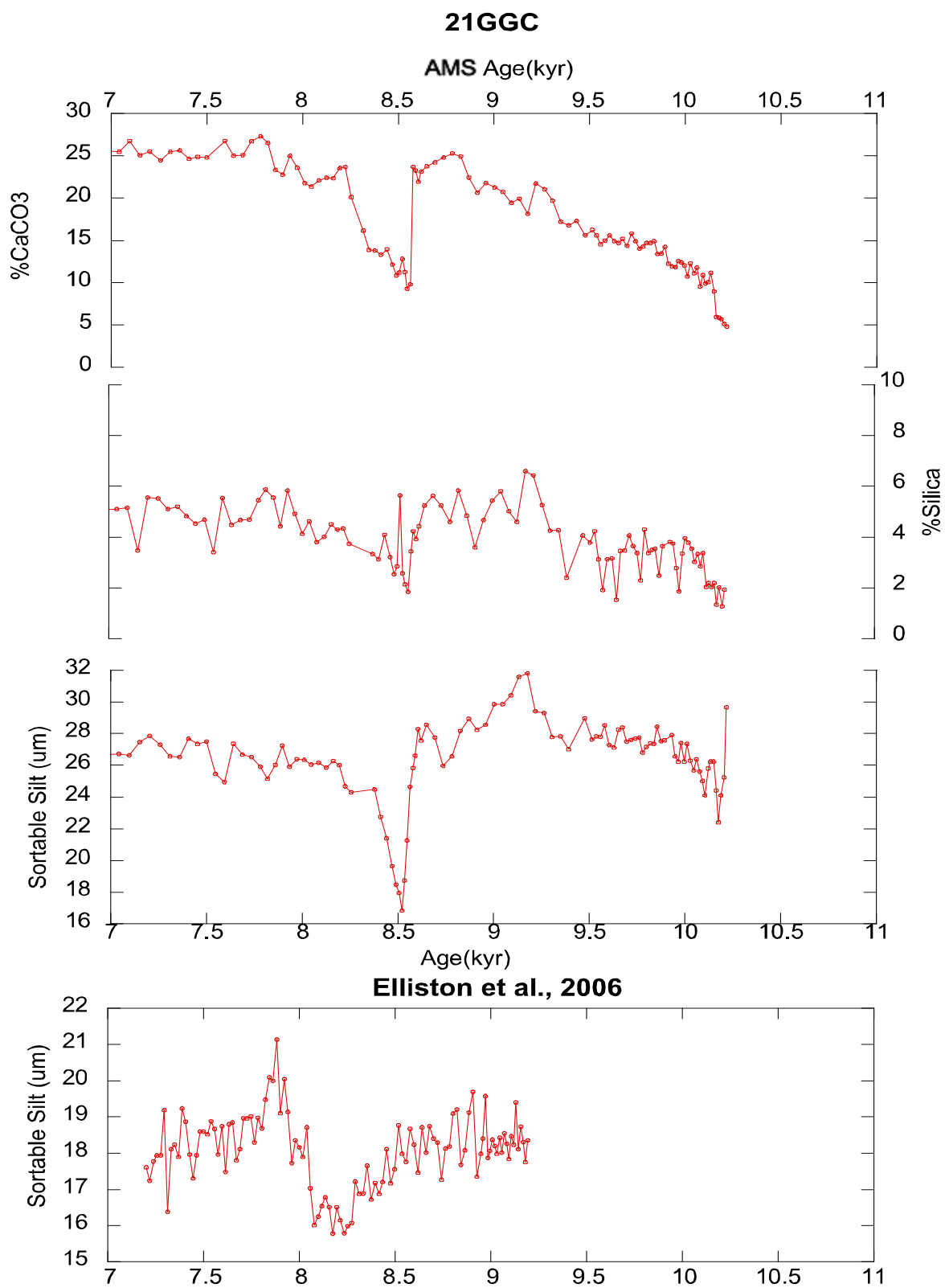
Figure 1.4

Figure 1.5



References

- Alley, R.B., Mayewski, P.A., Sowers, T., Stuiver, M., Taylor, K.C., Clark, P.U., 1997. Holocene climatic instability: A prominent, widespread event 8200 yr ago. *Geology*, 25, 483-486.
- Alley, R.B. and Agustsdottir, A.M., 2005. The 8k event: cause and consequences of a major Holocene abrupt climate change. *Quaternary Science Reviews*, 24(10-11): 1123-1149.
- Barber, D. C., et al. 1999, Forcing of the cold event of 8,200 years ago by catastrophic drainage of Laurentide lakes, *Nature*, 400(6742), 344-348.
- Bard, E., Hamelin, B., Fairbanks, R.G., and Zindler, A., 1987. Calibration of the ^{14}C timescale over the past 30,000 years using mass spectrometric U–Th ages from Barbados corals. *Nature*, 345(): 405-410.
- Bé, A.W.H., 1977. An ecological, zoogeographic and taxonomic review of recent planktonic foraminifera, in Ramsay, A.T.S. (ed.), *Oceanic Micropaleontology*, vol. 1, 1-100. Academic Press, London.
- Bé, A.W.H. & Tolderlund, D.S., 1971. Distribution and ecology of living planktonic foraminifera in surface waters of the Atlantic and Indian Oceans, in Funnel, B.M. and Riedel, W.R. (eds.), *The Micropaleontology of Oceans*, 105-149.
- Bianchi, G.G., and McCave, N., 1999. Holocene periodicity in North Atlantic climate and deep-ocean flow south of Iceland. *Nature*, 397: 515-517.
- Broecker, W.S. and Denton, G.H., 1990. The role of ocean-atmosphere reorganizations in glacial cycles. *Quaternary Science Reviews*, 9(4): 305-341.
- Charles, C.D., and Fairbanks, R.G., 1992. Evidence from Southern-Ocean sediments for the effect of North-Atlantic deepwater flux on climate. *Nature*, 355(6359): 416-419.
- Curry, W.B., Duplessy, J.C., Labeyrie, L. D., and Shackleton, N. J., 1988. Changes in the distribution of $\delta^{13}\text{C}$ of deepwater eCO_2 between the last glaciation and the Holocene. *Paleoceanography*, 3(3): 317-341.
- Demenocal, P.B., 1995. PlioPleistocene African climate. *Science*, 270(5233): 53-59.
- Duplessy, J. C., Shackleton, N. J., Fairbanks R. G., Labeyrie, L., Oppo D., and Kallel, N., 1988. Deepwater source variations during the last climatic cycle and their impact on the global deepwater circulation. *Paleoceanography*, 3(3): 343-360.
- Ellison, C.R.W., Chapman, M.R. and Hall, I.R., 2006. Surface and deep-ocean interactions during the cold climate event 8200 years ago. *Science*, 312(5782):

1929-1932.

- Fagel, N. et al., 2004. Nd and Pb isotope signatures of the clay-size fraction of Labrador Sea sediments during the Holocene: Implications for the inception of the modern deep circulation pattern. *Paleoceanography*, 19(3): 16.
- Fagel, N., Hillaire-Marcel, C. and Robert, C., 1997. Changes in the Western Boundary Undercurrent outflow since the Last Glacial Maximum, from smectite/illite ratios in deep Labrador Sea sediments. *Paleoceanography*, 12(1): 79-96.
- Fagel N., and Hillaire-Marcel, C., 1996. Clay mineral signature of the NW Atlantic Boundary undercurrent. *Marine Geology*, 130, 19-28.
- Fairbanks, R.G. et al., 2005. Radiocarbon calibration curve spanning 0 to 50,000 years BP based on paired Th-230/U-234/U-238 and C-14 dates on pristine corals. *Quaternary Science Reviews*, 24(16-17): 1781-1796.
- Hall, I.R., McCave, I.N., Shackleton, N.J., Weedon, G.P. and Harris, S.E., 2001. Intensified deep Pacific inflow and ventilation in Pleistocene glacial times. *Nature*, 412(6849): 809-812.
- Haug, G.H. and Tiedemann, R., 1998. Effect of the formation of the Isthmus of Panama on Atlantic Ocean thermohaline circulation. *Nature*, 393(6686): 673-676.
- Heezen, B.B., Hollister, C.D., and Ruddiman, W.F., Shaping of the continental rise by deep geostrophic currents. *Science*, 152(3721): 502-508
- Hillaire-Marcel, C., de Vernal, A., Bilodeau, G., Wu, G., (1994). Isotope Stratigraphy, sedimentation rates and paleoceanographic changes in the Labrador Sea. *Canadian Journal of Earth Sciences* 31, 63:89.
- Hoogakker, B.A.A., McCave, I.N. and Vautravers, M.J., 2007. Antarctic link to deep flow speed variation during Marine Isotope Stage 3 in the western North Atlantic. *Earth and Planetary Science Letters*, 257(3-4): 463-473.
- Hunter, S. et al., 2007. Deep western boundary current dynamics and associated sedimentation on the Eirik Drift, southern Greenland margin. *Deep-Sea Research Part I-Oceanographic Research Papers*, 54(12): 2036-2066.
- Innocent, C., Fagel, N., Stevenson, R.K. and Hillaire-Marcel, C., 1997. Sm-Nd signature of modern and late Quaternary sediments from the northwest North Atlantic: Implications for deep current changes since the Last Glacial Maximum. *Earth and Planetary Science Letters*, 146(3-4): 607-625.
- Keigwin, L.D., and Jones, G.A., 1994. Western North Atlantic evidence for millennial-scale changes in ocean circulation and climate. *Journal of Geophysical Research*,

99(c6): 12397-12410.

- Kleiven, H.F. et al., 2008. Reduced North Atlantic Deepwater coeval with the glacial Lake Agassiz freshwater outburst. *Science*, 319(5859): 60-64.
- Kohfeld, K.E., Fairbanks, R.G., Smith, S.L. and Walsh, I.D., 1996. *Neogloboquadrina pachyderma* (sinistral coiling) as paleoceanographic tracers in polar oceans: Evidence from northeast water Polynya plankton tows, sediment traps, and surface sediments. *Paleoceanography*, 11(6): 679-699.
- Lagerklint, I.M. and Wright, J.D., 1999. Late glacial warming prior to Heinrich event 1: The influence of ice rafting and large ice sheets on the timing of initial warming. *Geology*, 27(12): 1099-1102.
- McCave, I.N., Manighetti, B. and Robinson, S.G., 1995. Sortable silt and fine sediment size composition slicing-parameters for paleocurrent speed and *Paleoceanography*. *Paleoceanography*, 10(3): 593-610.
- McCave, I.N., Tucholke, B.E., 1986. Deep current-controlled sedimentation in the western North Atlantic. In: Vogt, P.R., Tucholke, B.E. (Eds.), *The Geology of North America, Vol. M, The Western North Atlantic Region*. Geological Society of America, Boulder, CO, 451-468.
- McManus, J.F., Francois, R., Gherardi, J.M., Keigwin, L.D. and Brown-Leger, S., 2004. Collapse and rapid resumption of Atlantic meridional circulation linked to deglacial climate changes. *Nature*, 428: 834-837.
- Oppo, D.W. and Lehman, S.J., 1995. Suborbital timescale variability of North-Atlantic deepwater during the past 200,000 years. *Paleoceanography*, 10(5): 901-910.
- Oppo, D.W. et al., 1995. A delta-C-13 record of upper North-Atlantic deepwater during the past 2.6 million years. *Paleoceanography*, 10(3): 373-394
- Praetorius, S.K., McManus, J.F., Oppo, D.W. and Curry, W.B., 2008. Episodic reductions in bottom-water currents since the last ice age. *Nature Geoscience*, 1(7): 449-452.
- Raymo, M.E. et al., 2004. Stability of North Atlantic water masses in face of pronounced climate variability during the Pleistocene. *Paleoceanography*, 19(2): 13.
- Raymo, M.E., Ruddiman, W.F., Shackleton, N.J. and Oppo, D.W., 1990. Evolution of Atlantic Pacific delta-C-13 gradients over the last 2.5 MY. *Earth and Planetary Science Letters*, 97(3-4): 353-368.

Chapter 2: Is the last glacial transition a good analogue for prior climate cycles: An examination of abrupt climatic events and establishment of deepwater flow across Terminations 1 and 2

Abstract

Surface and deep-ocean records of Termination 1 (T1) and Termination 2 (T2) are compared using two sites on the Eirik Drift. Termination 1 is punctuated by three climatic reversals (H1, YD and 8.2 kyr Event) while Termination 2 only records one reversal (H11). Benthic and planktonic $\delta^{18}\text{O}$ records indicate that continental ice volume melted more quickly across T2 relative to T1. The longer deglaciation across T1 indicates that continental ice was more resistant to North Atlantic temperature therefore, allowing storage of melt-waters and increasing probability of catastrophic freshwater events that could alter thermohaline circulation (THC) and climate in the Northern Hemisphere.

The establishment of the deepest flowing NCW was delayed in MIC 5e compared to the Holocene. After Termination 2, SS values reach maximum flow values, and hence, highest intensities at 123 ka, lagging full interglacial surface-water temperature conditions by 7kyr. Conversely, NCW quickly increases in density across Termination 1 with maximum flow velocities (9.3 ka) lagging the onset of Holocene temperatures by ~1.5 kyr. The deglaciation of Greenland throughout much of MIC 5e (deVernal and Hillaire-Marcel 2008) may be responsible for curtailing the full establishment of an NADW-like watermass during the more extreme interglacial MIC 5e.

Introduction

The saw-toothed shape of $\delta^{18}\text{O}$ records spanning the late Pleistocene show glacial-interglacial cycles that are marked by slow growth of continental ice sheets into full glacials followed by relatively rapid ice sheet melting and climate warming (Broecker and van Donk, 1970). These climate cycles are paced by small changes in insolation related to variations in Earth's orbit (Hays et al., 1976). It might be assumed that deglacial transitions operated in a similar fashion with the greatest rate of ice melting corresponding to insolation maxima. High-resolution records of the two most recent glacial terminations, however, show distinct differences. For example, three abrupt (H1, YD and the 8200 yr event) returns to colder climates interrupted Termination 1 (MIC 2 to 1) while Termination 2 (MIC 6 to 5e) only recorded a singular climatic event, H11. The mechanism most often called on to force these abrupt climate coolings is increased injections of ice and/or freshwater into the northern North Atlantic such that Northern Component Water (NCW, analogous to NADW) formation was disrupted. The effect on climate was that the alteration of heat distribution in the Northern Hemisphere (Broecker, 1994). If massive ice or freshwater discharge is the mechanism forcing abrupt climate cooling during deglaciations, the record of climate change during the last 2 terminations indicates that freshwater forcing across terminations may be climatically unique.

Large fluxes of freshwater into the North Atlantic have been shown to influence oceanic circulation on Milankovitch and millennial time scales through feedbacks associated with the slowing or complete shutting down of North Atlantic deepwater production (e.g.,

Boyle and Keigwin, 1987; Manabe and Stouffer, 1988, 2000; Barber et al., 1999; Broecker, 1994). Termination 1 produced abrupt climatic events during three different ice sheet configurations, representing near maximum, intermediate, and minimum volumes. The H1 and YD events occurred while NCW buoyancy was high, and characterized as glacial North Atlantic Intermediate Water (gNAIW; Oppo and Lehman, 1995). Conversely, the 8.2 kyr event (much smaller global extent than H1 and YD) occurred when NCW production resembled modern North Atlantic Deepwater (NADW) which is denser than the gNAIW flow state. These events have lead researchers to postulate that the gNAIW water state is less stable than NADW and more susceptible to freshwater forcing (e.g., Bianchi and McCave, 1999).

Only one abrupt climate event (H11) has been identified during Termination 2 (Rasmussen et al., 2003). Benthic foraminiferal $\delta^{13}\text{C}$ proxies indicate that NCW remained in its gNAIW state across Termination 2 and through a portion of MIC 5e (Oppo et al., 2001; McManus et al., 2002). Therefore, H11 occurred when NCW was in a gNAIW state, like the H1 and Younger Dryas Events during Termination 1, and potentially more susceptible to changes in the surface hydrographic budget. However, North Atlantic sedimentation rates indicate deepening depo-centers on sediment drifts across the climate transition suggesting a viable NADW-like watermass was formed soon after Termination 2 (Bianchi et al., 2001; Oppo et al., 2001, 2006). If gNAIW is more sensitive to freshwater flux, then the disagreement between sedimentological and geochemical proxies across Termination 2 must be resolved in order to make meaningful comparisons between Termination 1 and 2.

To determine if deep-ocean circulation was altered in response to abrupt events in the past, it is essential to have temporal resolution, precise age control, and knowledge of the prevailing state of NCW. The first concern is addressed by retrieving sedimentary archives from areas of the ocean where sedimentation rates are sufficiently high to resolve decadal to centennial changes. Cores collected on deep-sea sediment drifts (e.g., Bermuda Rise, Orphan Knoll, Fenni, Gardar and Eirik Drifts) have sedimentation rates in excess of 10 cm/kyr, affording the requisite temporal resolution (e.g., Boyle and Keigwin, 1987; Henderson Chapter 1; Solignac et al., 2004; Innocent et al., 2000).

Second, precise site-to-site correlation of records from multiple deep-sea locations is required to evaluate lead-lag relationships between the surface and deep ocean. Age control during Termination 1 is largely derived from AMS ^{14}C dates and allows for the generation of robust age models. Precise age control across Termination 2 is much more difficult. At present, oxygen isotopic stratigraphy provides the only means of site-to-site correlation, which is useful in generating age–depth picks across MIC boundaries.

However, sedimentation rates across glacial terminations are likely to be variable in nature adding uncertainty to constructed age models. A goal for Expedition 303 was the generation of paleointensity assisted chronologies (PACs) that extended through the Pleistocene. However, this new method of age constraint is unavailable at present, meaning that there is greater age uncertainty across Termination 2 than Termination 1.

A third requirement is that the buoyancy state of NCW must be considered. Geochemical

and sedimentologic evidence shows that NCW buoyancy varied significantly across Termination 1 (Curry et al., 1988; Duplessy et al., 1998; Oppo and Lehman, 1995). These buoyancy changes are linked to variations in freshwater which forced circulation patterns from one state to another (e.g., Manabe and Stauffer, 1988). Therefore, it is vital to incorporate paleo-records from cores spanning a sufficient depth range in the North Atlantic to constrain the dynamic range of NCW states and eliminate spurious findings that may result by monitoring changes at a single site.

This study addresses the issues outlined above that hinder an understanding of the relationship between deepwater circulation and abrupt climate change by monitoring the deep-ocean response at two sites on Eirik Drift. Eirik Drift is a large contourite deposit located off the southern tip of Greenland and is ideal for both surface and deepwater paleoceanographic study (Figure 2.1). Sedimentation rates on the drift reach maximum values that exceed 100 cm/kyr, but average ~20 cm/kyr (e.g., Hillaire-Marcel et al, 1994; Stoner et al., 1995; Shipboard party, Expedition 303; Henderson, Chapter 1). The drift occupies a large range of sea floor depths, extending from 1500 m down to depths that exceed 3500 m. Therefore, the sedimentary archives on Eirik Drift track NCW as it shifted between the deep flow (e.g., modern NADW) to the more buoyant water mass (e.g., gNAIW).

The East Greenland Current and Labrador Sea influence the surface waters over Eirik Drift. Therefore, proxies for surface water conditions above Eirik Drift reflect Laurentide, Inuitian and Greenland Ice Sheet variability (Hillaire-Marcel et al., 1994; Stoner et al.,

1995, 1998, 2000) including providing evidence for fresh water pulses that may have affected thermo-haline circulation (Hillaire-Marcel and Bilodeau, 2000). Deepwater currents focus and winnow sediments on Eirik Drift, most notably by the deep western boundary under current. Therefore, Eirik Drift is sensitive to geochemical and physical tracers of current position/strength as recorded in the depositional history of the drift. Because both surface and deep circulation changes are recorded at one site, ambiguities in correlating surface and deepwater changes are eliminated.

Comparison of North Atlantic Ocean Circulation during abrupt climate change

As noted previously, North Atlantic deepwater circulation operated in the deep mode across the 8.2 kyr event, similar to the modern NADW. However, deep-ocean circulation during the 8.2 kyr event differed from the modern in that Labrador Intermediate Water formation was absent in the early Holocene and deep convection was restricted to the eastern North Atlantic (Hillaire-Marcel et al., 1994; Fagel et al., 1997). Even though, deepwater buoyancy was highly variable throughout the first 1500 years of Holocene, by 9 ka deep NCW was flowing to the deepest depths on Eirik Drift (Henderson, Chapter 1).

Iceland Scotland Overflow Water (ISOW) constituted the bulk of NCW flow prior to the 8.2 kyr event (Fagel et al., 2004). Denmark Straights Overflow Water (DSOW) became a viable deepwater mass following the 8.2 kyr event at which time oceanic circulation may have collapsed briefly (Innocent et al., 2000; Kleiven et al., 2008). From 8 to 6 ka, the flux of DSOW increased at the expense of the previously dominant ISOW, indicating that there may be east-to-west compensation of flow across the Greenland and Norwegian

Seas . The lag in the formation of DSOW water compared to the onset of ISOW is often hypothesized to reflect remnant sea ice coverage in the Greenland Sea or localized freshening of the Greenland Sea from the Greenland ice sheets (Fagel et al., 2004). The surface conditions in the Greenland Sea across the interval most likely differ from conditions across the YD and H1 events and may provide a means for the 8.2 kyr event to recover in a different manner.

Circulation prior to and after the YD may be best described as spatially similar to the pre-8.2 kyr ocean; however, the density state of deepwaters was drastically different between the two events. Geochemical evidence suggests that ISOW started flowing at approximately 14.5 ka, but did not become a main constituent of the water mass until ~9.5 ka (Fagel et al., 2004). Sedimentation patterns across the North Atlantic show that NCW at this time was in a gNAIW state with active sedimentation occurring ~1200 m higher on Eirik Drift than during the modern (Henderson, Chapter 1). Insolation (65°N) across this interval approached a maximum at ~10 ka, promoting increased fluxes of freshwater as the ice sheets continued to melt. The increased freshwater kept NCW deepwater masses in its shallow mode. Interestingly, Pa/Th ratios of deep sea sediments show that while freshwater hindered formation of the denser variety of NCW, overall North Atlantic overturning was quite robust, approaching Holocene values during the Bolling-Allerod period (McManus et al., 2004).

Heinrich Events 1 and 11 occurred in an oceanic flow states much different than the YD and 8.2 kyr event. Sea level was ~100 m lower than today, which may have made it

more difficult for deepwater to flow from the Greenland and Norwegian Seas, across the Greenland-Scotland Ridge into the North Atlantic Ocean. Perennial sea ice cover in the Greenland and Norwegian seas was greatly expanded, making deep convection in this region difficult to improbable (CLIMAP, 1981; Oppo and Lehman, 1993; deVernal and Hillaire-Marcel, 2002). The polar front also moved south in response to increased sea ice expansion in the northern North Atlantic, reaching a maximum to a position south of Iceland. During this time, the warm salty North Atlantic Drift did not flow north of 45° N and as a result deepwater convection may not have occurred north of the Denmark Straights and Iceland-Scotland ridges. There are also questions as to how viable these deepwater formation sites were, considering fact that full glacial overturning rates were only 30 to 40% less than that of the modern (McManus et al., 2004).

Methods

The data used in this chapter are a compilation of stable isotopic and mean sortable silt (SS) data derived from chapters 1 and 3 of this dissertation (Site 1306 and 21GGC) as well as new SS data from Site 1305. For the methodology of the data pertaining to chapter 2, please see pages 25-28 of this dissertation.

Site 1305 data were generated in post cruise collaboration between C. Hillaire-Marcel and A. deVernal of GEOTOP and S. Henderson and J. Wright of Rutgers University. As a part of this agreement, all stable isotopic measurements from Site 1305 were conducted at GEOTOP while the SS measurements were conducted at Middlebury College on a Horiba LA-920 as part of an ongoing collaboration between P. Manley and S. Henderson.

Three cc samples of raw sediment were treated with a series of acetic acid and sodium hydroxide treatments to remove any biogenic carbonate and biogenic silica, respectively (McCave et al., 1995). By rinsing and drying the samples between each procedure we were able to calculate %CaCO₃ and %SiO₂. The prepared samples were then run in the Horiba LA-920 which uses a Helium-Neon Laser and a Tungsten lamp for calculating grain size measurements between 0.02 and 2000 microns with a precision of 0.6% per measurement (NIST-traceable standard particle, Horiba). The samples were pre-soaked in a 3% “Calgon” solution, stirred, and placed in a sonic bath for 4 minutes in order to deflocculate all silt and clay particles prior to analysis. After adequate agitation, the samples were placed into the Horiba auto sampler, with thirty samples comprising a run. Each sample was re-stirred by the Horibia autosampler and a small sub sample was taken for measurement. Upon entering the machine the sample was subjected to a sonic bath to ensure deflocculation of all particles while the measurement was performed. Several duplicate samples were run twice to ensure the preparation process was standardized and that the results were reproducible. Results are shown in Figure 2.2 and can be found in Appendix B.

Results

Termination 1 and Holocene

The $\delta^{18}\text{O}$ record of *N. pachyderma* (*s*) shows glacial highs of 4.7‰ to interglacial lows of 2.5‰ at Sites 1305 and 1306 (Figure 2.2). Mean SS values range from 20 to 26 μm at Site 1306 while Site 1305 records higher variability across the same interval with ranges from 15 to 28 μm . A SS maximum of 28 μm in Site 1305 occurs at a depth of 7.83 mcd

and is correlated to 21GGC at 9.2 kyr. The spliced record of 21GGC and Site 1305 ranges from 0 to 16.5 kyr providing a bottom water history for much of Termination 1 and the Holocene. Site 1306 records much of Termination 1, however, little to no variability is seen in the record from 0 to 1 mcd with $\delta^{18}\text{O}$ values trending along 3.5‰ and SS values ranging from 20 to 23 μm .

Termination 2 and MIC 5e

The $\delta^{18}\text{O}$ of *N. pachyderma* (*s*) across Termination 2 is much more variable than the Termination 1 record (Figure 2.3). At Site 1305, a short termination occurs from 32 to 31.7 mcd with $\delta^{18}\text{O}$ values ranging from 4.6‰ to 2.8‰. There is a brief increase in $\delta^{18}\text{O}$ at 31.9 mcd that records *N. pachyderma* (*s*) values of 3.7‰. MIC 5e at Site 1305 shows low amplitude variability in the $\delta^{18}\text{O}$ record with maximum values of 2.1‰ at 29.3 mcd and a long-term decrease to 2.8‰ at 24.9 mcd. Several spikes are seen in the $\delta^{18}\text{O}$ record at Site 1305 at 32.7 and 33.1 mcd with values approaching 3.1‰. A smaller spike at 34 mcd is also noted with $\delta^{18}\text{O}$ values of 4‰.

Mean Sortable Silt at Site 1305 is highly variable with values ranging from 14 to 26 μm (Figure 2.3). SS values increase in MIC 5e from a low of 14 μm at 31.7 mcd to a high of 26 μm at 28 mcd. From 28 to 27 mcd SS values decrease to 16 μm .

At Site 1306, *N. pachyderma* (*s*) $\delta^{18}\text{O}$ values range from highs of 4.7‰ to interglacial lows of 2.1‰ (Figure 2.3). Like Site 1305, Site 1306 records 3 excursions in the $\delta^{18}\text{O}$ record in MIC 6 and Termination 2 at 21.8, 22.3 and 22.6 mcd. Termination 2 at Site

1306 is expanded compared to Site 1305 occurring between 21.5 and 22 mcd while MIC 5e is compressed (relative to Site 1305) at Site 1306 occurring across 21 to 21.6 mcd. Site 1306 SS varies about a mean of 22 μm (Figure 2.3). The SS record shows low amplitude changes throughout MIC 6 and 5e, however, there are no long-term trends in the data.

Termination 1 vs Termination 2

Deepwater response across Terminations 1 and 2 share some similarities in the SS data. For example, SS values show long-term increases from 15 to 10 kyr at Site 1305 and 21GGC while a similar long-term increase is observed from 128 to 123 kyr at Site 1305 (Figure 2.4). The amplitude of SS variability across Terminations 1 and 2 are similar and both records show periods of increased and decreased flow.

Discussion

Insolation across Terminations 1 and 2

The total solar radiation received at 65°N is considered to be a driving force for the late Pleistocene glacial-interglacial cycles (e.g., Imbrie & Kipp 1971; Berger, 1978).

Insolation changes across Terminations 1 and 2 are similar, in general (Figure 2.4)

However, peak solar forcing at 65°N was $\sim 12 \text{ watts/m}^2$ higher during Termination 2 than in Termination 1 (Laskar et al., 2004). While relatively small (2.5% higher), the increased energy budget of the North Atlantic across Termination 2 was more destructive to continental ice sheets compared to Termination 1, which was manifested in a higher rate of ice sheet melting as well as the total ice melted.

The rate and magnitude of sea level change across Termination 1 is well constrained by drilled and uplifted corals (e.g., Fairbanks, 1989). Across Termination 1, the rate of sea level rise was generally constrained to 0.5 to 1 cm/kyr. This long-term trend is overlain by two rapid increases of sea level, Melt Water Pulse 1a and 1b, suggesting either massive iceberg discharge or the rapid release of freshwater from a continental source. The largest sea level jump, MWP 1a, occurred between 14.17 and 13.68 ka with sea levels rising 20 m at a rate of 3.2 ± 1 cm/kyr (Fairbanks, 1989; Stanford et al., 2006). MWP 1b occurred between ~ 11.5 -10.5 ka with sea levels rising ~ 5 m yielding a rate of ~ 2.5 cm/kyr (Stanford et al., 2006). Paradoxically, these large freshwater events seem to have little to no influence on North Atlantic circulation suggesting: 1) a large portion of these melt waters was derived from Antarctica, or 2) the continental melt water was injected into the North Atlantic in locations distal to the deepwater formation sites (for example, MWP 1a may have flowed into the Gulf of Mexico or the Arctic Ocean).

As noted above, our temporal constraints for Termination 2 rely on Milankovitch theory and assumption of relatively constant sedimentation rates within a specific location. However, it may be assumed that the changes in sedimentation rates across different terminations may be similar at one location. One expression of the rate of deglaciation is to compare benthic and planktonic $\delta^{18}\text{O}$ signatures across the terminations. Both records incorporate the $\delta^{18}\text{O}$ water decrease as the ice sheets melt. However, the surface waters will record the additional warming related to the high insolation forcing associated with the terminations. At ODP Site 983, there is only 0.3 m (~ 130 ka) where surface $\delta^{18}\text{O}$

becomes detached from benthic $\delta^{18}\text{O}$ across Termination 2 indicating that continental ice rapidly retreated as temperatures in the North Atlantic rose (Figure 2.5). In contrast, the deglacial offset between the surface and deep records is more expanded (0.84 m), providing a strong indication that the duration of Termination 1 was longer than for Termination 2. Thus, continental ice melting lagged the warmer temperatures much more so than during Termination 2. This lag allows for the creation of large-scale glacial lakes and, therefore, may explain why Termination 1 was punctuated by several climatic events while Termination 2 was not.

The magnitude of sea level rise across the terminations apparently differed. While MIC2 sea level is well constrained to be 120 m below the present level (Fairbanks, 1989), MIC6 is not known based on coral data. Benthic foraminiferal $\delta^{18}\text{O}$ values throughout the deep oceans yield similar values for MIC2 and 6, indicating similar ice volumes and deepwater temperatures for the two most recent glacial periods (e.g., Liseicki and Raymo, 2005). Uplifted coral terraces as well as siliciclastic shorelines indicate that sea level during MIC5e stood 5 meters higher than at present (e.g., Chen et al., 1991; Stirling et al., 1995; El-Asmar, 1997; Hearty et al., 2007a,b; Rohling et al., 2007). This extra 5 m of sea level rise is postulated to come from Greenland, West Antarctica, or a combination of both (e.g., Rohling et al., 2007).

The planktonic $\delta^{18}\text{O}$ records from Eirik Drift indicate that the surface response to Termination 2 was greater than in Termination 1. The $\Delta\delta^{18}\text{O}$ across Termination 2 is 2.5‰, in contrast to a 2.2‰ change across Termination 1, leaving a residual $\sim 0.3\text{‰}$ to

explain. The ice volume influence can only account of 0.05‰ of the difference. Thus, the remaining 0.25‰ reflects slightly warmer or fresher conditions during MIC5e relative to MIC 1.

Comparison of deepwater flow on Eirik Drift over Terminations 1 and 2 suggests that the resumption of interglacial flow conditions across each Termination is unique. The last deglaciation occurred roughly from 19 to 8 kyr BP. During this time SS values suggest that deepwater flow across the termination was highly variable. For example, at Site 1305/21GGC, deep-ocean circulation was curtailed in a two-step Younger Dryas before reaching Holocene flow intensities at ~11.5 kyr BP. Circulation was then briefly altered across the 8.2 kyr event; however this event is shorter than the previous YD interval. Interestingly, our gNAIW monitoring location, Site 1306, shows little variability in the deepwater system across the entire termination. This is perplexing because Site 1306 is well-suited to monitor circulation changes driven by H-events, however, there is no manifestation of H1 in our data. This discrepancy may be explained by low sedimentation rates at 1306 during H1 and is supported by Pa/Th data from McManus et al. (2004) who show that North Atlantic overturning collapsed across the H1 event.

Deepwater response across Termination 2 shows a very different transition from gNAIW to a NADW-like water mass. A singular climate reversal, Heinrich Event 11, occurs across Termination 2 at ~132 kyr; however, this event is only manifested in eastern shallow North Atlantic deepwater records (Carlson, 2008). At Sites 1306 and 1305 there is evidence for surface freshening in conjunction with H11 and increased flow velocities

at Site 1306 may indicate deep current shoaling. Across the termination into MIC 5e, Site 1306 becomes winnowed making SS interpretations unreliable (McCave, 1995). However, Site 1305 contains an expanded 5e section which shows a very expanded section comparable to establishment of an interglacial flow regime analogous to the Holocene.

Circulation MIC 5e vs. MIC 1

deVernal and Hillaire-Marcel (2008) show that a large portion of Greenland deglaciated during MIC 5e. Pollen increases in cores on and proximal to Eirik Drift beginning at 128 ka, reaching a maximum in pollen flux to the oceans between ~125 and 123 ka, suggesting during the prior 5 to 7 kyr, Greenland melt water must have discharged into the North Atlantic. The smaller ice sheet would produce warmer SSTs proximal to Greenland while the excess freshwater flux to the Greenland Sea to the east, Irminger Sea to the southeast, and Labrador Sea to the west would lower salinities and surface water $\delta^{18}\text{O}_{\text{water}}$ values regionally. This scenario is consistent with our measured planktonic foraminiferal values.

If the case stated above is correct, Greenland ice melt could have played a large role in the suppression of NCW across MIC 5e because: 1) the Laurentide and Fennoscandinavian ice sheets melted quickly; and 2) sea level was ~5 m higher in MIC 5e relative to today. This melt water suppressed true interglacial flow or made the deep waters more buoyant throughout MIC 5e and may provide insight as to how North Atlantic overturning will respond to increased Greenland ice melt due to global warming.

Higher insolation across Termination 2 may have also delayed the establishment of a deeply penetrating, NADW-like water mass throughout much MIC 5e. The SS proxy at Site 1305 takes approximately 7 kyr after the onset of full interglacial temperature to establish a maximum flow velocity at ~123 ka. This is a large departure from the 1.5 kyr lag in establishment of NADW at ~8ka seen across the Holocene. I suggest that Termination 1 differs when compared to Termination 2 and that the interglacial conditions seen across the Bolling/Allerod is the “true” onset of the Holocene that is reset to glacial conditions because of slower continental ice melt due to lower insolation forcing during this time. Therefore, the continental ice imbalance seen across Termination 1 overprinted the earliest part of the interglacial by sending freshwater into the North Atlantic thus causing the Younger Dryas.

Conclusions

Termination 1 is often thought to be a good analog for prior glacial/interglacial transitions; however, Termination 1 was punctuated by 3 climatic events vs 1 event across Termination 2. Higher insolation across Termination 2, is proposed to explain the different deglacial signatures forcing the rapid melt of Northern Hemisphere continental ice sheets, limiting continental freshwater storage. Conversely, lower insolation values across Termination 1 allow glacial ice to remain in large quantities in spite of warmer temperatures and store large volumes of freshwater on the continents. Therefore, Termination 1 is a unique climatic period and this period is particularly susceptible to abrupt climatic change.

Comparison of deepwater establishment during the last two interglacials also yields differing results. MIC 5e was warmer than the Holocene, and, therefore NCW circulation should have been enhanced. We find that NCW production is suppressed for ~ 7 kyr after the onset of MIC 5e temperatures contrary to what one may expect. A recent study by deVernal and Hillaire-Marcel (2008) shows that a large portion of Greenland deglaciated, from approximately 128 to 123 ka, concurrent with NCW suppression. We speculate that increased freshwater flux from Greenland is responsible for diminishing NCW production during a period of time in which flow should be vigorous.

Figure Captions

Figure 2.1

Basemap showing the locations of Sites 1306 (2270 m) and 1305/21GGC (3441 m) on the Eirik Drift. Using both the shallow and deep sites on the drift allows for the reconstruction of gross changes in NCW buoyancy as sedimentation rates change between the shallow and deep sites. ODP Site 983 on the Gardar Drift is also identified and is the location used to determine ice volume melt between Termination 1 and Termination 2.

Figure 2.2

SS (red) and $\delta^{18}\text{O}$ (blue) records generated at Sites 1306 (top, 1.5 mcd) and 1305/21GGC (bottom, 15 mcd). Site 1306 shows winnowing throughout the Holocene while Site 1305/21GGC is expanded indicating NCW is located deep on Eirik Drift. Likewise, across the last glacial maximum, Site 1306 shows a higher fidelity than Site 1305/21GGC indicating the current is in a gNAIW state.

Figure 2.3

SS (red) and $\delta^{18}\text{O}$ (blue) records generated from 110 to 140 kyr at Sites 1305 and 1306. Across termination 2 we see a $\delta^{18}\text{O}$ spike at ~133 kyr which is interpreted as surface freshening due to H11. Interestingly, at Site 1306, we find SS values increasing across H11 which may indicate shoaling of NCW. Site 1305 is expanded throughout MIC 5e indicating a less buoyant NCW however, SS shows an ~7 kyr lag in maximum flow velocity from the onset of interglacial temperatures interpreted as true interglacial flow suppression.

Figure 2.4

Comparison of Termination 1 and 2 surface and deep-ocean records through 20 kyr windows. Deep-ocean establishment occurs quite differently across the two terminations. After Termination 1, SS measurements indicate deepwater flow is quite robust over the deep coring sites on Eirik Drift. However, across Termination 2 deepwater velocities are reduced throughout much of MIC 5e, potentially because of Greenland ice melt (deVernal and Hillaire-Marcel 2008). SS (red), $\delta^{18}\text{O}$ (blue), insolation (green).

Figure 2.5

Changes in surface (red) and benthic (blue) oxygen isotopes across Terminations 1 and 2 from Site 983 on the Gardar Drift. Across Termination 1 there is a divergence of 0.84 m suggesting that continental glaciers resisted melting in spite of warmer North Atlantic temperatures. Across Termination 2 we find a much smaller divergence of 0.3 m suggesting continental ice melted quickly, probably due to higher insolation forcing during this time.

Figure 2.1

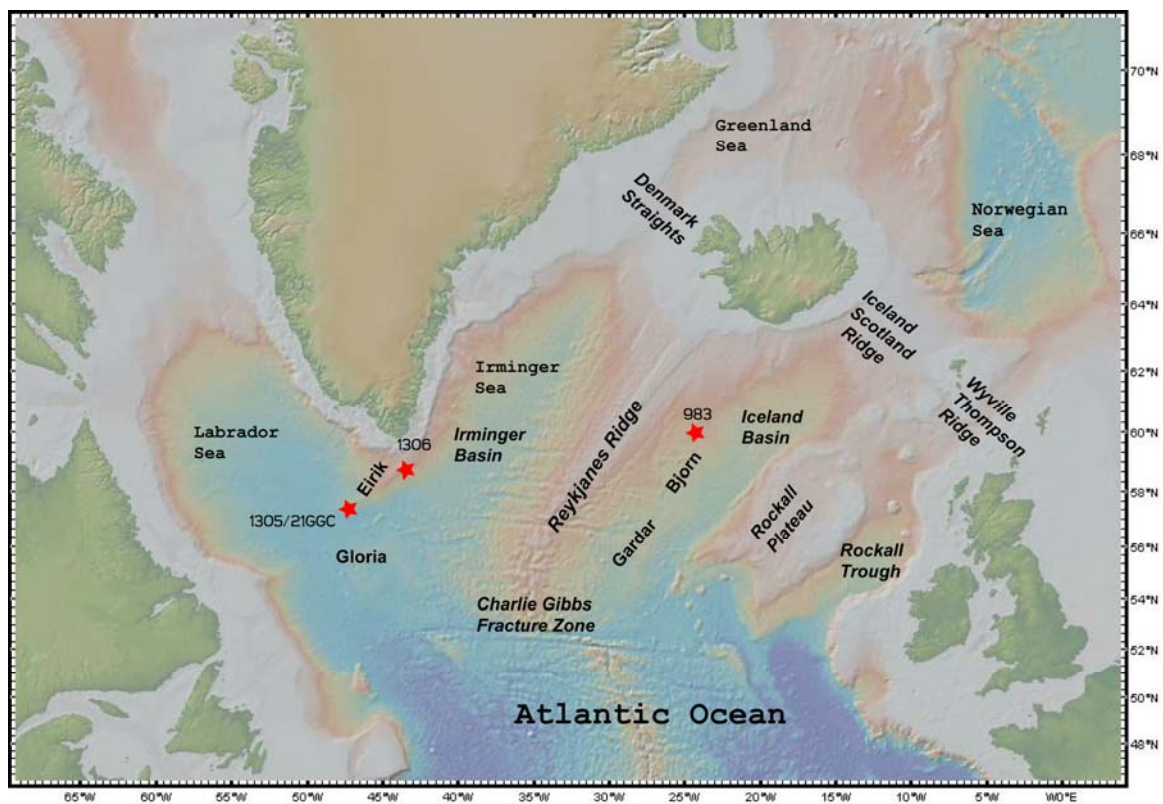
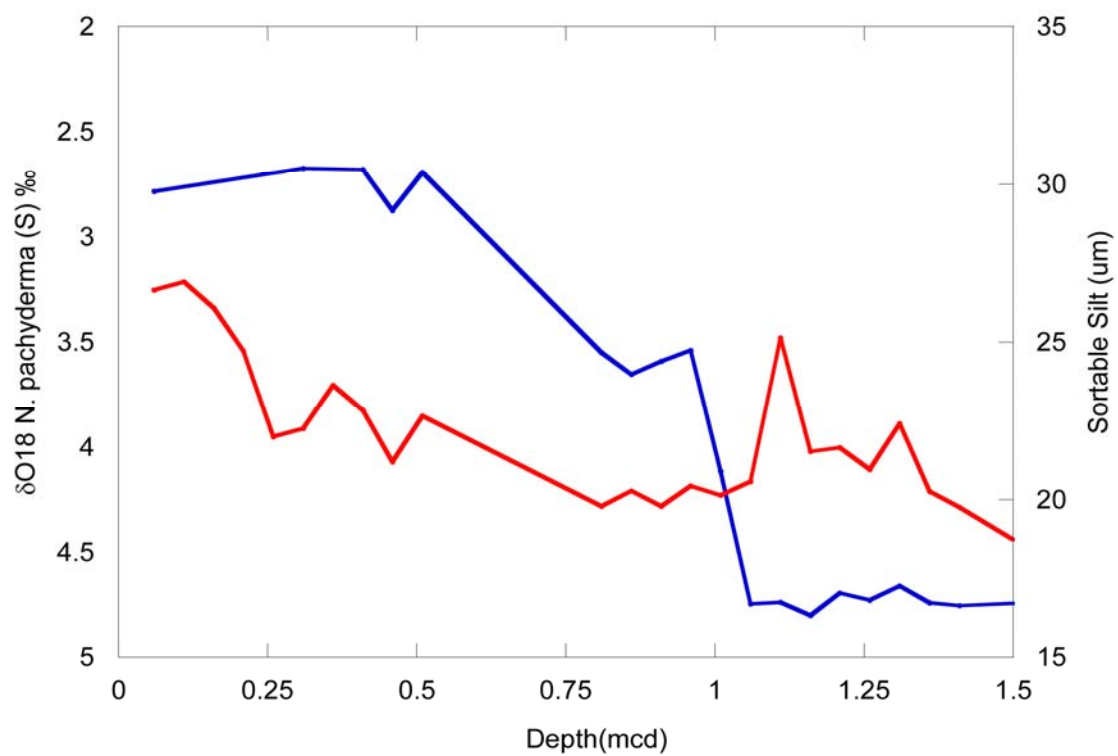


Figure 2.2

Termination 1 and Holocene
Site 1306



Termination 1 and Holocene
Site 1305/21GGC

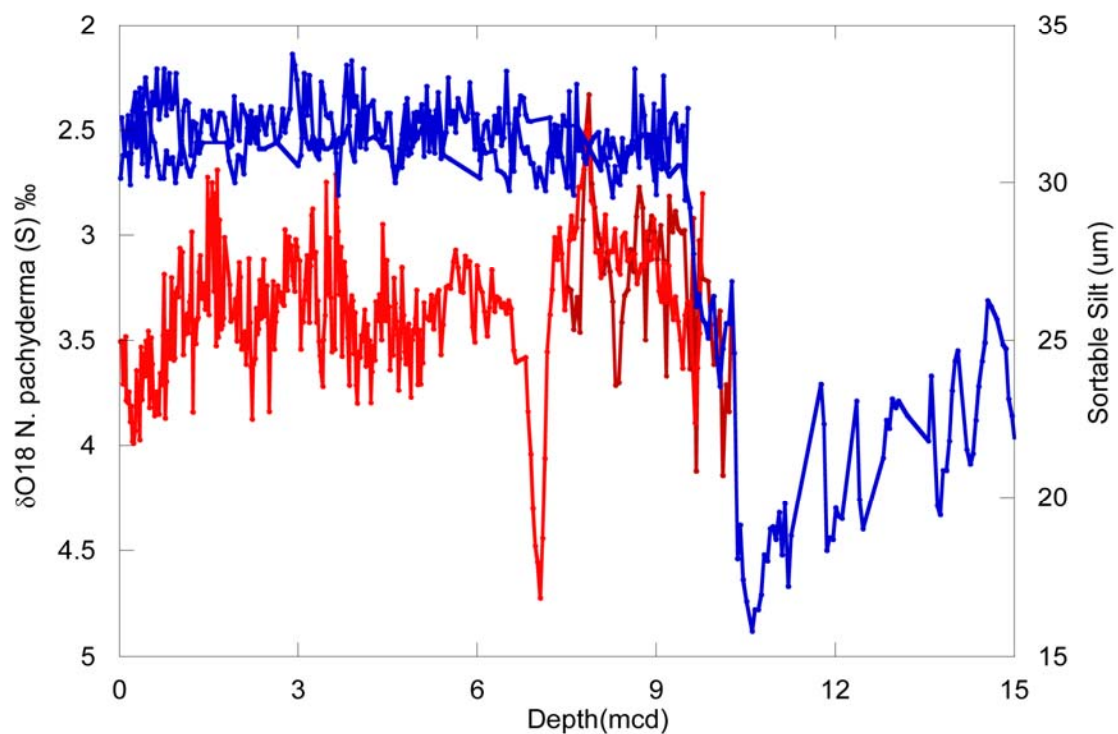
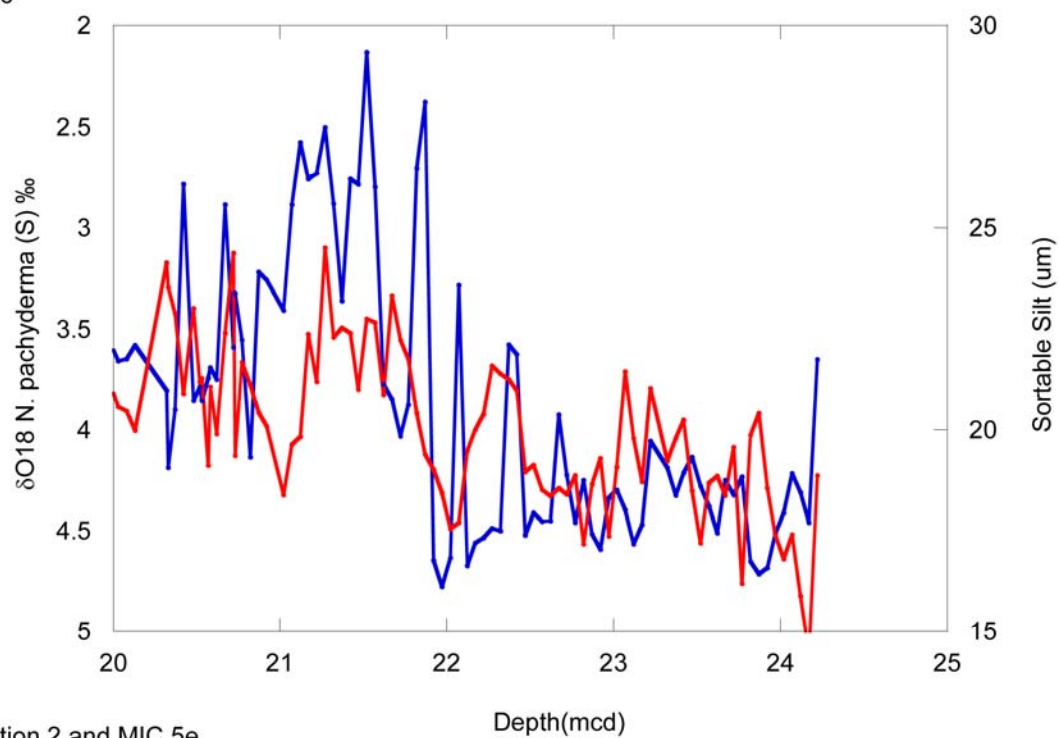


Figure 2.3

Termination 2 and MIC 5e
Site 1306



Termination 2 and MIC 5e
Site 1305

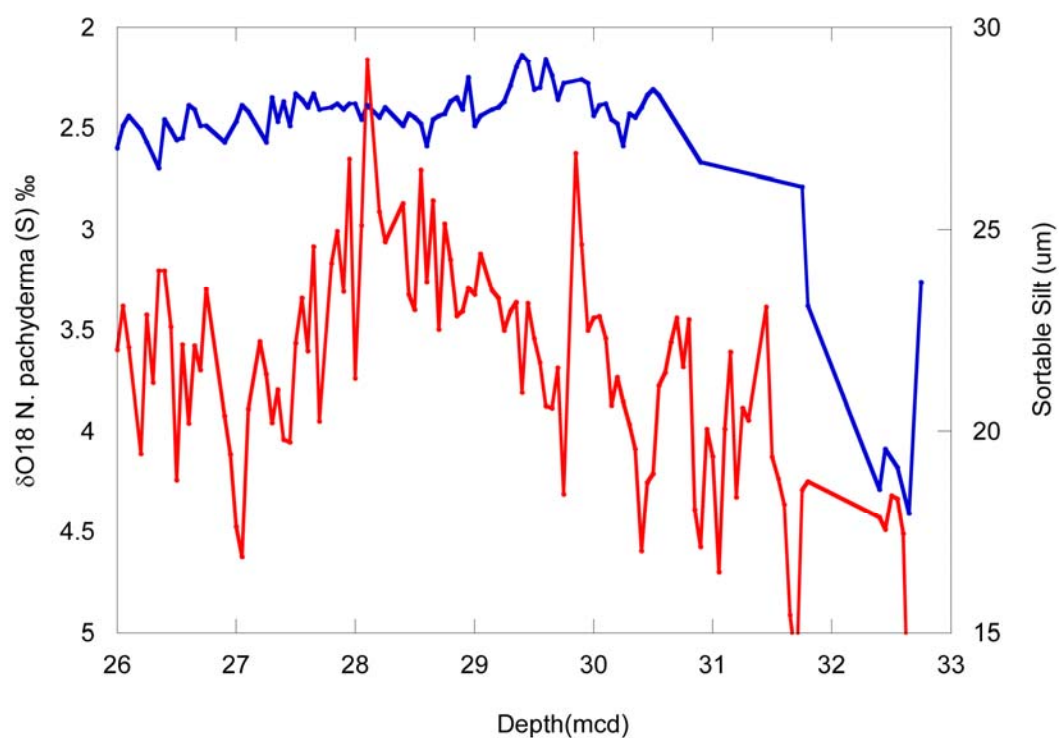
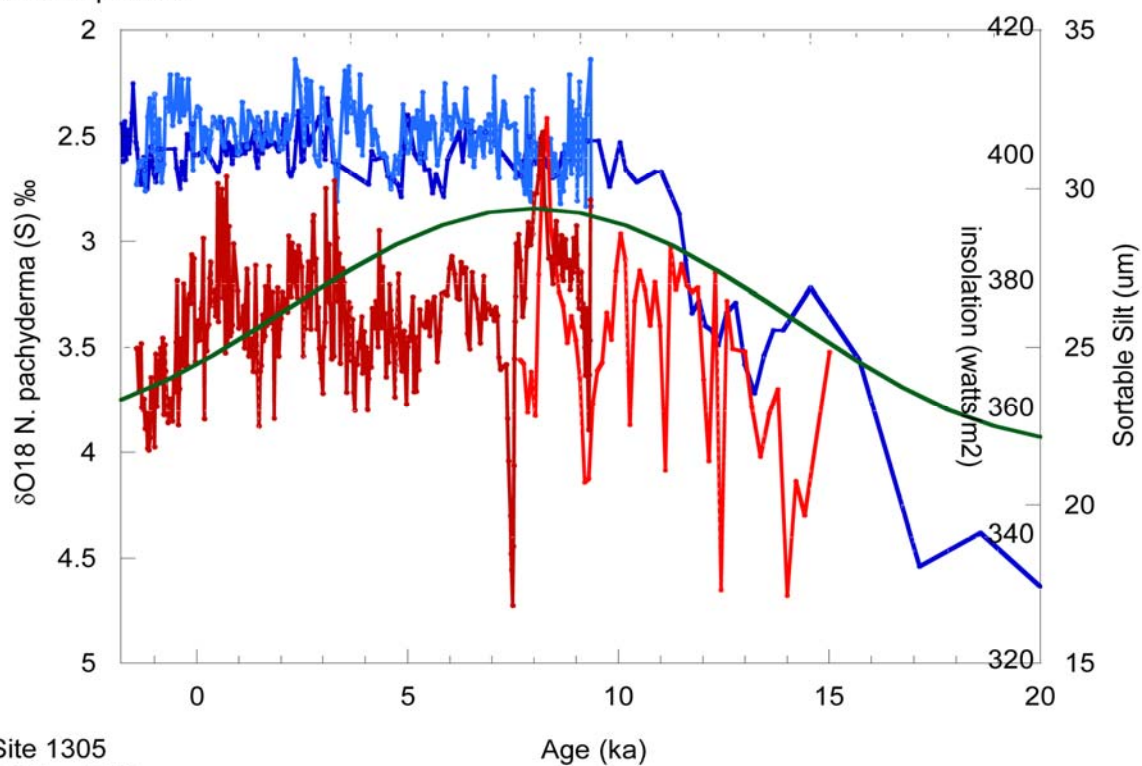
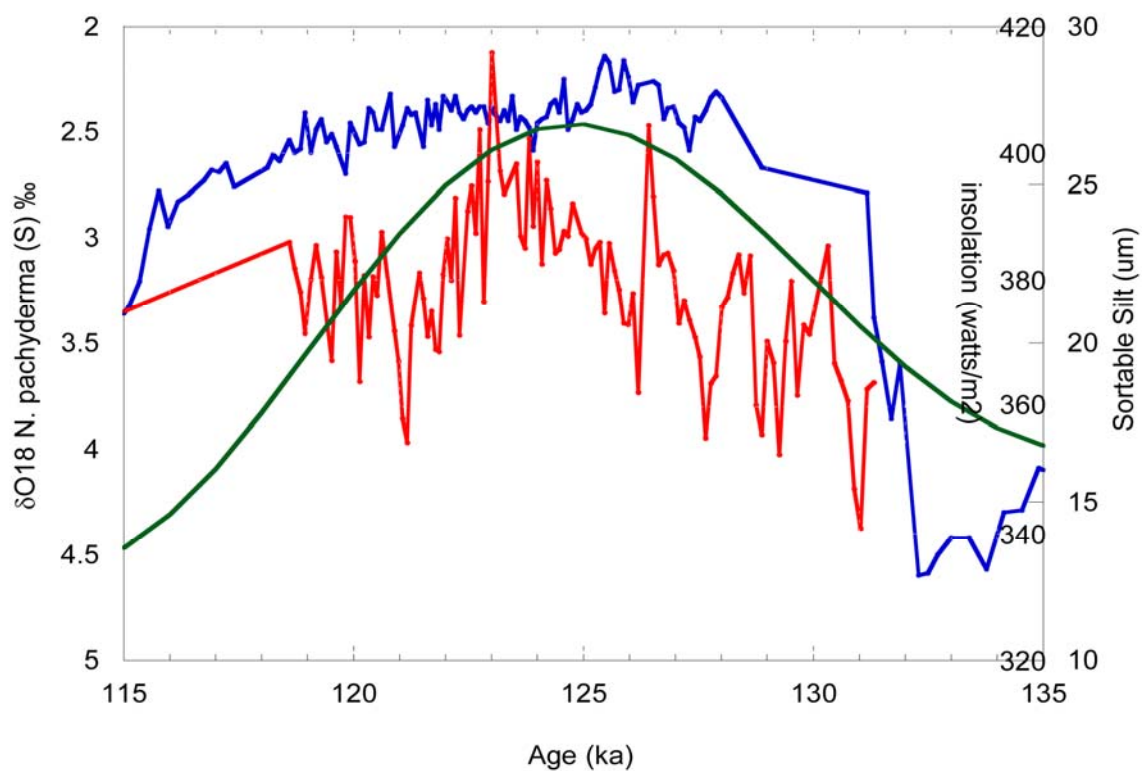


Figure 2.4

Site 1305/21GGC
20 ka to present



Site 1305
115 to 135 ka



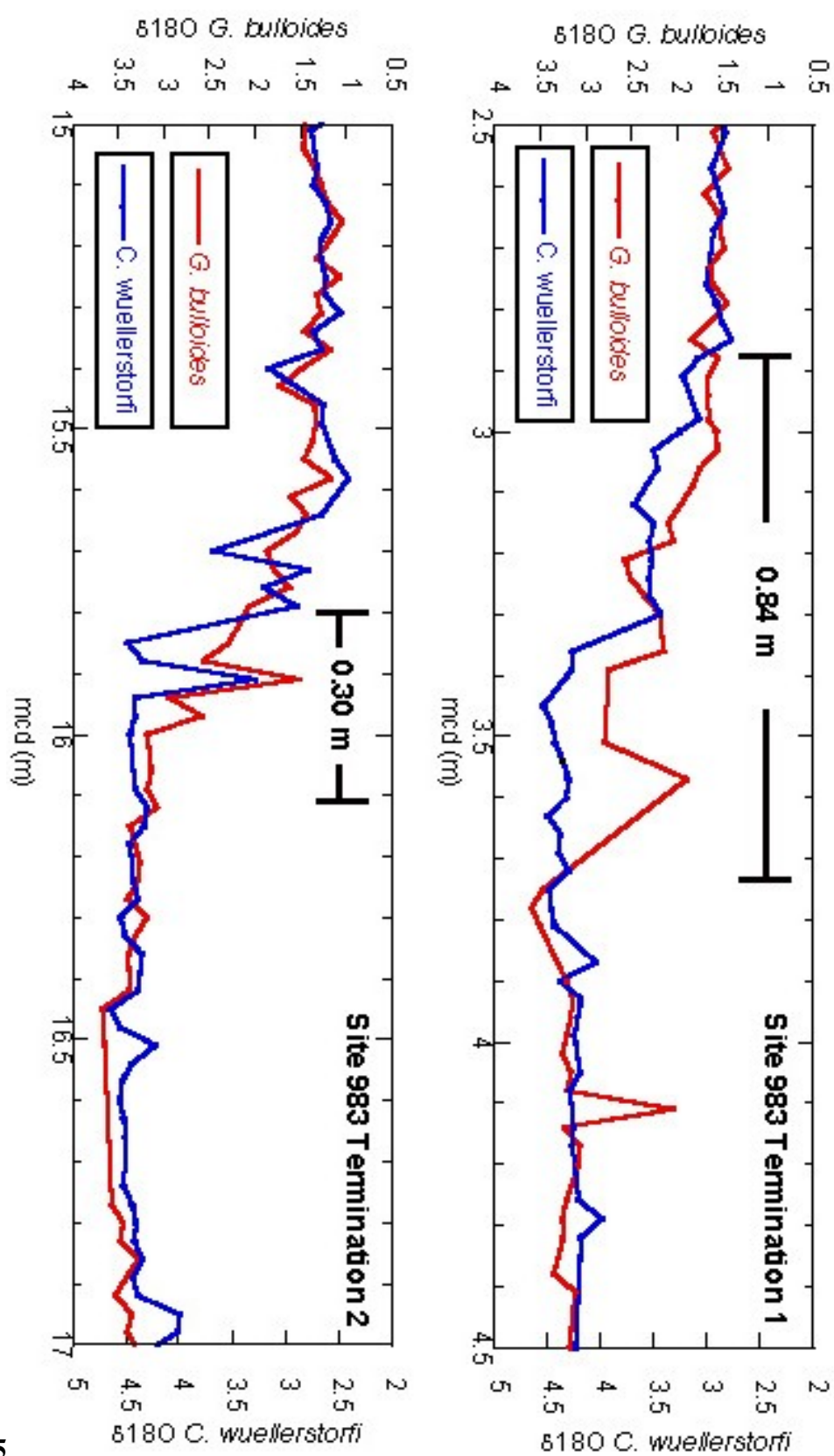


Figure 2.5

References

- Barber, D.C. et al., 1999. Forcing of the cold event of 8,200 years ago by catastrophic drainage of Laurentide lakes. *Nature*, 400(6742): 344-348.
- Berger A., 1978. Long-term variations of daily insolation and Quaternary climatic changes. *J. Atmos. Sc.*, 35(12), 2362-2367.
- Bianchi, G.G., and McCave, N., (1999). Holocene periodicity in North Atlantic climate and deep-ocean flow south of Iceland. *Nature*, 397: 515-517.
- Bianchi, G.G., Vautravers, M. and Shackleton, N.J., 2001. Deep flow variability under apparently stable North Atlantic Deepwater production during the last interglacial of the subtropical NW Atlantic. *Paleoceanography*, 16(3): 306-316.
- Boyle, E.A. and Keigwin, L., 1987. North-Atlantic thermohaline circulation during the past 20,000 years linked to high-latitude surface-temperature. *Nature*, 330(6143): 35-40.
- Broecker, W.S. and van Donk, J. (1970). Insolation changes, ice volumes, and the O18 record in deep-sea cores. *Reviews of Geophysics and Space Physics* 8, pp. 169–198
- Broecker, W.S., 1994. Massive iceberg discharges as triggers for global climate change. *Nature*, 372(6505): 421-424.
- Carlson, A.E., 2008. Why there was not a Younger Dryas-like event during the Penultimate Deglaciation. *Quaternary Science Reviews*, 27(9-10): 882-887.
- Chen, J. H., Curran, H. A., White, R. & Wasserburg, G. J. 1991. Precise chronology of the last interglacial period: 234U–230Th data from fossil coral reefs in the Bahamas. *Geol. Soc. Am. Bull.* 103, 82–97.
- Curry, W.B., Duplessy, J.C., Labeyrie, L. D., and Shackleton, N. J., 1988. Changes in the distribution of $\delta^{13}\text{C}$ of deepwater eCO_2 between the last glaciation and the Holocene. *Paleoceanography*, 3(3): 317-341.
- deVernal, A., and Hillaire-Marcel, C. 2008. Natural variability of Greenland climate, vegetation, and ice volume during the past million years. *Science*. 320(5883): 1622-1625.
- deVernal, A., Hillaire-Marcel, C., Turon, J.L. and Matthiessen, J., 2000. Reconstruction of sea- surface temperature, salinity, and sea-ice cover in the northern North Atlantic during the last glacial maximum based on dinocyst assemblages. *Canadian Journal of Earth Sciences*, 37(5): 725-750.
- Duplessy, J. C., Shackleton, N. J., Fairbanks R. G., Labeyrie, L., Oppo D., and Kallel, N., 1988. Deepwater source variations during the last climatic cycle and their impact on the

global deepwater circulation. *Paleoceanography*, 3(3): 343-360.

El-Asmar, H. M. 1997. Quaternary isotope stratigraphy and paleoclimate of coral reef terraces, Gulf of Aqaba, South Sinai, Egypt. *Quat. Sci. Rev.* 16, 911–924.

Fagel, N. et al., 2004. Nd and Pb isotope signatures of the clay-size fraction of Labrador Sea sediments during the Holocene: Implications for the inception of the modern deep circulation pattern. *Paleoceanography*, 19(3): 16.

Fagel, N., Hillaire-Marcel, C. and Robert, C., 1997. Changes in the Western Boundary Undercurrent outflow since the Last Glacial Maximum, from smectite/illite ratios in deep Labrador Sea sediments. *Paleoceanography*, 12(1): 79-96.

Fairbanks, R.G., 1989. A 17,000-year glacio-eustatic sea-level record – Influence of glacial melting rates on the Younger Dryas Event and deep-ocean circulation. *Nature*, 342(6250): 637-642.

Hays, J. D., John Imbrie, and N. J. Shackleton (1976). Variations in the Earth's Orbit: Pacemaker of the Ice Ages. *Science* 194 (4270): 1121 – 1132

Hearty, P.J., Hollin, J.T., Neumann, A.C., O'Leary, M.J. and McCulloch, M., 2007a. Global sea-level fluctuations during the Last Interglaciation (MIS 5e). *Quaternary Science Reviews*, 26(17-18): 2090-2112.

Hearty, P.J., Neumann, A.C. and O'Leary, M.J., 2007b. Comment on "Record of MIS 5 sea-level highstands based on U/Th dated coral terraces of Haiti" by Dumas et al. [Quaternary International 2006 106-118]. *Quaternary International*, 162: 205-208.

Hillaire-Marcel, C., de Vernal, A., Bilodeau, G., Wu, G., (1994). Isotope Stratigraphy, sedimentation rates and paleoceanographic changes in the Labrador Sea. *Canadian Journal of Earth Sciences* 31, 63:89.

Hillaire-Marcel, C. and Bilodeau, G., 2000. Instabilities in the Labrador Sea water mass structure during the last climatic cycle. *Canadian Journal of Earth Sciences*, 37(5): 795-809.

Innocent C., Fagel N., and Hillaire-Marcel C. (2000) Sm-Nd isotope systematics in deep-sea sediments: Clay size versus coarser fractions. *Mar. Geol.* **168**, 79–87.

Imbrie, J., Kipp, N.G., 1971. A new micropaleontological method for quantitative paleoclimatology. Application to a late Pleistocene Caribbean core. In: Turekian, K.K. (Ed.), *The Late Cenozoic glacial ages*. Yale Univ. Press, New Haven, pp. 71–131.

Kleiven, H.F. et al., 2008. Reduced North Atlantic Deepwater coeval with the glacial Lake Agassiz freshwater outburst. *Science*, 319(5859): 60-64.

- Laskar, J. et al. A long-term numerical solution for the insolation quantities of the Earth. *Astron. Astrophys.* 428, 261–285 (2004).
- Lisiecki, L.E. and Raymo, M.E., 2005. A Pliocene-Pleistocene stack of 57 globally distributed benthic delta O-18 records (vol 20, art no PA1003, 2005). *Paleoceanography*, 20(2).
- Manabe, S., and Stouffer, R.J. (1988). Two Stable Equilibria of a Coupled Ocean-Atmosphere Model: *Journal of Climate*. 1(9), p. 841-866.
- Manabe, S. and Stouffer, R.J., 2000. Study of abrupt climate change by a coupled ocean-atmosphere model, pp. 285-299.
- McCave, I.N., Manighetti, B. and Robinson, S.G., 1995. Sortable silt and fine sediment size composition slicing – Parameters for paleocurrent speed and *Paleoceanography*. *Paleoceanography*, 10(3): 593-610.
- McManus, J.F., Francois, R., Gherardi, J.M., Keigwin, L.D. and Brown-Leger, S., 2004. Collapse and rapid resumption of Atlantic meridional circulation linked to deglacial climate changes. *Nature*, 428: 834-837.
- Oppo, D.W., Keigwin, L.D., McManus, J.F. and Cullen, J.L., 2001. Persistent suborbital climate variability in marine isotope stage 5 and Termination II. *Paleoceanography*, 16(3): 280-292.
- Oppo, D.W. and Lehman, S.J., 1993. Mid-depth circulation of the subpolar North-Atlantic during the last glacial maximum. *Science*, 259(5098): 1148-1152.
- Oppo, D.W. and Lehman, S.J., 1995. Suborbital timescale variability of North-Atlantic deepwater during the past 200,000 years. *Paleoceanography*, 10(5): 901-910.
- Oppo, D.W., McManus, J.F. and Cullen, J.L., 2006. Evolution and demise of the Last Interglacial warmth in the subpolar North Atlantic. *Quaternary Science Reviews*, 25(23-24): 3268-3277.
- Rasmussen, T.L., Oppo, D.W., Thomsen, E. and Lehman, S.J., 2003. Deep sea records from the southeast Labrador Sea: Ocean circulation changes and ice-rafting events during the last 160,000 years. *Paleoceanography*, 18(1).
- Rohling, E.J., Grant, K., Hemleben, CH., Siddal, M., Hoogakker, B.A.A., Bolshaw, M., and Kucera, M. 2007. High rates of sea-level rise during the last interglacial period. *Nature Geoscience*. 1 38-42.
- Solignac, S., de Vernal, A. and Hillaire-Marcel, C., 2004. Holocene sea-surface conditions in the North Atlantic - contrasted trends and regimes in the western and

eastern sectors (Labrador Sea vs. Iceland Basin). *Quaternary Science Reviews*, 23(3-4): 319-334.

Stirling, C. H., Esat, T. M., McCulloch, M. T. & Lambeck, K. 1995. High-precision U-series dating of corals from Western Australia and implications for the timing and duration of the Last Interglacial. *Earth Planet. Sci. Lett.* 135, 115–130.

Stanford, J.D. et al., 2006. Timing of meltwater pulse 1a and climate responses to meltwater injections. *Paleoceanography*, 21(4).

Stoner, J.S., Channell, J.E.T. and Hillaire-Marcel, C., 1998. A 200 ka geomagnetic chronostratigraphy for the Labrador Sea: Indirect correlation of the sediment record to SPECMAP. *Earth and Planetary Science Letters*, 159(3-4): 165-181.

Stoner, J.S., Channell, J.E.T., Hillaire-Marcel, C. and Kissel, C., 2000. Geomagnetic paleointensity and environmental record from Labrador Sea core MD95-2024: global marine sediment and ice core chronostratigraphy for the last 110 kyr. *Earth and Planetary Science Letters*, 183(1-2): 161-177.

Stoner, J.S., Channell, J.E.T. and Hillaire-Marcel, C., 1995. Late Pleistocene relative geomagnetic paleointensity from the deep Labrador-Sea—Regional and global Correlations. . *Earth and Planetary Science Letters*, 134(3-4): 237-252.

Chapter 3: Surface water forcing of deepwater flow over Milankovitch and millennial time scales: Expedition 303 Site 1306 on the Eirik Drift.

Abstract

Over the past 160 kyr, Site 1306, located at a depth of 2270 m on the Eirik Drift, has undergone preferential deposition during intermediate climate states MIC 3 through MIC 5d. Here, I reconstruct a high-resolution $\delta^{18}\text{O}$ record from surface dwelling foraminifera *N. pachyderma* (*s*) and use mean sortable silt (SS) as a proxy of deep-ocean circulation to better understand how surface conditions are propagated to the deep ocean. At Site 1306, the $\delta^{18}\text{O}$ and SS proxies show an inverse relationship over the 160 kyr, supporting the idea that surface North Atlantic temperatures and salinities control NCW production rates. However, during the past 40 ka we find several periods, concurrent with Heinrich Events, where surface-ocean freshening over Eirik Drift is correlated to reductions in deepwater flow. I postulate that general ice sheet dynamics (size/melting rates) or resulting direction of melt-water flow have fundamentally changed causing the interval from 40 to 10 ka to be more susceptible to freshwater forcing.

Introduction

Some scenarios of global warming propose that continued warming may lead to partial collapse of the Greenland and Antarctic ice sheets. While “very unlikely” (e.g., Pfeffer et al., 2008), the presence of large masses of ice proximal to sites of deepwater formation should prompt thorough study of past ice sheet collapses and the different effects on deepwater circulation and climate change. Heinrich Events provide particularly good analogues for the consequences associated with previous ice sheet collapses because they

mark the release of large volumes of fresh water directly into the North Atlantic via freshwater pulses/iceberg armadas (Bond et al., 1992).

Several paleoceanographic and modeling studies have postulated/shown that melt water/ice rafting episodes are disrupt the North Atlantic component of thermohaline circulation (THC) causing shifts in the Earth's climate on hemispheric to global scale (e.g., Manabe and Stouffer, 1988; Broecker et al., 1989; Broecker 1994; Barber et al., 1999). North Atlantic deepwater formation was once viewed as an “on/off” system as climate oscillated between interglacial and glacial periods. However, many studies using nutrient tracers (benthic foraminiferal $\delta^{13}\text{C}$ and Cd/Ca) showed that the glacial/interglacial variations in Northern Component Water (NCW) are better characterized as buoyancy changes (Boyle and Keigwin, 1987; Curry et al., 1988; Duplessy et al., 1988), with shallow current operating during the glacial intervals and a deeper variety associated with the interglacials. More recent studies show that, while more buoyant than interglacial circulation, the flux of NCW during glacial times was reduced to no less than 60% of interglacial values (McManus et al., 2004; Lynch-Stieglitz et al., 2007). This concept is a large departure in thinking about general North Atlantic deepwater convection and may provide corollaries to impending future change due to global warming.

Heinrich Events have been the focus of many studies with the hope that the mechanism(s), timing, and global extent associated with these millennial-scale climate changes will lead to a better understanding of abrupt climate changes, including those

that may occur in the future. In the marine record, Heinrich Events appear as anomalous sedimentation events characterized by large amounts of ice-rafted detritus (IRD), approaching 100% of a collected sample, and can be deposited across a wide range of the North Atlantic north of 40°N (Heinrich 1988). While the mechanisms forcing iceberg discharge during H-events remain a matter of debate, the resulting ice armadas clearly escaped the continents and deposited IRD across large areas of the North Atlantic (e.g., Bond et al., 1992). However, several studies note that they may be associated with Dansgaard-Oeschger (D/O) cycles and may create abrupt climate changes (e.g., Bond et al., 1993).

Six well-defined Heinrich Events (H1-H6) have been identified in the last glacial interval with H1 being associated with the initial deglaciation (16.8 ka) and H6 having an age of approximately 60 ka (Bond et al., 1992; Hemming, 2004). Subsequent to Heinrich's (1988) scheme, Bond and Lotti (1995) proposed that the Younger Dryas (YD) be included as an irregular Heinrich Event and was designated as H0 (Andrews et al., 1995). The H0 Event is irregular because the YD is thought to result from increased freshwater rather than icebergs (e.g., Teller et al., 1983; Broecker, 2006); however, cores to the southeast of Hudson Straights show small increases of detrital carbonate suggesting that a small amount of ice rafting occurred (Andrews et al., 1994;1995). Several studies have examined previous glacial cycles for evidence of similar ice rafting events; however, support for this idea is limited at best. For example, studies have found the existence of Heinrich type layers in Marine Isotope Chron (MIC) 6 appear to have different provenance, sedimentation rate and magnetic susceptibility characteristics (Grousset et

al., 1993) suggesting that H1-H6 may be unique to the present glacial cycle.

The study, herein, builds on these recent findings and will use surface and deep-ocean proxies generated from a drill core located on the uppermost flanks of Eirik Drift to understand the surface hydrologic and deep-ocean changes associated during Heinrich Events. Eirik Drift has several attributes that make it a good place to study the relationships between surface water forcing and deepwater circulation during periods of rapid climate change. First, the major components of NADW comprise the deep-water mass that flows across Eirik Drift (e.g., Iceland-Scotland (ISOW) and Denmark Strait (DSOW) overflow waters). Sedimentation patterns indicate that the axis of the current was in a position such that drift sedimentation was focused on the uppermost flanks of Eirik Drift for the interval that spans the Younger Dryas to MIC 5d, accumulating at rates of >15 cm/kyr (Neitzke et al., 2007). Surface waters flowing above Eirik Drift incorporate the East Greenland and Irminger Current waters which have been shown to incorporate major hydrographic changes during H-events (Elliot et al., 1998). Furthermore, this region may contribute, via deepwater convection, a significant portion of Labrador Intermediate Water (LIW) and modern NADW (Pickart et al., 2003). Site 1306 on the Eirik Drift (this study) is, therefore, well located to examine the teleconnection between changes in surface water hydrography and the response of deep-ocean circulation below (Figure 2.1).

Identification and Provenance of H events

Heinrich Events have been identified by several lithologic and geochemical methods and

each event is thought to be caused by a similar mechanism. The H1, H2, H4, and H5 Events are all thought to have a Hudson Bay source and are characterized by high volumes of IRD relative to the bulk sample (Hemming, 2004). High lithic counts derived from IRD impart high values in MS relative to typical low MS and lithic counts found in open ocean sediments. Furthermore, these events are marked by increases in detrital carbonate, of which the largest source for this material is massive carbonate layers throughout the Hudson Bay. Similarly, several geochemical systems (Sm-ND, Pb for example) suggest that the IRD deposited in these layers is derived from an Archean source again pointing to a North American origin (see Hemming, 2004 for a review).

Heinrich 3 and 6 are manifested somewhat differently than H1, H2, H4, and H5. Within the IRD belt, the H3 and H6 layers contain much less %IRD and smaller MS spikes when compared to the “typical” H events noted above. The provenance of H3 and H6 also seems to deviate from the typical H event pattern. Lead isotopic analysis on IRD from these layers suggests that H3 and H6 were sourced in part from Europe (Grousset et al., 1993). However, data from Orphan Knoll shows H3 was partially sourced from the Hudson Bay, although this material was not transported as far east as a typical H event (Grousset et al., 1993; Bond and Lotti, 1995).

Methods

Approximately 20 cc of sediment was collected at 5 cm intervals down-core, following the spliced core record, from Expedition 303, Site 1306. Upon their arrival at Rutgers University, the original 20 cm³ samples were sub-sampled with 3 cm³ splits used for

grainsize analysis. The remaining 17 cm³ of sediment was washed in a 63µm sieve and dried. The dried samples were weighed allowing for calculation of percent coarse fraction (%CF), and were used for stable isotopic analysis. *N. pachyderma* (s) dominated the foraminiferal assemblage and was picked for isotopic analysis in the 150-212 µm size fraction.

Stable isotopic values ($\delta^{13}\text{C}$ and $\delta^{18}\text{O}$) were measured on a Micromass Optima mass spectrometer with Multiprep peripheral for the automated analysis of carbonate samples at Rutgers University. For each analysis, 8-12 individual foraminifera were picked from each sample. The samples were run in groups of 32 with an accompanying eight standards. Data are reported versus V-PDB through the analysis of an in-house standard which has been calibrated to NBS-19 (J.D. Wright, unpublished). This standard was routinely run against NBS-19 to ensure its accuracy; 1-sigma errors are 0.05‰ and 0.08‰ for $\delta^{13}\text{C}$ and $\delta^{18}\text{O}$, respectively.

Three cm³ samples of raw sediment were treated with a series of acetic acid and sodium hydroxide treatments to remove any biogenic carbonate and biogenic silica, respectively (McCave et al., 1995). By rinsing and drying the samples between each procedure, we were able to calculate % biogenic CaCO₃ and % biogenic SiO₂. Mean sortable silt measurements were conducted at Middlebury College on a Horiba LA-920. This machine uses a Helium-Neon Laser and a Tungsten lamp for calculating grainsize measurements between 0.02 and 2000 microns with a precision of 1% per measurement (P. Manley, unpublished). The samples were pre-soaked in a 3% sodium metaphosphate

solution, stirred, and placed in a sonic bath for 4 minutes in order to deflocculate all silt and clay particles prior to analysis. After the samples were adequately agitated they were placed into the Horiba auto sampler, with thirty samples comprising a run. Each sample was re-stirred by the Horiba autosampler and a small sub sample was taken for measurement. Upon entering the machine the sample was subjected to a sonic bath to ensure deflocculation of all particles while the measurement was performed. Several duplicate samples were run twice to ensure the preparation process was standardized and that the results were reproducible. Results are shown in Figure 3.2 and are archived in Appendix C.

The age model for this study was constructed using AMS ^{14}C dating and oxygen isotope stratigraphy (Figure 3.3; Table 1). Six to 10 mg of *N. pachyderma* (s) tests, the dominant taxa in all samples from Site 1306, were picked for AMS ^{14}C dating from five depths in the top 6 mcd (meter composite depth, depth model generated from splicing holes 1306A-1306D together). Samples were cleaned ultra-sonically in distilled water and sent to the Keck Carbon Cycle Accelerator Mass Spectrometry Laboratory at UC Irvine where ^{14}C ages were determined. To convert the ^{14}C ages to calendar years, the standard 400-year reservoir effect was applied to all ^{14}C ages prior to using the Fairbanks 08805 marine radiocarbon calibration program (Fairbanks et al., 2005). An additional age constraint is provided by the identification of the LaChamp excursion at 7.07 mcd in the Expedition 303 shipboard paleomagnetic records.

Age Model

Oxygen isotope stratigraphy is based on correlating a downcore $\delta^{18}\text{O}$ record to a target $\delta^{18}\text{O}$ curve. Most $\delta^{18}\text{O}$ target curves are derived by stacking benthic foraminiferal $\delta^{18}\text{O}$ records (e.g., Martinson et al., 1985; Shackleton et al., 1993). The choice of benthic foraminifera and stacking procedure are used to minimize local effects and retain the global signature common in all records. In this study, the stacked record of Lisiecki and Raymo (2005) is used as the target curve. Benthic foraminifera are rare at Site 1306 sediments, hindering the generation of a downcore benthic foraminiferal $\delta^{18}\text{O}$ record. Instead, a planktonic foraminiferal $\delta^{18}\text{O}$ record based on *N. pachyderma* (s) was generated (Figures 3.2, 3.3). Glacial terminations 1 and 2 are identified at 1.0 and 21.75 mcd, respectively. The MIC 5/4 boundary is also identifiable and placed at 10.6 mcd. The high amplitude, high frequency found throughout the *N. pachyderma* (s) record hinders placement of the other Marine Isotope Chron (MIC) boundaries. In particular the subdivision of MIC 5 is difficult because at least 6 cycles can be identified when 3 are expected. The subchrons of MIC 5 were aided by using the %CaCO₃ and %CF records, which record only 3 cycles (Figure 3.3). Distinct increases in the %CaCO₃ are found in both MIC 1 and 5e. Within the interval identified as MIC 5, two other intervals of high %CaCO₃ are found between 10.4-11.7 mcd and 14.7-16.4 mcd. MIC 5a and 5c sediments contain >20% CaCO₃ while MIC 5b and 5d contain <20 %CaCO₃. The tops and bottoms of these sections correspond to $\delta^{18}\text{O}$ maxima, and therefore, the intervals of high %CaCO₃ are assigned to be MIC5a and 5c, respectively (Table 1).

Results

Stable isotope values from *N. pachyderma* (s) vary from interglacial lows of 2.1‰ to glacial highs of 4.8‰ (Figure 3.2). The transition from MIC 1 to MIC 2 records an amplitude of ~2.2‰ in *N. pachyderma* (s) $\delta^{18}\text{O}$ values. Isolated intervals record $\delta^{18}\text{O}$ values lower than coretop values, indicating the presence of warmer temperatures and/or glacial meltwater. In the case of the values between 21 and 22 mcd, low values probably reflect warmer temperatures during MIC 5e (see below). However, unusually low values found between MIC 1 and MIC 5e must reflect the presence of glacial meltwater to some degree.

Mean SS values range from 13.9 to 27.1 μm and are highly variable down-core (Figure 3.2). Most SS values vary about a mean of 20 μm suggesting that this site remained under similar flow conditions throughout the entire record. In general, %CaCO₃ and %CF values increase where $\delta^{18}\text{O}$ values are low and vice versa reflecting the general relationship between warm (cold) climate and higher (lower) surface ocean productivity. Highest %CF measurements are found in MIC 1 and 5e suggesting Site 1306 is winnowed during these periods. Low sedimentation rates in MIC 1 and 5e also support this inference. Below, stable isotope and sedimentary results are presented based on the subdivision of the stratigraphic record in the individual Marine Isotope Chrons (Figure 3.3).

MIC1. The upper 0.56 mcd are assigned to MIC 1, or Holocene, based on *N. pachyderma* (s) $\delta^{18}\text{O}$ values that are <3‰. Within this interval, %CF values decrease

from 40% at the top to <10% at 0.56 mcd. Similarly, %CaCO₃ decreases >35% in the topmost sample to 11% at 0.56 mcd. SS values approach 27 µm and are the highest recorded throughout the record. Continuing downcore, SS values decrease to 22 µm at the base of MIC 1. As discussed below, AMS ¹⁴C ages and the high SS, %CF and %CaCO₃ indicate that the core top is heavily winnowed with accumulation ending in the early Holocene.

Termination 1. The interval between 0.71 mcd and 1.01 mcd contains *N. pachyderma* (s) δ¹⁸O values that are intermediate between the Holocene above and LGM values below. There is some structure in the δ¹⁸O record that may reflect Younger Dryas and Bolling-Allerod intervals; however, the resolution is insufficient to confidently identify either zone. %CF and %CaCO₃ values are ~10% in this interval. The SS values show a small decrease from 22 to 20 µm over this deglacial interval.

MIC2. In the upper part of MIC 2, or the LGM interval, *N. pachyderma* (s) δ¹⁸O values show little δ¹⁸O variability between 1.06 and 1.66 mcd, averaging 4.65‰ (Figures 2.2, 2.3). In contrast, the sedimentary proxies, SS, %CF and %CaCO₃, increase and then decrease in this interval. In particular, SS values peak at 25 µm before decreasing to 19 µm. In the lower part of MIC 2 (1.71 to 2.36 mcd), δ¹⁸O values vary greatly, with a range of >2‰ (Figures 3.2, 3.3). This indicates much greater instability in the overlying surface waters. As discussed below, the age model indicates that deposition of this interval coincided with the H2 climatological event. Within this interval, SS values continue to decrease downcore to nearly 16 µm at 2.36 mcd. Other than one point at 1.71

mcd (25%), %CF values are <10% with many values <3%. Likewise, %CaCO₃ values remain low at <10% in this interval.

MIC3. High variability in *N. pachyderma* (*s*) $\delta^{18}\text{O}$ values continues between 2.41 and 9.00 mcd (Figure 3.3). This variability is expected as Heinrich Events H3-H5 occurred during the deposition of this sediment package. SS values exhibit 8 distinct cycles throughout this interval. The most prominent low in the whole record is between 5.8 and 6.3 mcd. Small-scale variability can be seen in the %CaCO₃ and %CF records between 2.41 and 9.00 mcd. A small, but distinct, increase in the %CaCO₃ values occurs at 5.7 mcd and appears to be associated with lower and more variable $\delta^{18}\text{O}$ values.

MIC 4. There is low variability in *N. pachyderma* (*s*) $\delta^{18}\text{O}$ values throughout all of MIC 4, 9.0-10.6 mcd. The average $\delta^{18}\text{O}$ value across MIC 4 is 4.2‰ which is ~0.5‰ lower than recorded in MIC 2 and MIC 6. Across the MIC 5/4 transition, %CaCO₃ values decrease from 24 to 9 % carbonate and remain low for the rest of the stage. %CF shows little variability throughout this interval with values ranging from 10% across the MIC 5/4 transition and 0.5-1.5% throughout the MIC 4 record.

MIC 5. Identifying the sub-stages of MIC 5 is difficult because the $\delta^{18}\text{O}$ of *N. pachyderma* (*s*) shows 6 cycles when only three are expected. The lowest values in $\delta^{18}\text{O}$ occur between 21 and 21.6 mcd with values approaching 2.1‰, suggesting the extreme interglacial warmth of MIC 5e. This interval also showed marked increase in %CaCO₃ and %CF reaching 40 and 50 percent, respectively. Throughout the remainder of MIC 5

(10.6-21 mcd) the $\delta^{18}\text{O}$ record is highly variable making the identification of MIC 5a-5d difficult. Percent carbonate values record two peaks at 10.6-11.4 and 14.8-16.4 mcd which were used to define MIC 5a and 5c in the age model.

Termination 2. *N. pachyderma* (*s*) $\delta^{18}\text{O}$ values place the transition from MIC 6 to 5e between 21.5 and 21.9 mcd with values ranging from MIC 5e values of $<2.7\text{‰}$ to MIC 6 values of $>4.5\text{‰}$. Interestingly, across the MIC 6 to 5e transition, we find structure similar to that of the Bolling/Allerod to Younger Dryas transition associated with Termination 1 with values spiking to a high of 2.3‰ at 21.8 mcd and increasing to 3.8‰ before reaching stable MIC 5e conditions at 21.5 mcd.

Sedimentation Rates. Sedimentation rates at Site 1306 vary from 5 to 70 cm/kyr with highest sedimentation occurring during intermediate climate states (mid to late MIC 3, 5b, 5d). Sedimentation rates in the interglacial MIC 1 and 5e are low, supporting the sediment proxy evidence that these sediments were winnowed. Sedimentation rates for MIC 5a and 5c are slightly higher (~ 16 cm/kyr) indicating limited preferential deposition across the site during warmer intermediate climates. Lower sedimentation rates (~ 20 cm/kyr) also extend from MIC 5a through early MIC 3, suggesting limited current focusing during this time.

Discussion

The flux of Northern Component Water (NCW, analogous to NADW) has varied with Milankovitch and sub-Milankovitch timescales during the past 160 kyr (e.g., Raymo et al., 1990). During the extreme interglacials (100 kyr cyclicity), marked increases in %CF

and %CaCO₃ are coupled with very low sedimentation rates at Site 1306. These results indicate that a dense, fast moving NCW water mass occurred at ~2200 m on the Eirik Drift leading to erosion of sediments and redistribution at depth. Henderson (Chapters 1 and 2) shows that the depocenter for sediment accumulation during MIC 1 and 5e shifted from ~2200 m (this study) to ~3400 m water depth. Surface water conditions in the Greenland, Iceland and Norwegian (GIN) seas are the likely explanation for the shift from shallow to deep on Eirik Drift during MIC 1 and 5e because these intervals are characterized by low volumes of continental ice and therefore lessened freshwater flux to the surface-ocean and warm SST's throughout the North Atlantic.

Northern Component Water caused high sedimentation at Site 1306 during intermediate climate states (MIC 3, 5b, 5d) with maximum sedimentation rates of 70 cm/kyr. High sedimentation rates in drift settings are derived from winnowing sediments upstream from the core site (Keigwin and Jones, 1989). The density of NCW may also be unstable across these intervals because SS measurements are highly variable indicating changes in current strength over Site 1306. Studies of modern NADW flow on Eirik Drift suggest that buoyancy shifts in NADW are quite common (e.g., Hunter et al., 2007); however, these shifts must average out over long periods of time relative to the cores in drift settings would record high sedimentation rates. Furthermore, if density shifts did not occur, it is likely that the current would winnow sediments along its flow path to immovable foraminiferal/IRD sands preventing high sedimentation rates occurring over long periods of time. This relationship likely holds true in the past and density shifting may be amplified by D/O oscillations that can rapidly alter surface water hydrography in

the GIN seas.

Changes in the *N. pachyderma* (*s*) $\delta^{18}\text{O}$ record, corrected for ice volume, show an inverse relationship with the SS proxy record throughout the core (Figure 3.4). As $\delta^{18}\text{O}$ trends to lower values, SS increase, indicating that small warmings in surface ocean temperatures result in higher flow speeds over Site 1306. Similarly, as $\delta^{18}\text{O}$ increases, SS decreases suggesting slower flow speeds during cooler intervals. This relationship holds true for the entire down core record, indicating that surface water conditions over Eirik Drift and NCW production are coupled. This finding is of interest because deepwater convection sites are generally thought to be located to the north of the Iceland Basin in the Norwegian Seas during glacial and intermediate climate states. It may be possible that changes in the GIN seas outflow that occurs today nearby Site 1306 via the East Greenland Current (EGC) may have shifted south in the past, ending up directly over Site 1306. If this were true, changes in the surface waters over Site 1306 may be related to areas of deep convection accounting for the inverse relationship seen in the $\delta^{18}\text{O}$ and SS records. Another potential explanation may be the formation of deepwater in the Irminger Sea (Pickart et al., 2003) which is located adjacent to Site 1306.

Over the past 160 kyr periods of diminished deepwater production are indicated by lower SS values at Site 1306 (Figure 3.4). According to our age model, the largest decreases in SS occur during Heinrich Events as identified by other researchers (e.g., Praetorius et al., 2008). During the period from 40 to 160 ka, several periods of slowing occurred with little change in surface water hydrography. For example, SS decreased at 48, 56, 73, 80

and 88 ka which may be related to the H-events identified in Rasmussen et al. (2003).

Freshwater influences on the surface ocean become more pronounced from 40 ka to present with a co-varying relationship between large negative spikes of $\delta^{18}\text{O}$ and decreases in SS, overprinting the down core temperature derived relationship of *N. pachyderma* (*s*) and SS. The spikes in $\delta^{18}\text{O}$ occur during MIC 2 and 3 and must be driven by changes in the $\delta^{18}\text{O}$ of seawater and not temperature because the absolute value of change is much higher than records of temperature variability in nearby cores.

Interestingly, the timing of surface freshening and diminished deepwater production appears to occur in concert with Heinrich Events. This is a unique finding because large changes in surface hydrography are generally not seen at this latitude during Heinrich Events (Cortijo et al., 1999). Therefore, it becomes a curious observation as to why surface freshening occurs over Site 1306 in contrast to other nearby sites (e.g. Hillaire-Marcel et al., 1994). The freshening seen in the surface ocean over Site 1306 may be related to changes in the gross atmospheric and surface ocean circulation that is likely to become occur during large ice rafting events (Bond et al., 1992; Broecker, 1994). If the polar front was to shift southwards, as is thought to be the case during the LGM relative to the modern (CLIMAP, 1981), then it may be possible to deflect the outflow of the EGC southward over Site 1306 altering surface $\delta^{18}\text{O}$ values for short periods of time. The possibility also remains that this freshening could be directly sourced melt water from the Greenland ice sheet. However, this is an unlikely alternative because meltwater should travel across a wide range of sea surface and there is no record of these events in several nearby cores.

The best example of surface freshening with a corresponding change in deep-ocean circulation is during Heinrich Event 4 (H4) ~ 38 kyrs BP. During this event we find several peaks in $\delta^{18}\text{O}$ which are concurrent with decreases in the SS and MS records (Figure 2.5). Rapid $\delta^{18}\text{O}$ decreases are best explained by surface ocean freshening while SS records a slowing a current velocity. The MS record also shows a concurrent drop in susceptibility that arises from decreasing of current flow as sediment laden currents in this area are always high in magnetic mineral content (Kissel et al., 1999; Kleiven et al., 2008).

The H3 and H2 Events also show similar relationships with a surface freshening and corresponding deep-ocean current weakening, however these events are not clearly defined as H4. During the H3 Event, SS begins to decrease before any freshwater spikes are seen suggesting that H3 occurred after ocean circulation slowed. This finding is of interest because several studies have suggested that H3 is different from the typical H event from the lithologic differences in and amount of IRD deposited during other H events. If H3 was largely a water derived event (as indicated by the lack of IRD) then it may be possible that increased melt runoff into the North Atlantic started slowing circulation before any pulses of ice were launched.

From 25 to 22 ka, large changes in surface $\delta^{18}\text{O}$ values may be related to H2. At 25ka, a low spike in $\delta^{18}\text{O}$ values and drops in SS and MS, indicate that the start of the event is very similar to that of H4. However, another larger spike in $\delta^{18}\text{O}$ occurs at 23 ka while

SS and MS are increasing indicating a strengthening of the current. It may be possible that the initial pulse of freshwater at 25 ka was large enough to change the deepwater system into a different flow state as suggested by the slowing in the SS and MS records. The resulting increases in circulation seen across the H2 event remains puzzling and perhaps is related to a deep- current shoaling towards Site 1306, therefore skewing the SS records at this time.

The response of the surface ocean at Site 1306 during Heinrich Event 1 is also interesting because there is little change in the surface ocean compared to the corresponding ocean slowing in the MS and SS records. Perhaps one important observation is that the variability in the $\delta^{18}\text{O}$ record is much higher from 22-40 ka than it is from 5-22 ka, indicating that surface variability has been at a minimum over the past 22 ka. This lack of variability may be caused by clearly defined glacial and interglacial states over the past 22 ka while the preceding 20kyr occurred largely under an “intermediate” climate system where atmospheric temperature, rates of freshwater discharge and ocean circulation did not develop a steady state system.

Conclusions

Site 1306 provides an excellent history of NCW flow during the past 160 kyrs. Throughout this time, the highest sedimentation rates occurred during intermediate flow states of MIC 3, 5b and 5d. High NCW flow coupled with a deepening of the current axis in MIC 1 and 5e caused winnowing over the drill site making SS records from these intervals unreliable. An inverse relationship occurs between the surface proxy $\delta^{18}\text{O}$ of *N.*

pachyderma (*s*) and the deep flow proxy SS interpreted as small changes in ocean surface temperature being propagated into the deep-ocean system. For example, during warmer periods, SS values show increased NCW flow over Site 1306. Likewise, cooler temperatures show diminished relative current velocity. During the last 40 kyr this relationship becomes overprinted by periods of surface ocean freshening. These fresh water events are concurrent with Heinrich Events and show decreases in NCW velocity. Several periods of diminished SS flow in the 40 to 160 kyr interval that may be related to H-event activity. These events do not occur with the fresh water pulses seen in the 0-40 kyr interval, suggesting that 1) freshwater flux and surface ocean hydrography has changed between the 0-40 and 40-160 kyr intervals, and 2) these changes may potentially be related to how D/O or H-events have manifested themselves over time.

Table 1

Depth (mcd)	Reservoir Corrected ^{14}C Age	Measurement Error	Calendar Age (ka)	Standard Deviation
0.1	4930	15	5.6	16
0.81	11895	25	13.7	44
1.21	16200	70	19.3	79
1.66	18820	120	22.4	80
2.36	20080	110	24.0	106
3.51	23820	230	28.5	184
Stage boundary	Depth (mcd)	Calendar Age (ka)		
2/3	2.63	28.0		
LaChamp	7.07	40.0		
3/4	8.91	57.5		
4/5a	10.6	72.4		
5a/5b	12.06	85.5		
5b/5c	14.93	92.1		
5c/5d	16.5	105.7		
5d/5e	21.0	115.3		
5e/6	21.75	131.6		
6/7.1	33.05	191.2		

Table 1 shows data used to construct the age model for Site 1306. Clear cells show AMS ^{14}C data while shaded cells used stratigraphic correlation.

Figure Captions

Figure 3.1_Basemap showing the location of Site 1306 on the Eirik Drift. This site is located at a water depth of 2270 m and contains long-term sedimentation rates of ~16 cm/kyr. Multi-channel seismic and 3.5 khz data suggest that this site is ideal for monitoring changes in gNAIW, supporting the idea that NCW buoyancy shifts on glacial/interglacial timescales.

Figure 3.2_The $\delta^{18}\text{O}$, %coarse fraction, % CaCO_3 , % SiO_2 and mean sortable silt proxy records generated at Site 1306 in meter composite depth (mcd). Spikes in coarse fraction, carbonate and silica records at 0-0.5 mcd and 20-21 mcd indicated by the gray bars, are interpreted as winnowed sections, making SS values unreliable. Long-term trends down-core show an inverse (note the reverse scale on the $\delta^{18}\text{O}$ measurements) relationship between $\delta^{18}\text{O}$ and SS suggesting surface conditions are propagated to the deepwater system at Site 1306. Across the last 7 mcd several instances of strong negative spikes in the $\delta^{18}\text{O}$ record occur. Interpreted as freshwater pulses, these spikes occur during times of SS decreases indicating freshwater is altering deepwater circulation on millennial timescales.

Figure 3.3_Data used in order to construct the age model for Site 1306 using a combination of stable isotopic correlation (blue dots), AMS ^{14}C dates (red) and identification of paleomagnetic LaChamp event (orange). MIC transitions, especially during MIC 5 substages, were not always transparent in the stable isotope record due to changing sedimentation rates so %coarse fraction and % CaCO_3 proxies were used to better constrain our age model. The resulting picks show MIC 5a, 5c and 5e intervals containing high % CaCO_3 values as expected because these substages are warm. Calculated sedimentation rates show that the colder intermediate climate states of MIC 3, 5b and 5d preferentially deposit sediments at Site 1306 relative to full glacial or interglacial settings.

Figure 3.4 $\delta^{18}\text{O}$ (blue) and SS (red) smoothed by a 7 pt Gaussian filter. The top panel shows the complete record over the past 160 kyr while the bottom two panels show 0-80 kyr and 80-160 kyr, respectively. Across the 80-160 kyr a strong inverse relationship exists between the SS and $\delta^{18}\text{O}$ suggesting surface temperature is controlling the rates of deep-ocean circulation. Conversely, from 40 kyr to present strong negative spikes in $\delta^{18}\text{O}$ are seen with decreases in the SS record interpreted as freshwater capping of the surface oceans that slow deep-ocean circulation.

Figure 3.5 Magnetic Susceptibility (green) and SS (red) variability during the last 50 kyrs. MS and SS show decreases during Heinrich event periods, suggesting that deep ocean circulation over Site 1306 diminished.

Figure 3.1

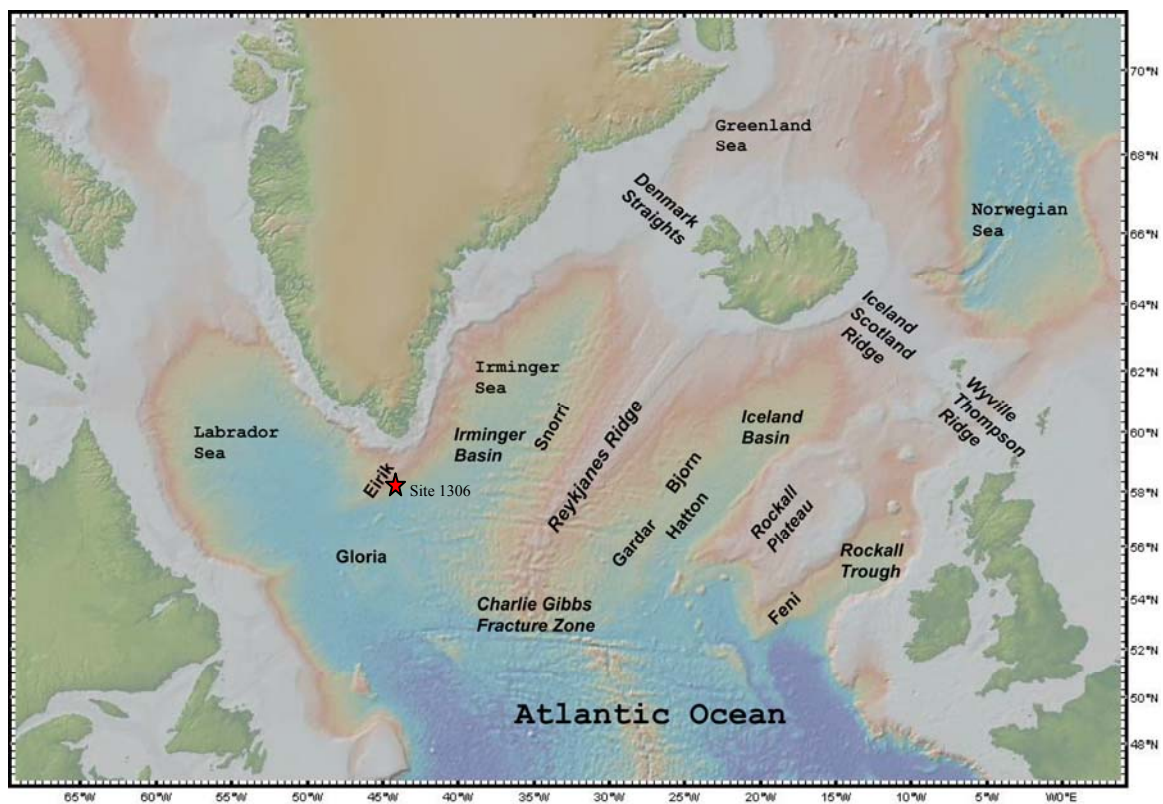


Figure 3.2

Expedition 303 Site U1306

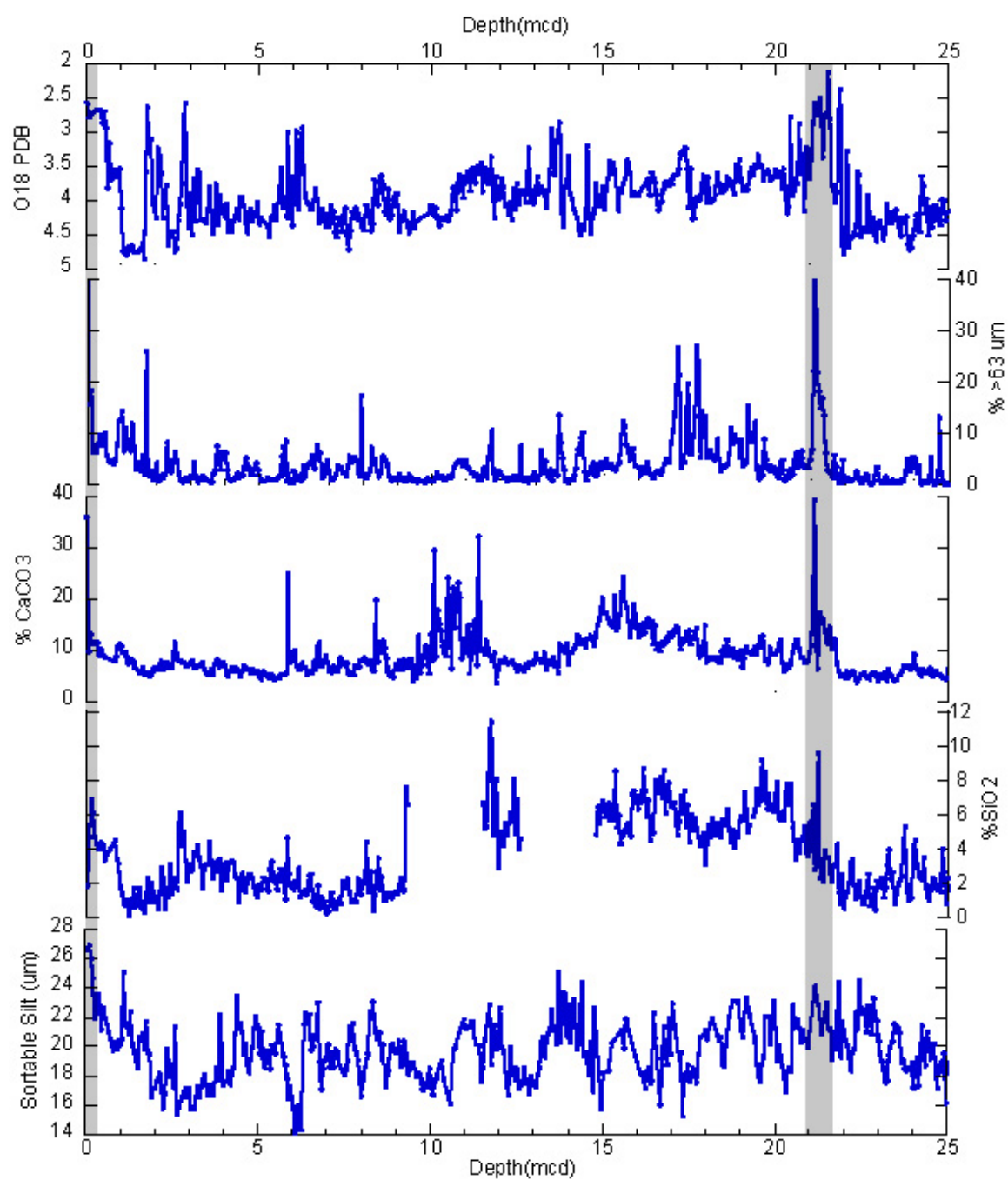


Figure 3.3

Expedition 303 Site U1306

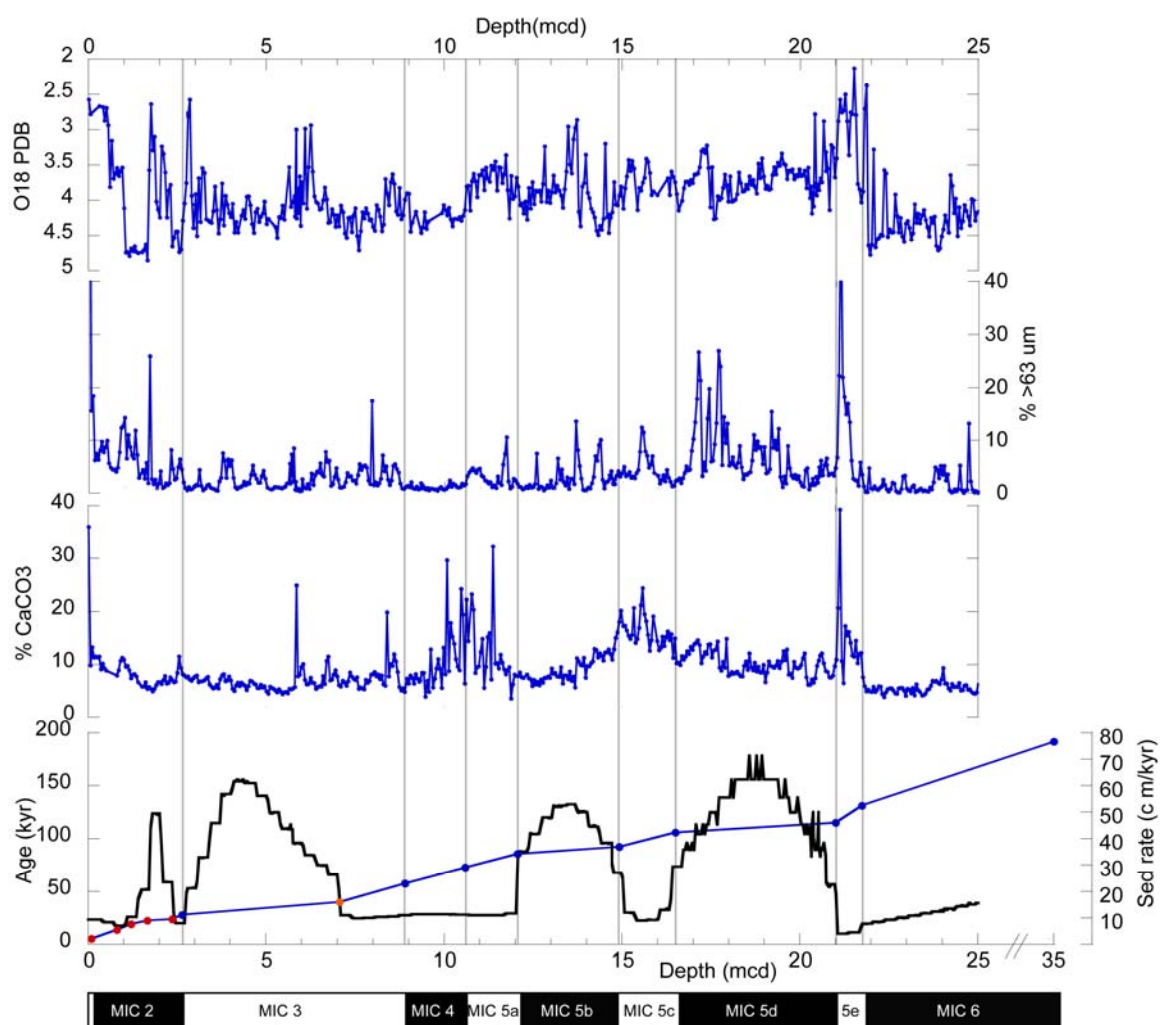


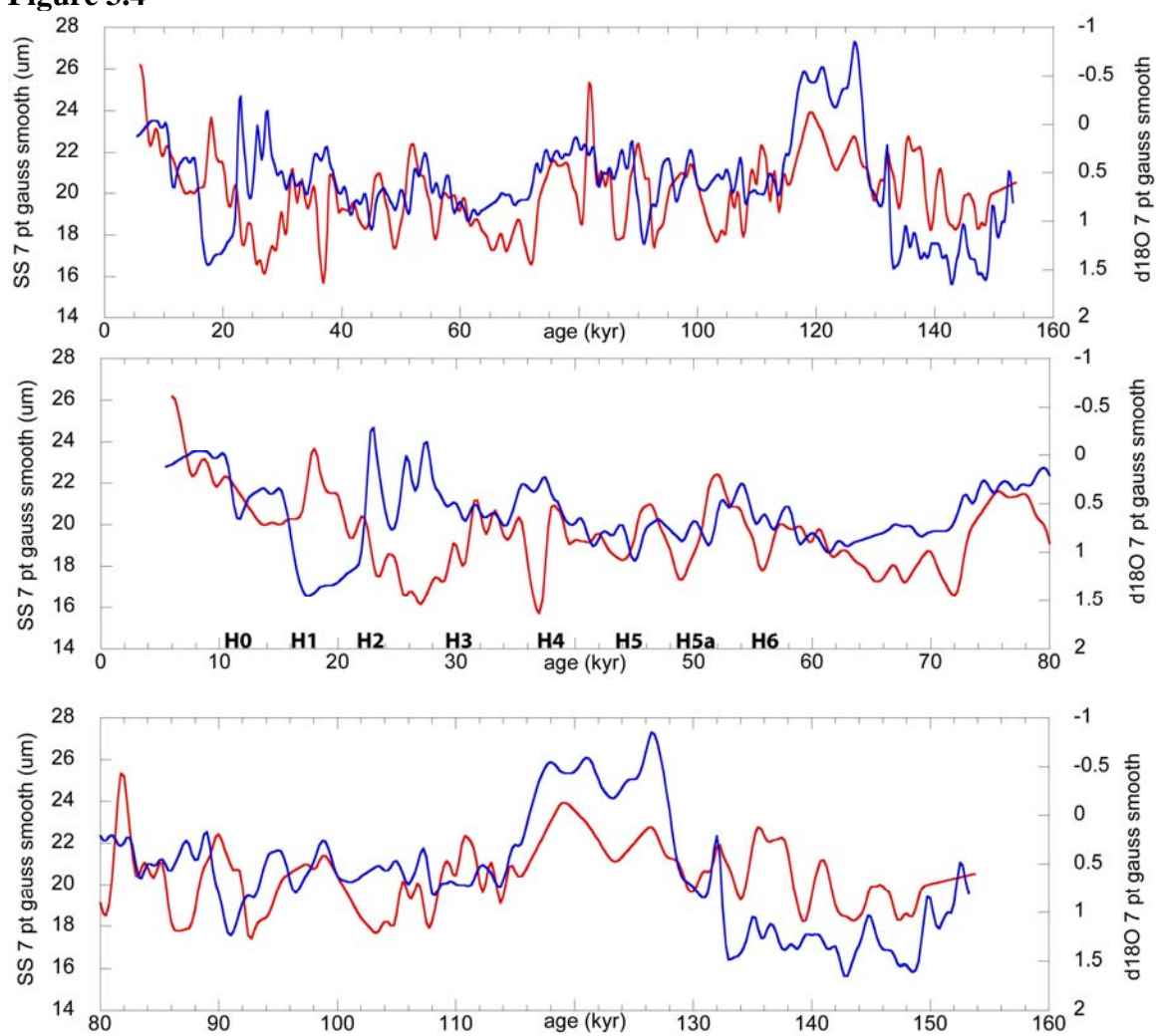
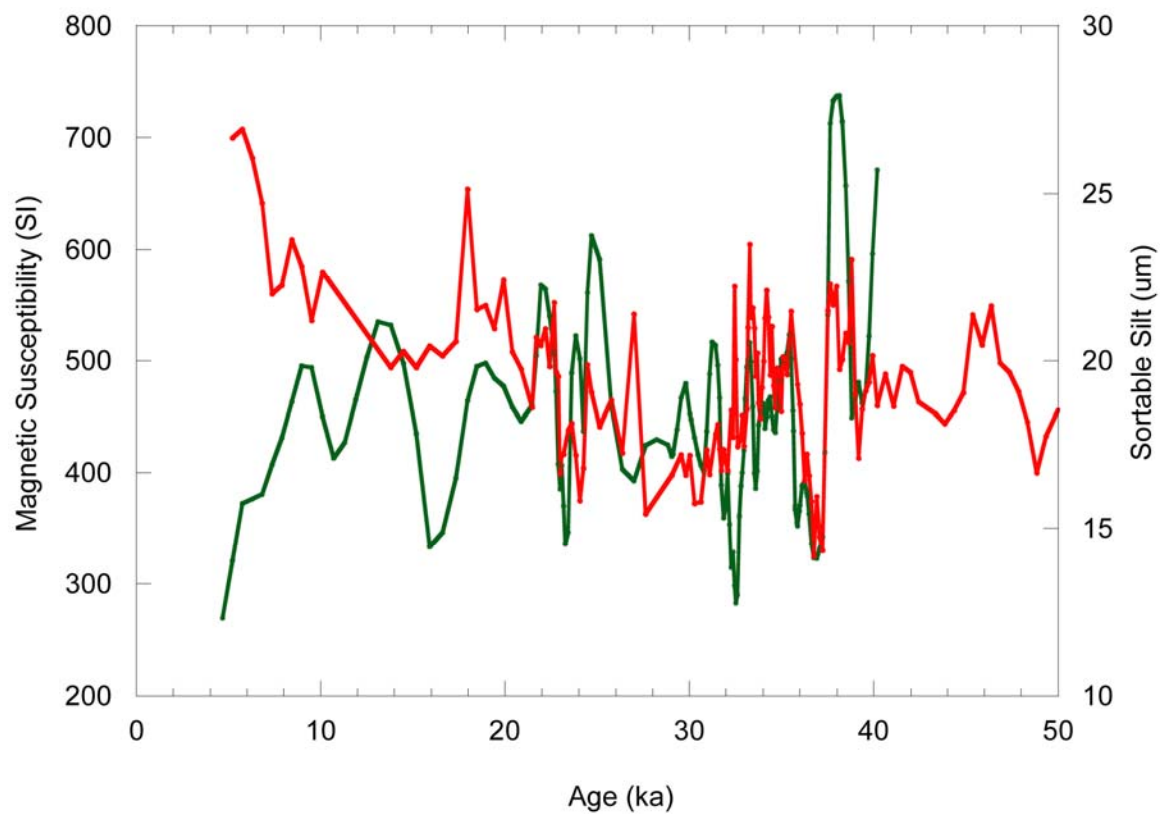
Figure 3.4

Figure 3.5

References

- Andrews, J.T., Erlenkeuser, H., Tedesco, K., Aksu, A.E. and Jull, A.J.T., 1994. Late Quaternary (Stage-2 and Stage-3) meltwater and Heinrich events, Northwest Labrador Sea. *Quaternary Research*, 41(1): 26-34.
- Andrews, J.T. et al., 1995. A Heinrich-like event, H-0 (DC-0) 0 Source(s) for detrital carbonate in the North-Atlantic during the Younger Dryas chronozone. *Paleoceanography*, 10(5): 943-952.
- Barber, D.C. et al., 1999. Forcing of the cold event of 8,200 years ago by catastrophic drainage of Laurentide lakes. *Nature*, 400(6742): 344-348.
- Bond, G. et al., 1993. Correlations between climate records from North-Atlantic sediments and Greenland ice. *Nature*, 365(6442): 143-147.
- Bond, G. et al., 1992. Evidence for massive discharges of icebergs into the North-Atlantic ocean during the last glacial period. *Nature*, 360(6401): 245-249.
- Bond, G. C. and Lotti, R., 1995. Iceberg discharges into the North-Atlantic on millennial time scales during the last glaciations. *Science*, 267(5200): 1005-1010.
- Boyle, E.A. and Keigwin, L., 1987. North-Atlantic thermohaline circulation during the past 20,000 years linked to high-latitude surface-temperature. *Nature*, 330(6143): 35-40.
- Broecker, W.S., 1994. Massive iceberg discharges as triggers for global climate-change. *Nature*, 372(6505): 421-424.
- Broecker, W.S., 2006. Abrupt climate change revisited. *Global and Planetary Change*, 54(3-4): 211-215.
- Broecker, W. S., et al. (1989). Routing of meltwater from the Laurentide ice-sheet during the Younger Dryas cold episode, *Nature*, 341(6240), 318-321.
- CLIMAP, 1981. Seasonal reconstruction of the Earth's surface at the last glacial maximum. Geological Society of America, Map and Chart Series, Vol. C36.
- Cortijo, E. et al., 1999. Changes in meridional temperature and salinity gradients in the North Atlantic Ocean (30 degrees-72 degrees N) during the last interglacial period. *Paleoceanography*, 14(1): 23-33.
- Curry, W.B., Duplessy, J.C., Labeyrie, L. D., and Shackleton, N. J., 1988. Changes in the distribution of delta13C of deepwater eCO2 between the last glaciation and the Holocene. *Paleoceanography*, 3(3): 317-341.

- Duplessy, J. C., Shackleton, N. J., Fairbanks R. G., Labeyrie, L., Oppo D., and Kallel, N., 1988. Deepwater source variations during the last climatic cycle and their impact on the global deepwater circulation. *Paleoceanography*, 3(3): 343-360.
- Elliot, M., Labeyrie, L., Bond, G., Cortijo, E., Turon, J.L., Tisnerat, N., Duplessy, J.-C., 1998. Millennial-scale iceberg discharges in the Irminger Basin during the last glacial period: relationship with the Heinrich events and environmental settings. *Paleoceanography* 13, 433-446.
- Fairbanks, R.G. et al., 2005. Radiocarbon calibration curve spanning 0 to 50,000 years BP based on paired Th-230/U-234/U-238 and C-14 dates on pristine corals. *Quaternary Science Reviews*, 24(16-17): 1781-1796.
- Grousset, F.E. et al., 1993. Patterns of ice-rafted detritus in the glacial North-Atlantic (40-degrees-55-degrees-N). *Paleoceanography*, 8(2): 175-192.
- Heinrich, H., 1988. Origin and Consequences of cyclic ice rafting in the Northeast Atlantic-Ocean during the past 130,00 years. *Quaternary Research*, 29(2): 142-152.
- Hemming, S.R., 2004. Heinrich Events: Massive late pleistocene detritus layers of the North Atlantic and their global climate imprint. *Reviews of Geophysics*, 42(1).
- Hillaire-Marcel, C., de Vernal, A., Bilodeau, G., Wu, G., (1994). Isotope Stratigraphy, sedimentation rates and paleoceanographic changes in the Labrador Sea. *Canadian Journal of Earth Sciences* 31, 63:89.
- Hunter, S. et al., 2007. Deep western boundary current dynamics and associated sedimentation on the Eirik Drift, southern Greenland margin. *Deep-Sea Research Part I-Oceanographic Research Papers*, 54(12): 2036-2066.
- Keigwin, L.D., and Jones, G.A., 1994. Western North Atlantic evidence for millennial-scale changes in ocean circulation and climate. *Journal of Geophysical Research*, 99(c6): 12397-12410.
- Keigwin, L.D. and Lehman, S.J., 1994. Deep circulation change linked to Heinrich Event-1 and Younger Dryas in a middepth North-Atlantic core. *Paleoceanography*, 9(2): 185-194.
- Kissel, C. et al., 1999. Rapid climatic variations during marine isotopic stage 3: magnetic analysis of sediments from Nordic Seas and North Atlantic. *Earth and Planetary Science Letters*, 171(3): 489-502.
- Kleiven, H.F. et al., 2008. Reduced North Atlantic Deepwater coeval with the glacial Lake Agassiz freshwater outburst. *Science*, 319(5859): 60-64.

- Lisiecki, L.E. and Raymo, M.E., 2005. A Pliocene-Pleistocene stack of 57 globally distributed benthic delta O-18 records (vol 20, art no PA1003, 2005). *Paleoceanography*, 20(2).
- Lynch-Stieglitz, J. et al., 2007. Atlantic meridional overturning circulation during the Last Glacial Maximum. *Science*, 316(5821): 66-69.
- Manabe, S., and Stouffer, R.J. (1988). Two Stable Equilibria of a Coupled Ocean-Atmosphere Model: *Journal of Climate*. 1(9), p. 841-866.
- Martinson, D.G. et al., 1987. Age dating and the orbital theory of the ice ages – Development of a high-resolution 0 to 300,000 year chronostratigraphy. *Quaternary Research*, 27(1): 1-29.
- McCave, I.N., Manighetti, B. and Robinson, S.G., 1995. Sortable silt and fine sediment size composition slicing-parameters for paleocurrent speed and *Paleoceanography*. *Paleoceanography*, 10(3): 593-610.
- McManus, J.F., Francois, R., Gherardi, J.M., Keigwin, L.D. and Brown-Leger, S., 2004. Collapse and rapid resumption of Atlantic meridional circulation linked to deglacial climate changes. *Nature*, 428: 834-837.
- Neitzke, L.C. and J.D. Wright, 2007. Variations in Deep-Water Circulation on Eirik Drift from the Last Glacial Maximum to early Holocene. *Geological Society of America, GSA 2007 Denver Annual Meeting*, Vol. 39, No. 6, Paper 114-20.
- Pfeffer, W.T., Harper, J.T. and O'Neel, S., 2008. Kinematic constraints on glacier contributions to 21st-century sea-level rise. *Science*, 321(5894): 1340-1343.
- Pickart, R.S., Straneo, F. and Moore, G.W.K., 2003. Is Labrador Sea Water formed in the Irminger basin? *Deep-Sea Research Part I-Oceanographic Research Papers*, 50(1): 23-52.
- Praetorius, S.K., McManus, J.F., Oppo, D.W. and Curry, W.B., 2008. Episodic reductions in bottom-water currents since the last ice age. *Nature Geoscience*, 1(7): 449-452.
- Rasmussen, T.L., Oppo, D.W., Thomsen, E. and Lehman, S.J., 2003. Deep sea records from the southeast Labrador Sea: Ocean circulation changes and ice-rafting events during the last 160,000 years. *Paleoceanography*, 18(1).
- Raymo, M.E., Ruddiman, W.F., Shackleton, N.J. and Oppo, D.W., 1990. Evolution of Atlantic Pacific delta-C-13 gradients over the last 2.5 MY. *Earth and Planetary Science Letters*, 97(3-4): 353-368.
- Shackleton, N.J., Hall, M.A., Pate, D., Meynadier, L. and Valet, P., 1993. High-

resolution stable isotope stratigraphy from bulk sediment. *Paleoceanography*, 8(2): 141-148.

Teller, J.T., Thorleifson, L.H., Dredge, L.A., Hobbs, H.C., Schreiner, B.T., 1983. Maximum extent and major features of Lake Agassiz. In: Teller, J.T., Clayton, L. (Eds.), *Glacial Lake Agassiz*. Geological Association of Canada Special Paper 26, pp. 43–45.

Conclusions of the Dissertation

The primary focus of this dissertation is to understand changes in deepwater circulation across Milankovitch and millennial time scales and, in particular, to resolve how changes in the cryosphere alter the surface/deep-ocean system. To accomplish this goal, the study examined several core holes from the Eirik Drift including cores KN166-14 21GGC and IODP Expedition 303 Sites 1305/1306 (Figure C.1). Proxy records including stable isotopes of planktonic foraminifera and mean sortable silt (SS) were utilized to monitor changes in both the surface and deep North Atlantic, respectively, in order to reconstruct many different “snapshots” of NCW flow history during the past 160 kyr.

Holocene establishment of deepwater flow

Establishing high-resolution records throughout the Holocene has been a major focus of the paleoceanographic community for several reasons. One area of interest is determining how the deep-ocean establishes itself from a glacial flowing gNAIW water mass to a more vigorously flowing, denser modern NADW water mass. This study uses 21GGC collected during KN166-14 from the southern terminus of the Eirik Drift to examine changes in the surface and deep-ocean from the earliest Holocene to the near present. The SS proxy suggests that 21GGC is subject to high velocity currents throughout most of the Holocene however, sedimentation at the site is Highest from 9 to 10.5 kyr BP (Figure C.2). High sedimentation rates are found during this time throughout the North Atlantic and are thought to occur as NCW remobilized sediments deposited during the last glacial interval (Keigwin and Jones 1989). This study adds to this idea, suggesting that the transition from shallow to deep flow in the Drift must have

been highly unstable (moved up and down many times across the drift) in order to keep sedimentation rates high throughout the early Holocene. I postulate that the earliest Holocene was subject to increased variability in continental freshwater flux which caused large density changes in NCW. The difference curve of *N. pachyderma* (*s*) and *G. bulloides* suggests that the surface ocean was more stratified in the early Holocene indicating the presence of freshwater (Kohfeld et al., 1996). Furthermore, the highest rates of sea level rise throughout the Holocene are seen across the 8 to 10 kyr interval (Fairbanks et al., 1989) adding additional support to the hypothesis.

Recent studies show that the Holocene, once thought to be an anomalously stable period of the Earth's history, is host to a wide variety of small amplitude climate changes that may be similar to previous climate states (eg., Bond et al., 1997, 2001; Bianichi and McCave, 1999; Alley et al., 1997). The 8.2 kyr event is arguably the largest climate excursion recorded during the Holocene and readily seen in a host of terrestrial records such as Greenland Ice cores, deep freshwater lakes and speleothems (Alley et al., 1997; Hu et al., 1999; Baldini et al., 2002). The event is thought to be caused by the release of freshwater from retreating ice sheets. This freshwater release, in turn, disrupts the formation of NCW, however convincing deepwater records of such change have been difficult to find (e.g., Keigwin and Jones 2001; Alley and Agustdottir, 2005). At 21GGC, a large decrease in the SS proxy from 8.6 to 8.2 ka suggests deep-ocean circulation was curtailed during this time. While this study finds convincing evidence for a reduction of deep-ocean flow during the 8.2 kyr event, numerous other studies have been inconclusive so I strongly caution the reader not to take this data as definitive proof that glacial Lake

Agassiz did in fact alter NCW.

Comparison of Termination 1 and 2

Often, the last deglaciation is thought to be a good analogue for previous glacial to interglacial transitions. However, across the last deglaciation (Termination 1) several abrupt climate events (8.2 kyr event, Younger Dryas and H1) interrupt the glacial to interglacial transition while the MIC 6 to 5e transition (Termination 2) only records one event (H11). This study uses surface and deepwater proxies including $\delta^{18}\text{O}$ of *N.*

pachyderma (*s*) and SS measurements from Expedition 303 Sites 1305 and 1306 to better understand surface hydrologic conditions and the resulting deepwater flow across each Termination and into MIC 1 and 5e, respectively.

Changes in Northern Hemisphere insolation have long been thought to be an important control of glacial/interglacial cycles (Hays et al., 1976; Imbrie et al., 1994). Likewise, the rate of change in insolation across the previous two glacial Terminations may provide some insights as to why the Terminations manifest themselves differently. I suggest that Termination 2 differs from Termination 1 because higher insolation across Termination 2 forces continental ice to melt quickly, limiting its ability to form large ice dams that can store and reroute water as is the case in Termination 1. A comparison of surface and deep $\delta^{18}\text{O}$ records from ODP Site 983 allows us to see the agreement between ice volume and surface temperatures across each Termination (Figure C.3). Across Termination 2 there is only a 0.3 m offset (ca. 130 ka) indicating that continental ice volume quickly melted as surface temperatures in the North Atlantic increased. Conversely, across

Termination 1 an expanded offset of 0.84 m exists suggesting that continental ice/freshwater lingered after the onset of warmer temperatures.

The establishment of deepwater flow during MIC 5e and the Holocene are also quite different. Deepwater establishment of a vigorously flowing dense NADW-like water mass is formed within 1.5 kyr after the onset of interglacial conditions (Henderson, Chapter 1; Innocent et al., 2002). Across MIC 5e, sedimentation rates suggest a dense NADW-like water mass is being formed, however, intensities do not reach their height until ~7 kyr after the onset of interglacial temperatures. This result is perplexing because the $\delta^{18}\text{O}$ records across MIC 5e indicate that this period was warmer or slightly fresher than the Holocene. Sea level across MIC 5e was 5 m higher relative to the modern and has been attributed to a Greenland or Western Antarctic source (Mesolella et al., 1969). A recent study by deVernal and Hillaire-Marcel (2008) shows that a significant portion of this 5 m must have come from Greenland based on pollen records contained in marine sediments. I postulate that the deglaciation of Greenland is responsible for curtailing full NCW circulation throughout much of MIC 5e because melt water from Greenland will flow into areas of the ocean thought to convect deepwater.

Deepwater flow over the past 160 kyr

Original hypotheses derived from $\delta^{13}\text{C}$ reconstructions of deepwater circulation suggested that the ocean conveyor operated in an on/off mode across interglacial/glacial periods, respectively (Manabe and Stouffer, 1988; Oppo and Fairbanks, 1987). However,

new tools in paleoceanographic reconstruction (such as the Pa/Th proxy) suggest that glacial circulation was reduced at most 40% relative to modern meridional overturning circulation (MOC) (e.g., McManus et al., 2004). This study expands on the idea that ocean circulation is rarely in an off state as well as examining how surface ocean conditions alter NCW formation by using drill core Expedition 303 Site 1306 on the Eirik Drift. This site is a good candidate for a deepwater reconstruction because this area was in the locus or proximal to the locus of sedimentation when the North Atlantic deepwater was in the gNAIW mode. This area is also excellent for surface ocean reconstructions because it is close to sites of deepwater formation during glacial and intermediate climate states.

This study finds that Site 1306 is an excellent recorder of gNAIW throughout the intermediate climate states of MIC 3, 5b and 5d where sedimentation rates approach 70 cm/kyr (Figure C.4). Typically in oceanic studies ocean circulation is either in a modern NADW-like state or in a gNAIW water state. This variation in sedimentation rates, interpreted as movement of NCW relative to Site 1306, suggest that gNAIW is highly variable in nature, for example a MIC 2 gNAIW must have very different density characteristics compared to gNAIW of MIC 3. I suggest caution be used in applying gNAIW as a catchall phrase for any NCW flow state unlike the modern.

This study also finds unique interactions between surface water control of deep-ocean circulation across much of the past 160 kyr. An inverse relationship in $\delta^{18}\text{O}$ of *N. pachyderma* (*s*) and SS suggests that the warming of the surface North Atlantic is linked

to the increase in deepwater flow over Eirik Drift and vice versa (Figure C.5). During the past 40 kyr, an overprint of the long-term inverse relationship is present where large negative spikes in the $\delta^{18}\text{O}$ record are shown in conjunction with decreasing current velocities. The age model puts the large co-varying events concurrent with Heinrich Events 2 and 3 indicating the $\delta^{18}\text{O}$ excursions are likely caused by surface-ocean freshening due to large ice rafting. This result suggests 1) Heinrich-type events have had a stronger influence on ocean circulation over the past 40 kyr than they did during the 40 to 160 ka ocean and 2) the surface ocean over Eirik Drift records surface hydrographic conditions similar to those areas where deepwater convection occurs, therefore suggesting that the Irminger Sea may operate as a deep-ocean convection site during intermediate and glacial climate states.

Future Work

As with any academic study, the research conducted in this dissertation has opened more avenues of question than it has resolved. Several areas of additional data collection and revision will carry this foundation forward in better understanding the interactions between the cryosphere and oceans. For example, H1 has been identified in a wide variety of marine cores throughout the North Atlantic; however, it is not certain if this event disrupted deep-ocean flow for 400 or 1500 years (Hemming 2004). The development of better constrained age models by combining magnetic paleointensity and $\delta^{18}\text{O}$ measurements is a primary objective of Expedition 303/306. When these chronologies become available for Sites 1305 and 1306 we may be able to better constrain the duration and deep-ocean response to Heinrich events. The improved

chronology will also better constrain NCW flow history across Termination 2 into MIC5e so that a more robust comparison may be made to Termination 1.

Further data collection will also be essential to address the concerns raised over the course of this study. Obviously, SS data gaps at Site 1305 SS from MIC 5e to the Holocene should be filled. Samples throughout this interval have undergone carbonate and silica removal and are currently stored in the GSBL rock lab and ready for SS analysis at Middlebury. Completing these analyses may provide further insights into tracking deep-ocean currents during the warmer intermediate climate states of MIC 5a and 5c and will allow for complete comparisons of NCW circulation variability between Sites 1305 and 1306.

I also recommend the generation of benthic foraminiferal $\delta^{13}\text{C}$ records at Site 1306. SS is an excellent measure of current intensity; however, one must be aware of two different current processes: shifts in the current axis and changes in current velocity are indistinguishable by SS alone. Adding benthic isotopic records will compliment this work greatly because the combination of $\delta^{13}\text{C}$ and SS records will allow for the better interpretation of changes in NCW production vs. changes in NCW buoyancy state.

The scope of this work can also be expanded in time, for example looking at several other glacial terminations to determine if the climate system has become more susceptible to abrupt climate change during the past 40 kyr. A logical corollary for a Holocene type glacial termination lies across the MIC 12/11 boundary because insolation was similar to

that of the Holocene. I also suggest examination of other glacial/interglacial terminations to see if Termination 2 is a good model for comparison.

Finally, I suggest the addition of core sites on the Eirik Drift at depths between 2200 and 3400 m. Much of this study has shown that Sites 1306 and 1305 are suitable end member sites when reconstructing gNAIW and NADW type water masses. The addition of Site 1307 (2575 m) or KN166-14 JPC 18/19 (3435/3184 m) should aid in tracking current buoyancy shifts and will help constrain how quickly these shifts are propagated in the deep ocean.

Figure Captions

Figure C.1

Basemap showing the locations of Sites 1306 (2200 m) and 1305/21GGC (3400 m) on the Eirik Drift. Using both the shallow and deep sites on the drift allows for the reconstruction of gross changes in NCW buoyancy as sedimentation rates change between the shallow and deep sites. ODP Site 983 on the Gardar Drift is also identified and is the location used to determine ice volume melt between Termination 1 and Termination 2.

Figure C.2

Several Proxy records generated from 21GGC. All graphs are plotted on a common depth scale from 0 to 500 cm. The blue proxy records are $\delta^{18}\text{O}$ records of *N. pachyderma* (s), *G. bulloides* and the difference curve of *N. pachyderma* (s) – *G. bulloides*. In all records we find highly variable small amplitude changes down core. Sediment from 342 to 354 cm within 21GGC is barren of all foraminifera. The difference curve suggests that the early Holocene (300-500 cm) more stratified than the mid to late Holocene with divergence rising above 0.8 per mil 5 times. The two red curves show the %CaCO₃ and SS proxy records. %CaCO₃ increases from ~10 to 40% throughout the Holocene while SS ranges from 16 to 30 microns. Both records show a large negative excursion from 325 to 358 cm with values approaching or exceeding that of earliest Holocene sediment in 21GGC. The green record shows calculated sedimentation rates derived from our age model. Two periods of high sedimentation rates are found in the resulting model, 344-362 and 400 to 482 cm. A longer term Holocene sedimentation rate of ~40 cm/kyr is seen from 0 to 344 and 362 to 400 cm.

Figure C.3

Changes in surface (red) and benthic (blue) oxygen isotopes across Terminations 1 and 2 from Site 983 on the Gardar Drift. Across Termination 1 there is a divergence of 0.84 m suggesting that continental glaciers resisted melting in spite of warmer North Atlantic temperatures. Across Termination 2 we find a much smaller divergence of 0.3 m suggesting continental ice melted quickly, probably due to higher insolation forcing during this time.

Figure C.4 Data used in order to construct the age model for Site 1306 using a combination of stable isotopic correlation (blue dots), AMS ¹⁴C dates (red) and identification of paleomagnetic LaChamp event (orange). MIC transitions, especially during MIC 5 substages, were not always transparent in the stable isotope record due to changing sedimentation rates so %coarse fraction and %CaCO₃ proxies were used to better constrain the age model. The resulting picks show MIC 5a, 5c and 5e intervals containing high %CaCO₃ values as expected because these substages are warm. Calculated sedimentation rates show that the colder intermediate climate states of MIC 3, 5b and 5d preferentially deposit sediments at Site 1306 relative to full glacial or interglacial settings

Figure C.5

Figure 2.4 shows $\delta^{18}\text{O}$ (blue) and SS (red) smoothed by a 7 pt Gaussian filter. The top panel shows the complete record over the past 160 kyr while the bottom two panels show 0-80 kyr and 80-160 kyr, respectively. Across the 80-160 kyr a strong inverse relationship exists between the SS and $\delta^{18}\text{O}$ suggesting surface temperature is controlling the rates of deep-ocean circulation. Conversely, from 40 kyr to present strong negative spikes in $\delta^{18}\text{O}$ are seen with decreases in the SS record interpreted as freshwater capping of the surface oceans that slow deep-ocean circulation.

Figure C.1

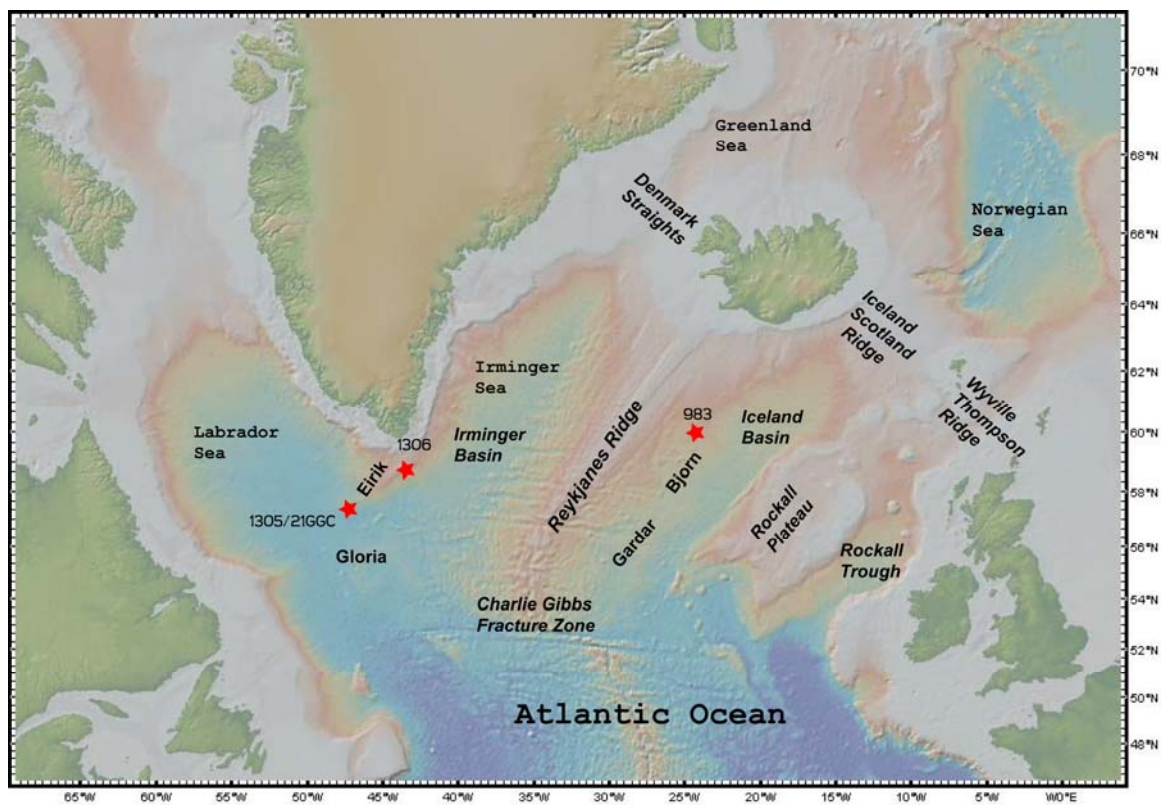
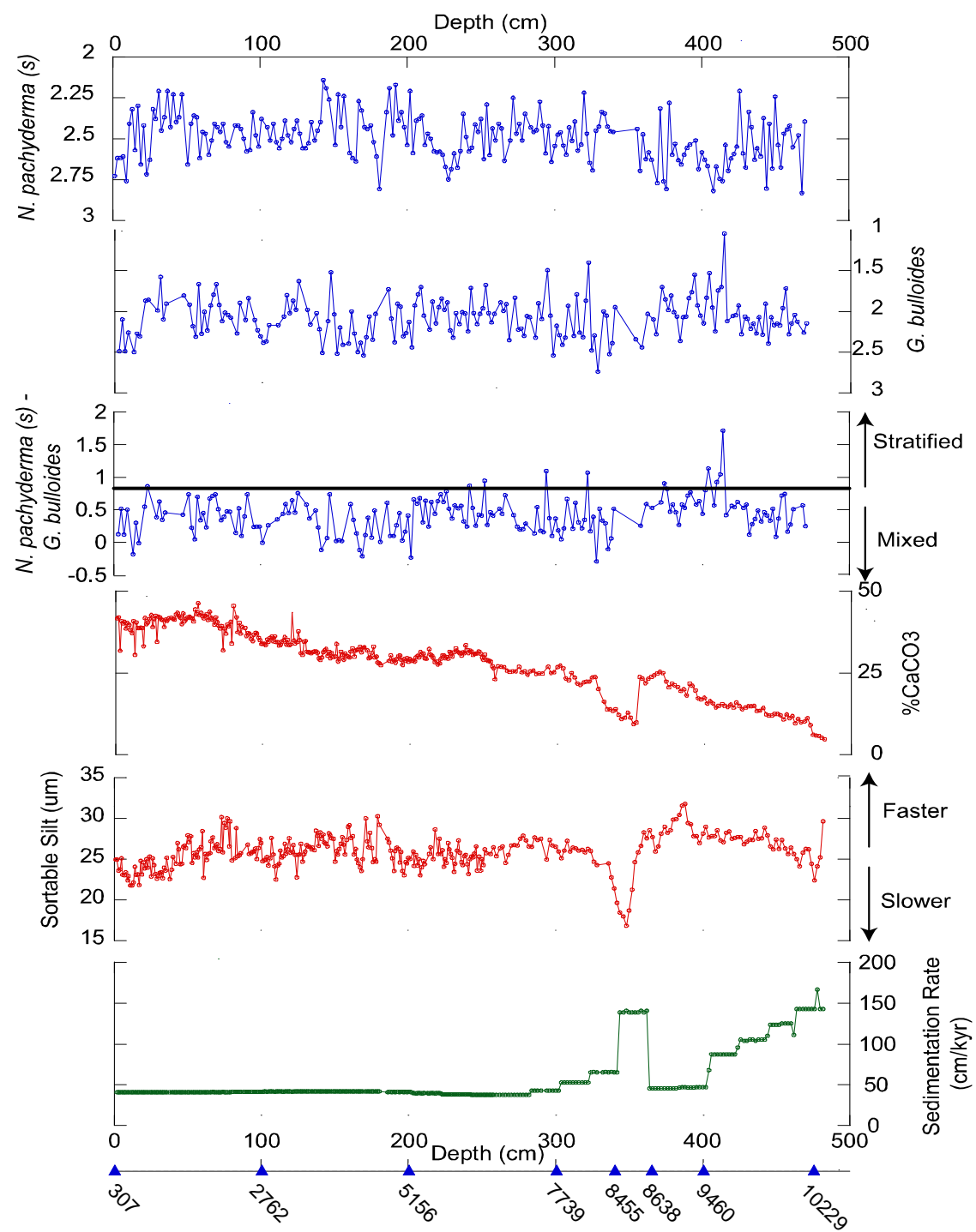


Figure C.2



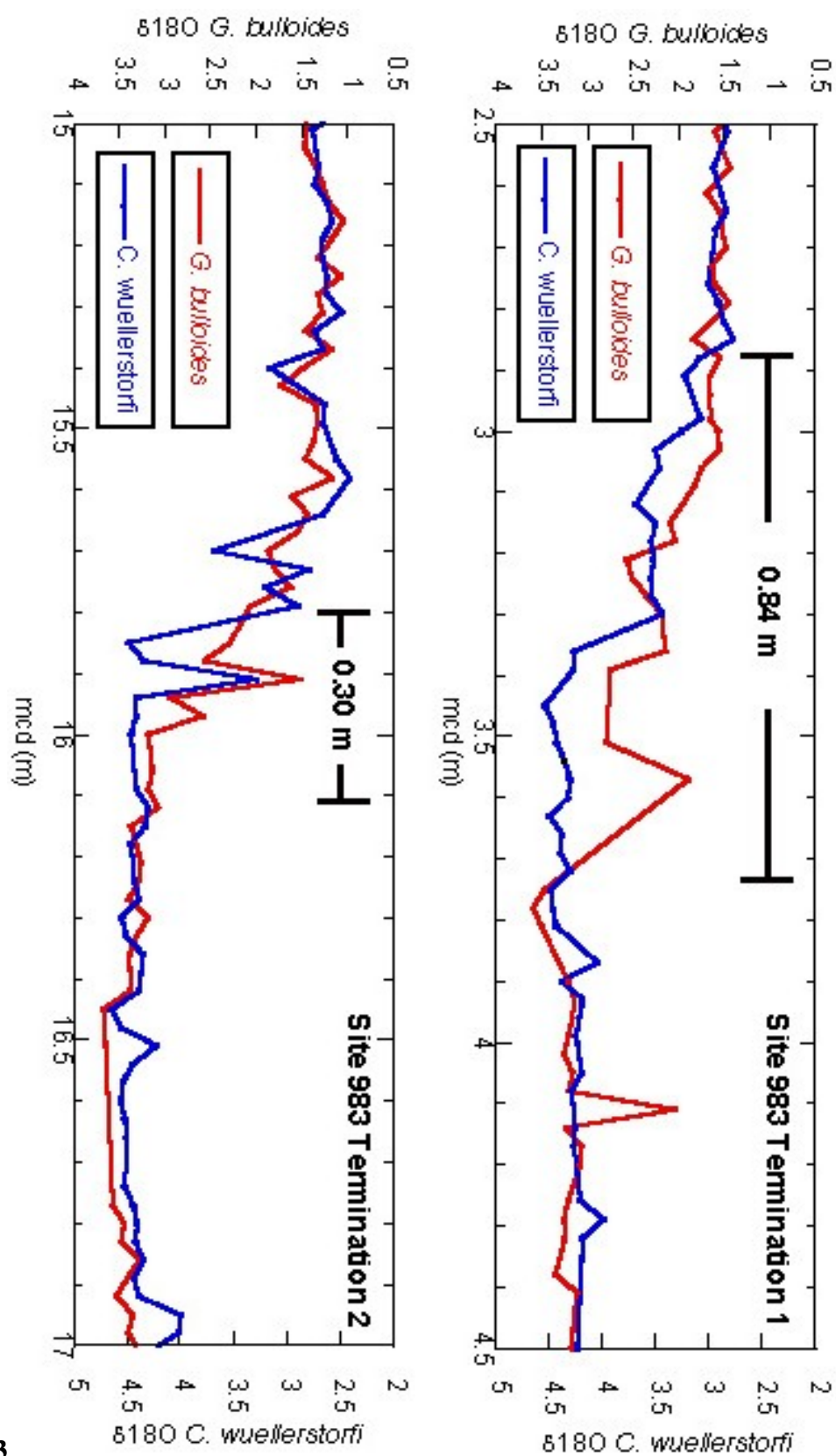


Figure C.3

Figure C.4

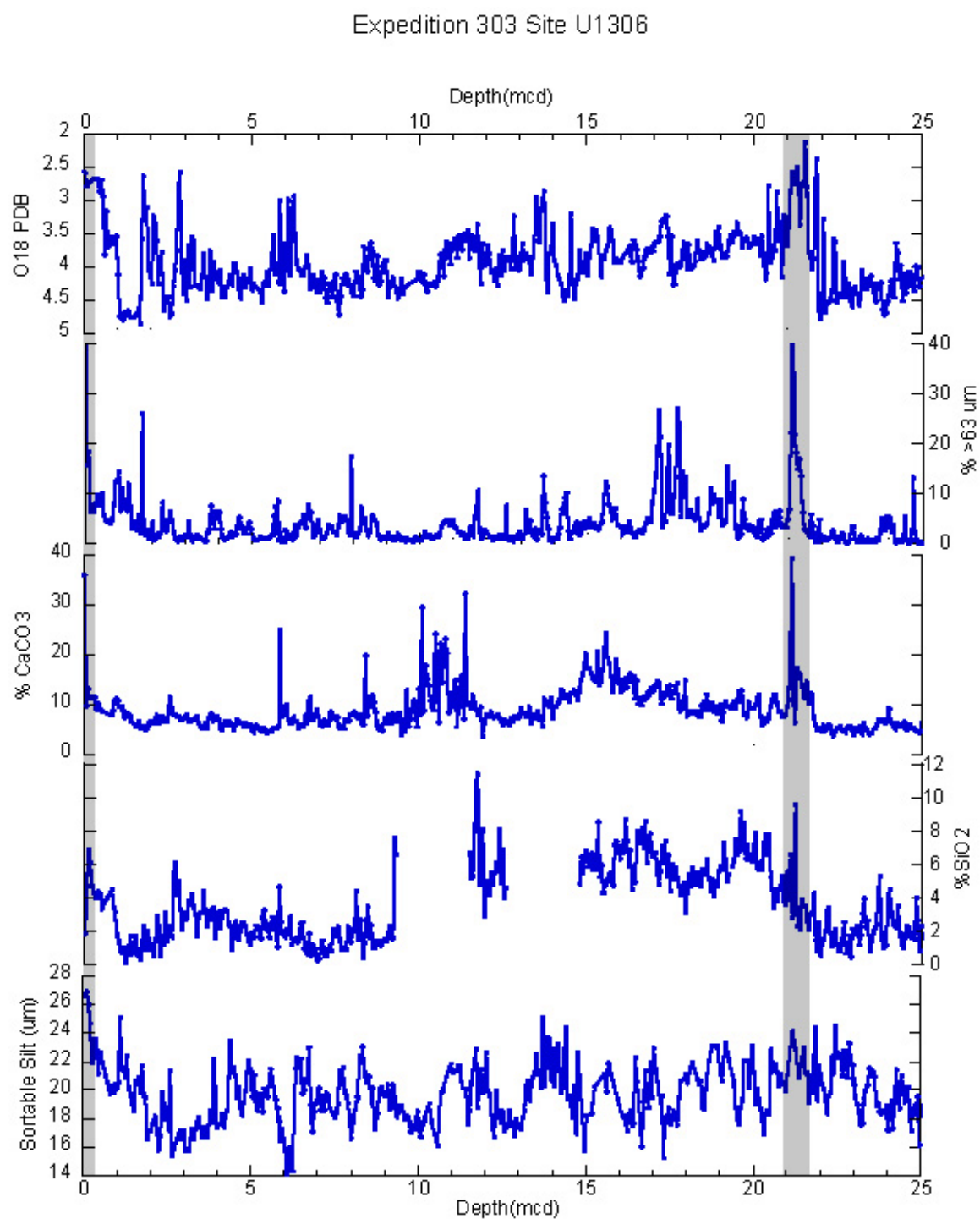
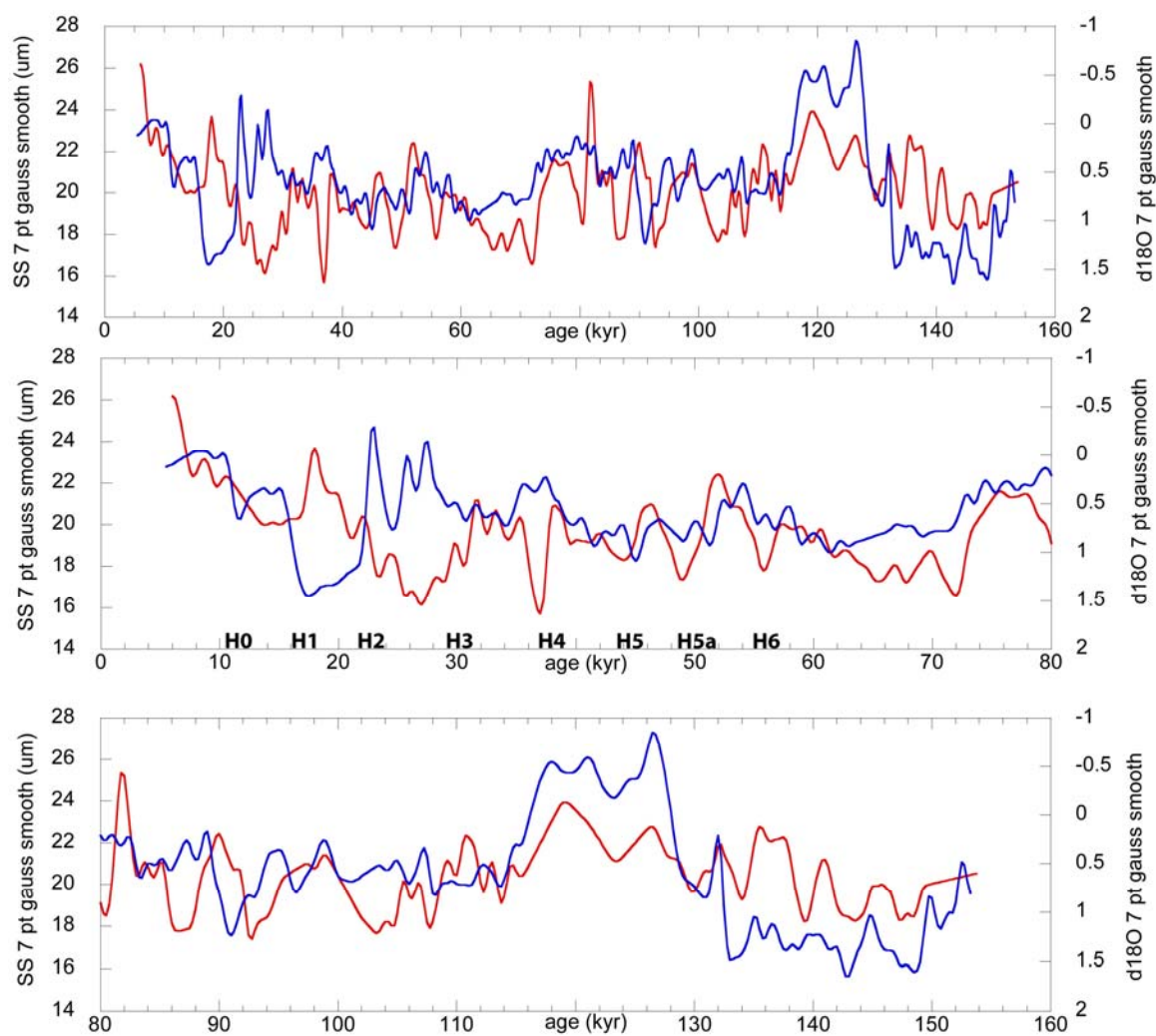


Figure C.5

References

- Alley, R. B., et al. (1997), Holocene climatic instability: A prominent, widespread event 8200 yr ago, *Geology*, 25(6), 483-486.
- Alley, R. B., and A. M. Agustsdottir (2005), The 8k event: cause and consequences of a major Holocene abrupt climate change, *Quaternary Science Reviews*, 24(10-11), 1123-1149.
- Baldini, J. U. L., et al. (2007), Structure of the 8200-year cold event revealed by a speleothem trace element record (vol 296, pg 2203, 2002), *Science*, 317(5839), 748-748.
- Bianchi, G. G., and I. N. McCave (1999), Holocene periodicity in North Atlantic climate and deep-ocean flow south of Iceland, *Nature*, 397(6719), 515-517.
- Bond, G., et al. (1997), A pervasive millennial-scale cycle in North Atlantic Holocene and glacial climates, *Science*, 278(5341), 1257-1266.
- Bond, G., et al. (2001), Persistent solar influence on north Atlantic climate during the Holocene, *Science*, 294(5549), 2130-2136.
- Fairbanks, R.G., 1989. A 17,000-year glacio-eustatic sea-level record – Influence of glacial melting rates on the Younger Dryas Event and deep-ocean circulation. *Nature*, 342(6250): 637-642.
- Hu, F. S., et al. (1999), Abrupt changes in North American climate during early Holocene times, *Nature*, 400(6743), 437-440.
- Innocent C., Fagel N., and Hillaire-Marcel C. (2000) Sm-Nd isotope systematics in deep-sea sediments: Clay size versus coarser fractions. *Mar. Geol.* **168**, 79–87.
- Imbrie, J., Kipp, N.G., 1971. A new micropaleontological method for quantitative paleoclimatology. Application to a late Pleistocene Caribbean core. In: Turekian, K.K. (Ed.), *The Late Cenozoic glacial ages*. Yale Univ. Press, New Haven, pp. 71–131.
- Keigwin, L.D., and G.A. Jones. 1989. Glacial-Holocene stratigraphy, chronology and paleoceanographic observations on some North-Atlantic sediment drifts. *Deep-Sea Research Part a-Oceanographic Research Papers*, 36(6), 845-867.
- Keigwin, L. D., and E. A. Boyle (2000), Detecting Holocene changes in thermohaline circulation, *Proceedings of the National Academy of Sciences of the United States of America*, 97(4), 1343-1346.
- Kohfeld, K. E., et al. (1996), *Neogloboquadrina pachyderma* (sinistral coiling) as paleoceanographic tracers in polar oceans: Evidence from northeast water Polynya

plankton tows, sediment traps, and surface sediments, *Paleoceanography*, 11(6), 679-699.

Manabe, S., and Stouffer, R.J. (1988). Two Stable Equilibria of a Coupled Ocean-Atmosphere Model: *Journal of Climate*. 1(9), p. 841-866.

K. J. Mesolella, R. K. Matthews, W. S. Broecker, D. L. Thurber, (1969), The astronomical theory of climate change: Barbados data. *J. Geol.* 77, 250-274.

McManus, J. F., et al. (2004), Collapse and rapid resumption of Atlantic meridional circulation linked to deglacial climate changes, *Nature*, 428, 834-837.

Oppo, D.W., and R. G. Fairbanks (1987), Variability in the deep and intermediate water circulation of the Atlantic-Ocean during the past 25,000 years – Northern-Hemisphere modulation of the Southern-Ocean, *Earth and Planetary Science Letters*, 86(1), 1-15.

Appendix A

Sampe (core-depth)	depth (cm)	Age Model (ka)	Sed. Rate (cm/kyr)	d18O Npachy (s)	d18O Gbull	d18O difference	%CaCO3	Sortable Silt
21GGC 4-1	1	0.34						
21GGC 4-2	2	0.36		2.73			41.69	24.97
21GGC 4-3	3	0.39	40.49				42.06	24.98
21GGC 4-4	4	0.41	40.50	2.62	2.49	0.13	31.74	23.61
21GGC 4-5	5	0.44	40.50				40.86	23.75
21GGC 4-6	6	0.46	40.49	2.62	2.10	0.52	40.13	25.13
21GGC 4-7	7	0.49	40.50				40.59	23.10
21GGC 4-8	8	0.51	40.49	2.61	2.49	0.12	38.59	23.03
21GGC 4-9	9	0.54	40.50				40.25	23.38
21GGC 4-10	10	0.56	40.50	2.76	2.26	0.50	39.69	22.41
21GGC 4-11	11	0.59	40.49				38.27	22.92
21GGC 4-12	12	0.61	40.50	2.41			37.28	21.79
21GGC 4-13	13	0.64	40.50				40.83	21.75
21GGC 4-14	14	0.66	40.49	2.32	2.50	-0.18	30.42	22.14
21GGC 4-15	15	0.69	40.50				40.52	24.05
21GGC 4-16	16	0.71	40.49	2.57	2.27	0.30	38.78	23.07
21GGC 4-17	17	0.73	40.50				38.82	23.15
21GGC 4-18	18	0.76	40.50	2.30	2.31	-0.01	39.01	21.84
21GGC 4-19	19	0.78	40.49				38.90	24.79
21GGC 4-20	20	0.81	40.50	2.66			33.25	23.14
21GGC 4-21	21	0.83	40.50				41.79	24.57
21GGC 4-22	22	0.86	40.63	2.42	1.87	0.55	39.99	23.88
21GGC 4-23	23	0.88	40.67				40.54	24.99
21GGC 4-24	24	0.91	40.67	2.72	1.86	0.86	41.54	23.95
21GGC 4-25	25	0.93	40.67				42.66	25.31
21GGC 4-26	26	0.96	40.67	2.63			39.16	22.87
21GGC 4-27	27	0.98	40.65				41.57	25.09
21GGC 4-28	28	1.01	40.67	2.32			42.61	24.26
21GGC 4-29	29	1.03	40.70				34.58	23.17
21GGC 4-30	30	1.05	40.65	2.38	1.99	0.39	42.14	22.61
21GGC 4-31	31	1.08	40.65				42.13	22.93
21GGC 4-32	32	1.10	40.65	2.21	1.58	0.63	41.41	23.37
21GGC 4-33	33	1.13	40.65				41.20	23.38
21GGC 4-34	34	1.15	40.65	2.45	2.10	0.35	39.05	22.67
21GGC 4-35	35	1.18	40.65				41.25	23.96
21GGC 4-36	36	1.20	40.65	2.37	1.91	0.46	41.07	23.59
21GGC 4-37	37	1.23	40.82				41.67	25.16
21GGC 4-38	38	1.25	40.65	2.21				27.10
21GGC 4-39	39	1.28	40.65				41.92	22.55
21GGC 4-40	40	1.30	40.65	2.43			41.56	23.71

Sampe (core-depth)	depth (cm)	Age Model (ka)	Sed. Rate (cm/kyr)	d18O Npachy (s)	d18O Gbull	d18O difference	%CaCO3	Sortable Silt
21GGC 4-1	1	0.34						
21GGC 4-2	2	0.36		2.73			41.69	24.97
21GGC 4-3	3	0.39	40.49				42.06	24.98
21GGC 4-4	4	0.41	40.50	2.62	2.49	0.13	31.74	23.61
21GGC 4-5	5	0.44	40.50				40.86	23.75
21GGC 4-6	6	0.46	40.49	2.62	2.10	0.52	40.13	25.13
21GGC 4-7	7	0.49	40.50				40.59	23.10
21GGC 4-8	8	0.51	40.49	2.61	2.49	0.12	38.59	23.03
21GGC 4-9	9	0.54	40.50				40.25	23.38
21GGC 4-41	41	1.33	40.65				41.47	25.29
21GGC 4-42	42	1.35	40.82	2.23			42.89	
21GGC 4-43	43	1.37	40.82				43.38	24.43
21GGC 4-44	44	1.40	40.82	2.40			42.42	26.99
21GGC 4-45	45	1.42	40.82				41.89	26.19
21GGC 4-46	46	1.45	40.82	2.37			39.95	24.38
21GGC 4-47	47	1.47	40.82				43.30	24.44
21GGC 4-48	48	1.50	40.82	2.23	1.81	0.42	40.98	26.51
21GGC 4-49	49	1.52	40.98				41.56	26.67
21GGC 4-50	50	1.55	40.82				42.05	26.39
21GGC 4-51	51	1.57	40.82				42.19	27.92
21GGC 4-52	52	1.59	40.82	2.66	1.92	0.74	41.77	27.09
21GGC 4-53	53	1.62	40.82				41.76	27.80
21GGC 4-54	54	1.64	40.82	2.41	2.18	0.23	40.83	24.56
21GGC 4-55	55	1.67	40.82				44.40	25.74
21GGC 4-56	56	1.69	40.82	2.36	2.31	0.05	43.15	25.21
21GGC 4-57	57	1.72	40.98				46.31	25.85
21GGC 4-58	58	1.74	40.82	2.37	1.67	0.70	42.66	25.24
21GGC 4-59	59	1.77	40.82				43.43	26.22
21GGC 4-60	60	1.79	40.82	2.62	2.28	0.34	42.40	26.44
21GGC 4-61	61	1.81	40.82				41.68	28.44
21GGC 4-62	62	1.84	40.98	2.46	2.01	0.45	42.59	22.72
21GGC 4-63	63	1.86	40.98				42.99	25.65
21GGC 4-64	64	1.89	40.98	2.47	2.24	0.23	41.25	24.89
21GGC 4-65	65	1.91	40.98				43.81	25.65
21GGC 4-66	66	1.94	40.98	2.60	1.93	0.67	41.86	25.73
21GGC 4-67	67	1.96	40.98				41.43	27.18
21GGC 4-68	68	1.99	41.15	2.51	1.80	0.71	39.88	27.69
21GGC 4-69	69	2.01	40.98				42.10	26.34
21GGC 4-70	70	2.03	40.98	2.41	1.67	0.74	40.71	26.54
21GGC 4-71	71	2.06	40.98				39.50	26.81
21GGC 4-72	72	2.08	40.98	2.43	1.92	0.51	38.56	26.00
21GGC 4-73	73	2.11	40.98				39.48	26.25
21GGC 4-74	74	2.13	40.98	2.46	2.12	0.34	31.92	30.18

Sampe (core-depth)	depth (cm)	Age Model (ka)	Sed. Rate (cm/kyr)	d18O Npachy (s)	d18O Gbull	d18O difference	%CaCO3	Sortable Silt
21GGC 4-1	1	0.34						
21GGC 4-2	2	0.36		2.73			41.69	24.97
21GGC 4-3	3	0.39	40.49				42.06	24.98
21GGC 4-4	4	0.41	40.50	2.62	2.49	0.13	31.74	23.61
21GGC 4-5	5	0.44	40.50				40.86	23.75
21GGC 4-6	6	0.46	40.49	2.62	2.10	0.52	40.13	25.13
21GGC 4-7	7	0.49	40.50				40.59	23.10
21GGC 4-8	8	0.51	40.49	2.61	2.49	0.12	38.59	23.03
21GGC 4-9	9	0.54	40.50				40.25	23.38
21GGC 4-75	75	2.16	41.15				38.51	25.82
21GGC 4-76	76	2.18	40.98	2.41	2.02	0.39	37.06	29.42
21GGC 4-77	77	2.21	40.98				39.81	28.88
21GGC 4-78	78	2.23	40.98	2.52	2.04	0.48	39.32	30.00
21GGC 4-79	79	2.25	40.98				40.68	26.57
21GGC 4-80	80	2.28	40.98	2.55	2.08	0.47	34.06	29.66
21GGC 4-81	81	2.30	41.15				45.53	24.83
21GGC 4-82	82	2.33	40.98		1.79			30.39
21GGC 4-83	83	2.35	41.15				42.08	25.10
21GGC 4-84	84	2.38	41.15	2.42	2.27	0.15	37.50	28.82
21GGC 4-85	85	2.40	41.32				40.41	25.36
21GGC 4-86	86	2.42	41.15	2.42	1.90	0.52	36.99	25.49
21GGC 4-87	87	2.45	41.15				39.03	25.72
21GGC 4-88	88	2.47	41.15	2.44	2.34	0.10		28.26
21GGC 4-89	89	2.50	41.15				38.86	
21GGC 4-90	90	2.52	41.15	2.50	2.10	0.40	36.38	
21GGC 3-1	91	2.55	41.32				37.29	
21GGC 3-2	92	2.57	41.15	2.58	1.84	0.74	36.95	26.77
21GGC 3-3	93	2.59	41.15				35.42	25.61
21GGC 3-4	94	2.62	41.15	2.57			34.78	25.71
21GGC 3-5	95	2.64	41.15				36.69	25.90
21GGC 3-6	96	2.67	41.32	2.34	2.10	0.24	37.36	25.93
21GGC 3-7	97	2.69	41.15				37.00	26.30
21GGC 3-8	98	2.72	41.15	2.48	2.23	0.25	35.82	24.98
21GGC 3-9	99	2.74	41.15				35.05	26.37
21GGC 3-10	100	2.76	41.15	2.55	2.31	0.24	33.84	27.47
21GGC 3-11	101	2.79	41.15				33.86	27.01
21GGC 3-12	102	2.81	41.32	2.38	2.38	0.00	33.86	24.74
21GGC 3-13	103	2.84	41.49				33.57	24.91
21GGC 3-14	104	2.86	41.49		2.37		35.36	24.92
21GGC 3-15	105	2.88	41.32				34.60	25.29
21GGC 3-16	106	2.91	41.49	2.43	2.17	0.26	35.79	24.24
21GGC 3-17	107	2.93	41.49				36.06	25.14
21GGC 3-18	108	2.96	41.49	2.51			34.83	27.60

Sampe (core-depth)	depth (cm)	Age Model (ka)	Sed. Rate (cm/kyr)	d18O Npachy (s)	d18O Gbull	d18O difference	%CaCO3	Sortable Silt
21GGC 4-1	1	0.34						
21GGC 4-2	2	0.36		2.73			41.69	24.97
21GGC 4-3	3	0.39	40.49				42.06	24.98
21GGC 4-4	4	0.41	40.50	2.62	2.49	0.13	31.74	23.61
21GGC 4-5	5	0.44	40.50				40.86	23.75
21GGC 4-6	6	0.46	40.49	2.62	2.10	0.52	40.13	25.13
21GGC 4-7	7	0.49	40.50				40.59	23.10
21GGC 4-8	8	0.51	40.49	2.61	2.49	0.12	38.59	23.03
21GGC 4-9	9	0.54	40.50				40.25	23.38
21GGC 3-19	109	2.98	41.49				36.17	25.58
21GGC 3-20	110	3.01	41.32	2.41			34.35	24.15
21GGC 3-21	111	3.03	41.49				34.41	22.50
21GGC 3-22	112	3.05	41.49	2.52	2.17	0.35	33.38	24.24
21GGC 3-23	113	3.08	41.49				33.57	24.42
21GGC 3-24	114	3.10	41.49	2.56			34.66	26.02
21GGC 3-25	115	3.13	41.49				34.90	25.21
21GGC 3-26	116	3.15	41.32	2.50	2.06	0.44	35.90	25.38
21GGC 3-27	117	3.17	41.49				33.73	26.91
21GGC 3-28	118	3.20	41.49	2.39	1.80	0.59	35.19	25.69
21GGC 3-29	119	3.22	41.49				33.69	26.20
21GGC 3-30	120	3.25	41.49	2.48	2.02	0.46	33.80	27.56
21GGC 3-31	121	3.27	41.49				43.60	25.78
21GGC 3-32	122	3.29	41.32	2.52	1.87	0.65	34.90	25.91
21GGC 3-33	123	3.32	41.84				34.13	26.74
21GGC 3-34	124	3.34	41.84	2.44	1.98	0.46	34.42	25.56
21GGC 3-35	125	3.37	41.84				37.72	22.75
21GGC 3-36	126	3.39	41.67	2.39	1.63	0.76	35.09	25.53
21GGC 3-37	127	3.41	41.84				30.95	25.57
21GGC 3-38	128	3.44	41.84	2.47			30.42	26.87
21GGC 3-39	129	3.46	41.84				34.70	24.72
21GGC 3-40	130	3.49	41.67	2.56			34.75	25.59
21GGC 3-41	131	3.51	41.84				31.54	25.92
21GGC 3-42	132	3.53	41.84	2.56	1.98	0.58	31.33	26.74
21GGC 3-43	133	3.56	41.84				31.24	26.55
21GGC 3-44	134	3.58	41.67	2.53	2.16	0.37	31.08	26.53
21GGC 3-45	135	3.61	41.84				31.41	26.21
21GGC 3-45	136	3.63	41.84	2.40			31.62	26.41
21GGC 3-47	137	3.65	41.67				31.64	26.11
21GGC 3-48	138	3.68	41.84	2.51	2.02	0.49	31.10	28.52
21GGC 3-49	139	3.70	41.84				29.50	27.89
21GGC 3-50	140	3.73	41.84	2.45	2.22	0.23	28.94	26.61
21GGC 3-51	141	3.75	41.67				29.69	28.29
21GGC 3-52	142	3.77	41.84	2.40	2.51	-0.11	31.25	27.53

Sampe (core-depth)	depth (cm)	Age Model (ka)	Sed. Rate (cm/kyr)	d18O Npachy (s)	d18O Gbull	d18O difference	%CaCO3	Sortable Silt
21GGC 4-1	1	0.34						
21GGC 4-2	2	0.36		2.73			41.69	24.97
21GGC 4-3	3	0.39	40.49				42.06	24.98
21GGC 4-4	4	0.41	40.50	2.62	2.49	0.13	31.74	23.61
21GGC 4-5	5	0.44	40.50				40.86	23.75
21GGC 4-6	6	0.46	40.49	2.62	2.10	0.52	40.13	25.13
21GGC 4-7	7	0.49	40.50				40.59	23.10
21GGC 4-8	8	0.51	40.49	2.61	2.49	0.12	38.59	23.03
21GGC 4-9	9	0.54	40.50				40.25	23.38
21GGC 3-53	143	3.80	42.02				31.88	28.01
21GGC 3-54	144	3.82	42.02	2.14			32.31	27.06
21GGC 3-55	145	3.84	42.02				30.28	26.91
21GGC 3-56	146	3.87	42.02	2.19	2.12	0.07	31.49	26.57
21GGC 3-57	147	3.89	42.02				29.44	28.19
21GGC 3-58	148	3.92	42.02	2.26	1.52	0.74	31.07	27.95
21GGC 3-59	149	3.94	42.02				29.82	27.58
21GGC 3-60	150	3.96	42.02		2.04		30.14	27.53
21GGC 3-61	151	3.99	42.02				33.82	24.72
21GGC 3-62	152	4.01	42.02	2.54	2.52	0.02	28.54	26.00
21GGC 3-63	153	4.03	42.02				29.29	25.60
21GGC 3-64	154	4.06	42.02	2.23	2.20	0.03	31.57	26.29
21GGC 3-65	155	4.08	42.02				30.44	26.90
21GGC 3-66	156	4.11	42.02	2.43	2.41	0.02	29.08	27.69
21GGC 3-67	157	4.13	42.02				30.89	26.76
21GGC 3-68	158	4.15	42.02	2.24		2.24	30.24	25.58
21GGC 3-69	159	4.18	42.02				29.96	27.36
21GGC 3-70	160	4.20	42.02		2.40		29.77	28.97
21GGC 3-71	161	4.23	42.02				31.50	29.17
21GGC 3-72	162	4.25	42.02	2.59	2.00	0.59	32.53	27.63
21GGC 3-73	163	4.27	42.02				30.03	27.79
21GGC 3-74	164	4.30	41.84	2.62	2.27	0.35	31.73	25.58
21GGC 3-75	165	4.32	42.02				32.20	26.27
21GGC 3-76	166	4.34	42.02	2.64	2.50	0.14	32.04	24.98
21GGC 3-77	167	4.37	41.84				32.97	24.52
21GGC 3-78	168	4.39	42.02	2.27	2.39	-0.12	31.23	24.01
21GGC 3-79	169	4.42	42.02				32.69	23.54
21GGC 3-80	170	4.44	41.84	2.33	2.54	-0.21	32.81	25.02
21GGC 3-81	171	4.46	42.02				53.66	25.81
21GGC 3-82	172	4.49	42.02	2.43	2.32	0.11	31.94	30.02
21GGC 3-83	173	4.51	41.84				29.44	27.17
21GGC 3-84	174	4.53	42.02	2.44	2.06	0.38	29.73	26.47
21GGC 3-85	175	4.56	42.02				31.13	28.25
21GGC 3-86	176	4.58	42.02	2.42	2.35	0.07	33.06	26.36

Sampe (core-depth)	depth (cm)	Age Model (ka)	Sed. Rate (cm/kyr)	d18O Npachy (s)	d18O Gbull	d18O difference	%CaCO3	Sortable Silt
21GGC 4-1	1	0.34						
21GGC 4-2	2	0.36		2.73			41.69	24.97
21GGC 4-3	3	0.39	40.49				42.06	24.98
21GGC 4-4	4	0.41	40.50	2.62	2.49	0.13	31.74	23.61
21GGC 4-5	5	0.44	40.50				40.86	23.75
21GGC 4-6	6	0.46	40.49	2.62	2.10	0.52	40.13	25.13
21GGC 4-7	7	0.49	40.50				40.59	23.10
21GGC 4-8	8	0.51	40.49	2.61	2.49	0.12	38.59	23.03
21GGC 4-9	9	0.54	40.50				40.25	23.38
21GGC 3-87	177	4.61	41.84				29.67	24.64
21GGC 3-88	178	4.63	42.02	2.52	2.03	0.49	29.90	25.03
21GGC 3-89	179	4.65	42.02				28.11	24.73
21GGC 3-90	180	4.68	41.84	2.61			27.86	30.26
21GGC 3-91	181	4.70	42.02				27.32	29.23
	182	4.73	42.02	2.81	2.80	0.01		28.46
Core compacted	183	4.75	41.49					26.46
No mud	184	4.77	40.98					27.95
	185	4.80	41.15					24.50
21GGC 2-5	186	4.82	41.15					
21GGC 2-6	187	4.85	40.98	2.34	1.73	0.61	28.72	27.49
21GGC 2-7	188	4.87	41.15				30.41	27.04
21GGC 2-8	189	4.90	41.15	2.19	2.09	0.10	28.53	26.03
21GGC 2-9	190	4.92	40.98				28.90	25.09
21GGC 2-10	191	4.94	41.15	2.48	2.38	0.10	28.15	23.58
21GGC 2-11	192	4.97	40.98				29.24	26.00
21GGC 2-12	193	4.99	41.15	2.17	1.91	0.26	30.05	26.42
21GGC 2-13	194	5.02	41.15				30.41	26.28
21GGC 2-14	195	5.04	40.98	2.39	1.94	0.45	28.90	24.60
21GGC 2-15	196	5.07	41.15				27.49	25.89
21GGC 2-16	197	5.09	41.15	2.34	2.31	0.03	29.27	23.58
21GGC 2-17	198	5.12	40.98				28.67	23.01
21GGC 2-18	199	5.14	41.15	2.43	2.27	0.16	29.62	24.63
21GGC 2-19	200	5.16	40.98				28.47	24.47
21GGC 2-20	201	5.19	41.15	2.54	2.13	0.41	29.21	25.17
21GGC 2-21	202	5.21	41.15				28.64	25.00
21GGC 2-22	203	5.24	40.49	2.21	2.44	-0.23	28.69	
21GGC 2-23	204	5.26	39.53				28.50	25.98
21GGC 2-24	205	5.29	39.53	2.59	1.93	0.66	29.64	24.20
21GGC 2-25	206	5.31	39.37				30.26	25.51
21GGC 2-26	207	5.34	39.53	2.39	1.79	0.60	29.78	24.24
21GGC 2-27	208	5.36	39.53				31.38	25.01
21GGC 2-28	209	5.39	39.53	2.38	1.70	0.68	30.60	23.03
21GGC 2-29	210	5.42	39.37				30.91	24.01

Sampe (core-depth)	depth (cm)	Age Model (ka)	Sed. Rate (cm/kyr)	d18O Npachy (s)	d18O Gbull	d18O difference	%CaCO3	Sortable Silt
21GGC 4-1	1	0.34						
21GGC 4-2	2	0.36		2.73			41.69	24.97
21GGC 4-3	3	0.39	40.49				42.06	24.98
21GGC 4-4	4	0.41	40.50	2.62	2.49	0.13	31.74	23.61
21GGC 4-5	5	0.44	40.50				40.86	23.75
21GGC 4-6	6	0.46	40.49	2.62	2.10	0.52	40.13	25.13
21GGC 4-7	7	0.49	40.50				40.59	23.10
21GGC 4-8	8	0.51	40.49	2.61	2.49	0.12	38.59	23.03
21GGC 4-9	9	0.54	40.50				40.25	23.38
21GGC 2-30	211	5.44	39.53	2.36	2.05	0.31	29.50	24.83
21GGC 2-31	212	5.47	39.53				29.29	24.38
21GGC 2-32	213	5.49	39.53	2.54	1.90	0.64		26.23
21GGC 2-33	214	5.52	39.53				32.27	
21GGC 2-34	215	5.54	39.37	2.47	2.22	0.25	30.66	25.63
21GGC 2-35	216	5.57	39.53				30.18	26.47
21GGC 2-36	217	5.59	39.53	2.50	1.88	0.62	29.56	
21GGC 2-37	218	5.62	39.53				28.28	25.02
21GGC 2-38	219	5.64	39.37	2.58	2.14	0.44	28.54	28.69
21GGC 2-39	220	5.67	39.53				27.55	
21GGC 2-40	221	5.69	39.53	2.58	1.95	0.64	27.87	25.62
21GGC 2-41	222	5.72	39.53				29.35	27.54
21GGC 2-42	223	5.75	39.22	2.58	1.84	0.74	30.37	25.64
21GGC 2-43	224	5.77	38.31				30.41	26.09
21GGC 2-44	225	5.80	38.31	2.60	1.98	0.62	29.50	24.07
21GGC 2-45	226	5.82	38.31				29.82	25.02
21GGC 2-46	227	5.85	38.31	2.68	1.89	0.78	29.27	24.53
21GGC 2-47	228	5.88	38.31				31.49	26.98
21GGC 2-48	229	5.90	38.31	2.75	2.23	0.52	31.08	26.19
21GGC 2-49	230	5.93	38.31				30.09	25.61
21GGC 2-50	231	5.95	38.31	2.69	2.32	0.37	31.33	25.18
21GGC 2-51	232	5.98	38.31				32.60	23.43
21GGC 2-52	233	6.01	38.31	2.59	2.02	0.57	31.82	24.42
21GGC 2-53	234	6.03	38.31				31.35	26.06
21GGC 2-54	235	6.06	38.31	2.68	2.15	0.52	31.02	27.31
21GGC 2-55	236	6.08	38.31				30.17	25.81
21GGC 2-56	237	6.11	38.31	2.58	2.01	0.56	31.21	24.64
21GGC 2-57	238	6.14	38.31				31.08	24.26
21GGC 2-58	239	6.16	38.31	2.35	2.03	0.32	33.46	25.36
21GGC 2-59	240	6.19	38.31				32.05	25.52
21GGC 2-60	241	6.22	38.31	2.49	2.25	0.24	31.15	24.39
21GGC 2-61	242	6.24	38.31				31.87	23.20
21GGC 2-62	243	6.27	38.31	2.58	1.71	0.87	31.65	25.03
21GGC 2-63	244	6.29	37.45				30.49	25.34

Sampe (core-depth)	depth (cm)	Age Model (ka)	Sed. Rate (cm/kyr)	d18O Npachy (s)	d18O Gbull	d18O difference	%CaCO3	Sortable Silt
21GGC 4-1	1	0.34						
21GGC 4-2	2	0.36		2.73			41.69	24.97
21GGC 4-3	3	0.39	40.49				42.06	24.98
21GGC 4-4	4	0.41	40.50	2.62	2.49	0.13	31.74	23.61
21GGC 4-5	5	0.44	40.50				40.86	23.75
21GGC 4-6	6	0.46	40.49	2.62	2.10	0.52	40.13	25.13
21GGC 4-7	7	0.49	40.50				40.59	23.10
21GGC 4-8	8	0.51	40.49	2.61	2.49	0.12	38.59	23.03
21GGC 4-9	9	0.54	40.50				40.25	23.38
21GGC 2-64	245	6.32	37.45	2.55	2.02	0.53	30.74	25.23
21GGC 2-65	246	6.35	37.45				30.89	25.70
21GGC 2-66	247	6.38	37.45	2.41	2.16	0.26	31.01	26.59
21GGC 2-67	248	6.40	37.45				31.70	23.60
21GGC 2-68	249	6.43	37.45	2.46	2.03	0.43	30.91	25.33
21GGC 2-69	250	6.46	37.45				29.74	23.61
21GGC 2-70	251	6.48	37.45	2.38	1.96	0.42	28.88	25.00
21GGC 2-71	252	6.51	37.31				30.66	24.29
21GGC 2-72	253	6.54	37.45	2.63	1.68	0.95	29.03	26.20
21GGC 2-73	254	6.56	37.45				28.64	25.76
21GGC 2-74	255	6.59	37.45	2.29	2.02	0.27	28.73	
21GGC 2-75	256	6.62	37.45				28.37	
21GGC 2-76	257	6.64	37.45	2.60	2.14	0.47	27.10	25.65
21GGC 2-77	258	6.67	37.45				26.49	
21GGC 2-78	259	6.70	37.45	2.44	2.03	0.41	23.09	26.45
21GGC 2-79	260	6.72	37.45					
21GGC 2-80	261	6.75	37.45	2.51			27.12	25.37
21GGC 2-81	262	6.78	37.45					
21GGC 2-82	263	6.80	37.31	2.41	1.89	0.52	26.92	26.31
21GGC 2-83	264	6.83	37.45					
21GGC 2-84	265	6.86	37.31	2.44	2.00	0.44	26.68	26.60
21GGC 2-85	266	6.88	37.45					
21GGC 2-86	267	6.91	37.31	2.64	1.91	0.72	25.65	24.56
21GGC 2-87	268	6.94	37.31					
21GGC 2-88	269	6.96	37.45		2.36		25.29	25.51
21GGC 2-89	270	6.99	37.31					
21GGC 2-90	271	7.02	37.31	2.51			25.62	26.69
21GGC 2-91	272	7.04	37.45					
21GGC 2-92	273	7.07	37.31	2.25	1.83	0.42	25.47	26.74
21GGC 2-93	274	7.10	37.45					
21GGC 2-94	275	7.12	37.31	2.47	2.23	0.24	26.80	26.65
21GGC 2-95	276	7.15	37.31					
21GGC 2-96	277	7.18	37.45	2.41	2.21	0.20	25.10	27.48
21GGC 2-97	278	7.20	37.31					

Sampe (core-depth)	depth (cm)	Age Model (ka)	Sed. Rate (cm/kyr)	d18O Npachy (s)	d18O Gbull	d18O difference	%CaCO3	Sortable Silt
21GGC 4-1	1	0.34						
21GGC 4-2	2	0.36		2.73			41.69	24.97
21GGC 4-3	3	0.39	40.49				42.06	24.98
21GGC 4-4	4	0.41	40.50	2.62	2.49	0.13	31.74	23.61
21GGC 4-5	5	0.44	40.50				40.86	23.75
21GGC 4-6	6	0.46	40.49	2.62	2.10	0.52	40.13	25.13
21GGC 4-7	7	0.49	40.50				40.59	23.10
21GGC 4-8	8	0.51	40.49	2.61	2.49	0.12	38.59	23.03
21GGC 4-9	9	0.54	40.50				40.25	23.38
21GGC 2-98	279	7.23	37.31	2.51	2.30	0.21	25.55	27.87
21GGC 2-99	280	7.26	37.45					
21GGC 2-100	281	7.28	37.31	2.35	2.06	0.29	24.46	27.31
21GGC 2-101	282	7.31	37.31					
21GGC 2-102	283	7.34	37.45		2.07		25.48	26.57
21GGC 2-103	284	7.36	40.65					
21GGC 2-104	285	7.38	42.74	2.43			25.64	26.53
21GGC 2-105	286	7.41	42.55					
21GGC 2-106	287	7.43	42.74	2.46	2.32	0.14	24.63	27.68
21GGC 2-107	288	7.45	42.55					
21GGC 2-108	289	7.48	42.55	2.45	1.90	0.54	24.89	27.35
21GGC 2-109	290	7.50	42.74					
21GGC 2-110	291	7.52	42.55	2.27	2.09	0.18	24.81	27.51
21GGC 2-111	292	7.55	42.74					
21GGC 2-112	293	7.57	42.55	2.42	2.26	0.16	53.49	25.45
21GGC 2-113	294	7.59	42.74					
21GGC 2-114	295	7.62	42.55	2.59	1.49	1.10	26.81	24.96
21GGC 2-115	296	7.64	42.74					
21GGC 2-116	297	7.66	42.55	2.42	2.05	0.37	25.00	27.37
21GGC 2-117	298	7.69	42.55					
21GGC 2-118	299	7.71	42.74	2.64	2.54	0.10	25.14	26.67
21GGC 2-119	300	7.73	42.55					
21GGC 2-120	301	7.76	42.74	2.54	2.18	0.37	26.74	26.53
21GGC 2-121	302	7.78	42.55					
21GGC 2-122	303	7.80	42.74	2.48	2.29	0.19	27.27	25.93
21GGC 2-123	304	7.82	47.17					
21GGC 2-124	305	7.84	52.63	2.46	2.41	0.05	26.51	25.14
21GGC 2-125	306	7.86	52.91					
21GGC 2-126	307	7.88	52.63	2.54	2.32	0.22	23.36	26.04
21GGC 2-127	308	7.90	52.91					
21GGC 2-128	309	7.92	52.91	2.60	1.93	0.66	22.76	27.25
21GGC 2-129	310	7.93	52.63					
21GGC 2-130	311	7.95	52.91	2.43			24.98	25.93
21GGC 2-131	312	7.97	52.63					

Sampe (core-depth)	depth (cm)	Age Model (ka)	Sed. Rate (cm/kyr)	d18O Npachy (s)	d18O Gbull	d18O difference	%CaCO3	Sortable Silt
21GGC 4-1	1	0.34						
21GGC 4-2	2	0.36		2.73			41.69	24.97
21GGC 4-3	3	0.39	40.49				42.06	24.98
21GGC 4-4	4	0.41	40.50	2.62	2.49	0.13	31.74	23.61
21GGC 4-5	5	0.44	40.50				40.86	23.75
21GGC 4-6	6	0.46	40.49	2.62	2.10	0.52	40.13	25.13
21GGC 4-7	7	0.49	40.50				40.59	23.10
21GGC 4-8	8	0.51	40.49	2.61	2.49	0.12	38.59	23.03
21GGC 4-9	9	0.54	40.50				40.25	23.38
21GGC 2-132	313	7.99	52.91	2.51	2.30	0.21	23.61	26.40
21GGC 2-133	314	8.01	52.91					
21GGC 2-134	315	8.03	52.63	2.40	1.79	0.60	21.80	26.33
21GGC 2-135	316	8.05	52.91					
21GGC 2-136	317	8.07	52.63	2.57	2.26	0.31	21.35	26.06
21GGC 2-137	318	8.09	52.91					
21GGC 2-138	319	8.11	52.91	2.54	2.32	0.22	22.07	26.18
21GGC 2-139	320	8.12	52.63					
21GGC 2-140	321	8.14	52.91	2.22	1.87	0.35	22.42	25.86
21GGC 2-141	322	8.16	52.63					
21GGC 2-142	323	8.18	52.91	2.47	1.40	1.07	22.35	26.27
21GGC 2-143	324	8.20	56.50					
21GGC 2-144	325	8.21	65.36	2.65	2.48	0.17	23.58	26.01
21GGC 2-145	326	8.23	65.36					
21GGC 2-146	327	8.24	65.79	2.70	2.30	0.40	23.71	24.69
21GGC 2-147	328	8.26	65.36					
21GGC 2-148	329	8.27	65.36	2.45	2.74	-0.29	20.11	24.31
21GGC 2-149	330	8.29	65.36					
21GGC 2-150	331	8.30	65.79	2.43	1.91	0.51		
21GGC 1-1	332	8.32	65.36					
21GGC 1-2	333	8.33	65.36	2.34	2.00	0.34	16.18	
21GGC 1-3	334	8.35	65.36					
21GGC 1-4	335	8.36	65.79	2.35	2.05	0.29	13.84	
21GGC 1-5	336	8.38	65.36					
21GGC 1-6	337	8.39	65.36	2.43	2.53	-0.10	13.80	24.47
21GGC 1-7	338	8.41	65.36					
21GGC 1-8	339	8.42	65.79	2.46	2.39	0.06	13.34	22.75
21GGC 1-9	340	8.44	65.36					
21GGC 1-10	341	8.45	65.36	2.46	1.95	0.51	13.98	21.40
21GGC 1-11	342	8.47	65.79					
21GGC 1-12	343	8.48	65.36				12.14	19.65
21GGC 1-13	344	8.49	71.94					
21GGC 1-14	345	8.50	138.89				10.83	18.47
21GGC 1-15	346	8.51	138.89					

Sampe (core-depth)	depth (cm)	Age Model (ka)	Sed. Rate (cm/kyr)	d18O Npachy (s)	d18O Gbull	d18O difference	%CaCO3	Sortable Silt
21GGC 4-1	1	0.34						
21GGC 4-2	2	0.36		2.73			41.69	24.97
21GGC 4-3	3	0.39	40.49				42.06	24.98
21GGC 4-4	4	0.41	40.50	2.62	2.49	0.13	31.74	23.61
21GGC 4-5	5	0.44	40.50				40.86	23.75
21GGC 4-6	6	0.46	40.49	2.62	2.10	0.52	40.13	25.13
21GGC 4-7	7	0.49	40.50				40.59	23.10
21GGC 4-8	8	0.51	40.49	2.61	2.49	0.12	38.59	23.03
21GGC 4-9	9	0.54	40.50				40.25	23.38
21GGC 1-16	347	8.51	138.89				11.21	17.96
21GGC 1-17	348	8.52	138.89					
21GGC 1-18	349	8.53	140.85				12.83	16.85
21GGC 1-19	350	8.53	138.89					
21GGC 1-20	351	8.54	138.89				11.24	18.72
21GGC 1-21	352	8.55	138.89					
21GGC 1-22	353	8.56	138.89				9.31	21.26
21GGC 1-23	354	8.56	140.85					
21GGC 1-24	355	8.57	138.89		2.34		9.80	24.64
21GGC 1-25	356	8.58	138.89					
21GGC 1-26	357	8.58	138.89	2.44			23.72	25.83
21GGC 1-27	358	8.59	138.89					
21GGC 1-28	359	8.60	140.85	2.70	2.44	0.26	23.28	26.61
21GGC 1-29	360	8.61	138.89					
21GGC 1-30	361	8.61	138.89	2.47		2.47	21.93	28.28
21GGC 1-31	362	8.62	138.89					
21GGC 1-32	363	8.63	140.85	2.62	2.03	0.59	23.14	27.56
21GGC 1-33	364	8.65	138.89					
21GGC 1-34	365	8.67	45.25	2.58			23.75	28.57
21GGC 1-35	366	8.69	45.25					
21GGC 1-36	367	8.72	45.25	2.63	2.10	0.53	24.24	27.75
21GGC 1-37	368	8.74	45.25					
21GGC 1-38	369	8.76	45.25		2.28		24.80	25.97
21GGC 1-39	370	8.78	45.25					
21GGC 1-40	371	8.80	45.25	2.77			25.34	26.57
21GGC 1-41	372	8.83	45.25					
21GGC 1-42	373	8.85	45.25	2.32	1.70	0.61	24.98	28.16
21GGC 1-43	374	8.87	45.25					
21GGC 1-44	375	8.89	45.45	2.76	1.85	0.91	22.46	28.95
21GGC 1-45	376	8.91	45.25					
21GGC 1-46	377	8.94	45.25	2.81	1.98	0.83	20.65	28.23
21GGC 1-47	378	8.96	45.25					
21GGC 1-48	379	8.98	45.25	2.28	1.81	0.47	21.78	28.58
21GGC 1-49	380	9.00	45.25					

Sampe (core-depth)	depth (cm)	Age Model (ka)	Sed. Rate (cm/kyr)	d18O Npachy (s)	d18O Gbull	d18O difference	%CaCO3	Sortable Silt
21GGC 4-1	1	0.34						
21GGC 4-2	2	0.36		2.73			41.69	24.97
21GGC 4-3	3	0.39	40.49				42.06	24.98
21GGC 4-4	4	0.41	40.50	2.62	2.49	0.13	31.74	23.61
21GGC 4-5	5	0.44	40.50				40.86	23.75
21GGC 4-6	6	0.46	40.49	2.62	2.10	0.52	40.13	25.13
21GGC 4-7	7	0.49	40.50				40.59	23.10
21GGC 4-8	8	0.51	40.49	2.61	2.49	0.12	38.59	23.03
21GGC 4-9	9	0.54	40.50				40.25	23.38
21GGC 1-50	381	9.03	45.25	2.60	2.01	0.58	21.24	29.86
21GGC 1-51	382	9.05	45.25					
21GGC 1-52	383	9.07	45.25	2.53	2.07	0.46	20.76	29.88
21GGC 1-53	384	9.09	45.25					
21GGC 1-54	385	9.11	46.51	2.63	2.37	0.27	19.46	30.43
21GGC 1-55	386	9.13	46.51					
21GGC 1-56	387	9.16	46.73	2.66	2.07	0.59	19.96	31.59
21GGC 1-57	388	9.18	46.51					
21GGC 1-58	389	9.20	46.73	2.60	2.07	0.53	18.13	31.81
21GGC 1-59	390	9.22	46.73					
21GGC 1-60	391	9.24	46.51	2.56	1.84	0.72	21.72	29.43
21GGC 1-61	392	9.26	46.73					
21GGC 1-62	393	9.28	46.51	2.54	1.77	0.77	21.03	29.31
21GGC 1-63	394	9.31	46.73					
21GGC 1-64	395	9.33	46.51		1.55		19.67	27.80
21GGC 1-65	396	9.35	46.73					
21GGC 1-66	397	9.37	46.73	2.51	1.93	0.58	17.21	27.85
21GGC 1-67	398	9.39	46.51					
21GGC 1-68	399	9.41	46.73	2.69	2.05	0.64	16.79	26.99
21GGC 1-69	400	9.43	46.51					
21GGC 1-70	401	9.46	46.73	2.58	2.15	0.43	17.30	28.15
21GGC 1-71	402	9.48	46.51					
21GGC 1-72	403	9.50	46.73	2.63	1.83	0.80	15.64	28.98
21GGC 1-73	404	9.51	46.51					
21GGC 1-74	405	9.52	68.03	2.67	1.53	1.14	16.27	27.65
21GGC 1-75	406	9.54	86.96					
21GGC 1-76	407	9.55	87.72		1.95		15.60	27.83
21GGC 1-77	408	9.56	87.72					
21GGC 1-78	409	9.57	86.96	2.82	2.25	0.57	14.53	27.82
21GGC 1-79	410	9.58	87.72					
21GGC 1-80	411	9.59	87.72	2.67	1.75	0.93	15.01	28.53
21GGC 1-81	412	9.60	86.96					
21GGC 1-82	413	9.62	87.72	2.75	1.70	1.04	15.57	27.28
21GGC 1-83	414	9.63	87.72					

Sampe (core-depth)	depth (cm)	Age Model (ka)	Sed. Rate (cm/kyr)	d18O Npachy (s)	d18O Gbull	d18O difference	%CaCO3	Sortable Silt
21GGC 4-1	1	0.34						
21GGC 4-2	2	0.36		2.73			41.69	24.97
21GGC 4-3	3	0.39	40.49				42.06	24.98
21GGC 4-4	4	0.41	40.50	2.62	2.49	0.13	31.74	23.61
21GGC 4-5	5	0.44	40.50				40.86	23.75
21GGC 4-6	6	0.46	40.49	2.62	2.10	0.52	40.13	25.13
21GGC 4-7	7	0.49	40.50				40.59	23.10
21GGC 4-8	8	0.51	40.49	2.61	2.49	0.12	38.59	23.03
21GGC 4-9	9	0.54	40.50				40.25	23.38
21GGC 1-84	415	9.64	86.96	2.76	1.05	1.71	14.88	27.11
21GGC 1-85	416	9.65	87.72					
21GGC 1-86	417	9.66	87.72	2.54	2.12	0.42	14.68	28.26
21GGC 1-87	418	9.67	86.96					
21GGC 1-88	419	9.68	87.72	2.70			15.23	28.40
21GGC 1-89	420	9.70	87.72					
21GGC 1-90	421	9.71	86.96	2.62	2.06	0.56	14.40	27.52
21GGC 1-91	422	9.72	87.72					
21GGC 1-92	423	9.73	87.72	2.60	2.05	0.55	15.85	27.60
21GGC 1-93	424	9.74	86.96					
21GGC 1-94	425	9.75	96.15	2.55	1.93	0.62	14.92	27.71
21GGC 1-95	426	9.76	104.17					
21GGC 1-96	427	9.77	105.26	2.21	2.29		14.00	27.75
21GGC 1-97	428	9.78	105.26					
21GGC 1-98	429	9.79	104.17	2.59	2.07	0.53	14.31	26.81
21GGC 1-99	430	9.80	105.26					
21GGC 1-100	431	9.81	104.17	2.68	2.10	0.58	14.70	27.16
21GGC 1-101	432	9.82	105.26					
21GGC 1-102	433	9.83	105.26	2.34	2.22	0.12	14.70	27.41
21GGC 1-103	434	9.84	104.17					
21GGC 1-104	435	9.85	105.26	2.43	2.15	0.28	14.91	27.36
21GGC 1-105	436	9.86	105.26					
21GGC 1-106	437	9.86	104.17	2.63	2.27	0.36	13.38	28.44
21GGC 1-107	438	9.87	105.26					
21GGC 1-108	439	9.88	105.26	2.56	2.07	0.49	13.42	27.54
21GGC 1-109	440	9.89	104.17					
21GGC 1-110	441	9.90	105.26	2.61	2.29	0.32	14.22	27.58
21GGC 1-111	442	9.91	104.17					
21GGC 1-112	443	9.92	105.26	2.38	1.91	0.47	12.26	28.85
21GGC 1-113	444	9.93	105.26					
21GGC 1-114	445	9.94	109.89	2.81	2.40	0.41	11.92	27.92
21GGC 1-115	446	9.95	125.00					
21GGC 1-116	447	9.96	123.46	2.41	2.07	0.34	11.85	26.56
21GGC 1-117	448	9.96	123.46					

Sampe (core-depth)	depth (cm)	Age Model (ka)	Sed. Rate (cm/kyr)	d18O Npachy (s)	d18O Gbull	d18O difference	%CaCO3	Sortable Silt
21GGC 4-1	1	0.34						
21GGC 4-2	2	0.36		2.73			41.69	24.97
21GGC 4-3	3	0.39	40.49				42.06	24.98
21GGC 4-4	4	0.41	40.50	2.62	2.49	0.13	31.74	23.61
21GGC 4-5	5	0.44	40.50				40.86	23.75
21GGC 4-6	6	0.46	40.49	2.62	2.10	0.52	40.13	25.13
21GGC 4-7	7	0.49	40.50				40.59	23.10
21GGC 4-8	8	0.51	40.49	2.61	2.49	0.12	38.59	23.03
21GGC 4-9	9	0.54	40.50				40.25	23.38
21GGC 1-118	449	9.97	123.46	2.69	2.17	0.52	12.55	26.23
21GGC 1-119	450	9.98	125.00					
21GGC 1-120	451	9.99	123.46	2.24	2.15	0.09	12.40	27.43
21GGC 1-121	452	10.00	123.46					
21GGC 1-122	453	10.00	123.46	2.54	2.17	0.37	12.05	26.24
21GGC 1-123	454	10.01	121.95					
21GGC 1-124	455	10.02	125.00	2.68	1.96	0.72	10.72	27.37
21GGC 1-125	456	10.03	125.00					
21GGC 1-126	457	10.04	125.00	2.47	1.72	0.75	12.31	26.31
21GGC 1-127	458	10.04	125.00					
21GGC 1-128	459	10.05	125.00	2.45	2.28	0.16	11.10	25.66
21GGC 1-129	460	10.06	125.00					
21GGC 1-130	461	10.07	125.00	2.42	2.15	0.28	11.78	26.40
21GGC 1-131	462	10.08	125.00					
21GGC 1-132	463	10.09	111.11	2.55	2.04	0.51	9.54	25.61
21GGC 1-133	464	10.09	125.00					
21GGC 1-134	465	10.10	142.86		2.13		10.88	25.01
21GGC 1-135	466	10.11	142.86					
21GGC 1-136	467	10.11	142.86	2.48			9.91	24.12
21GGC 1-137	468	10.12	142.86					
21GGC 1-138	469	10.13	142.86	2.83	2.26	0.57	10.06	25.81
21GGC 1-139	470	10.13	142.86					
21GGC 1-140	471	10.14	142.86	2.40	2.15	0.25	11.14	26.24
21GGC 1-141	472	10.15	142.86					
21GGC 1-142	473	10.16	142.86				8.96	26.23
21GGC 1-143	474	10.16	142.86					
21GGC 1-144	475	10.17	142.86				5.95	24.42
21GGC 1-145	476	10.18	142.86					
21GGC 1-146	477	10.18	142.86				5.84	22.38
21GGC 1-147	478	10.19	142.86					
21GGC 1-148	479	10.20	166.67				5.71	24.13
21GGC 1-149	480	10.20	142.86					
21GGC 1-150	481	10.21	142.86				5.09	25.24
21GGC 1-151	482	10.22	142.86					

Appendix B

Leg	Site	H	Core	Section	Top(cm)	Bot(cm)	Depth(mbsf)	Depth(mcd)	Age (kyr)	%CaCO3	%SiO2	Sortable Silt
303	1305	B	1	1	4	5	0.04	0.04	0.024146	42.246	6.768	
303	1305	B	1	1	9	10	0.09	0.09	0.054328	43.390	8.998	
303	1305	B	1	1	14	15	0.14	0.14	0.08451	40.197	8.297	
303	1305	B	1	1	19	20	0.19	0.19	0.11469	43.446	8.202	
303	1305	B	1	1	24	25	0.24	0.24	0.14487	41.781	8.682	
303	1305	B	1	1	29	30	0.29	0.29	0.17506	40.044	8.294	
303	1305	B	1	1	34	35	0.34	0.34	0.20524	41.775	6.994	
303	1305	B	1	1	39	40	0.39	0.39	0.23632	41.411	7.478	
303	1305	B	1	1	44	45	0.44	0.44	0.26774	41.769	6.545	
303	1305	B	1	1	49	50	0.49	0.49	0.29917	42.294	7.484	
303	1305	B	1	1	54	55	0.54	0.54	0.33059	41.949	7.350	
303	1305	B	1	1	59	60	0.59	0.59	0.36201	42.324	8.623	
303	1305	B	1	1	64	65	0.64	0.64	0.39343	42.405	8.311	
303	1305	B	1	1	69	70	0.69	0.69	0.42485	42.001	8.100	
303	1305	B	1	1	74	75	0.74	0.74	0.45714	40.368	8.238	
303	1305	B	1	1	79	80	0.79	0.79	0.48988	39.573	7.430	
303	1305	B	1	1	84	85	0.84	0.84	0.52261	40.789	6.573	
303	1305	B	1	1	89	90	0.89	0.89	0.55535	38.198	7.121	
303	1305	B	1	1	94	95	0.94	0.94	0.58809	36.750	7.528	
303	1305	B	1	1	99	100	0.99	0.99	0.62083	38.415	6.381	
303	1305	B	1	1	104	105	1.04	1.04	0.65357	39.155	5.951	
303	1305	B	1	1	109	110	1.09	1.09	0.68713	35.634	5.517	
303	1305	B	1	1	114	115	1.14	1.14	0.72127	37.241	5.704	
303	1305	B	1	1	119	120	1.19	1.19	0.75541	36.088	5.233	
303	1305	B	1	1	124	125	1.24	1.24	0.78955	36.205	5.846	
303	1305	B	1	1	129	130	1.29	1.29	0.82369	33.713	5.082	
303	1305	B	1	1	134	135	1.34	1.34	0.85783	35.778	6.786	
303	1305	B	1	1	139	140	1.39	1.39	0.89197	35.629	4.750	
303	1305	B	1	1	144	145	1.44	1.44	0.92688	34.912	6.301	
303	1305	B	1	1	149	150	1.49	1.49	0.96251	33.509	5.705	
303	1305	B	1	2	4	5	1.54	1.54	0.99814	-14.297	0.006	
303	1305	B	1	2	9	10	1.59	1.59	1.0338	30.611	5.990	
303	1305	B	1	2	14	15	1.64	1.64	1.0694	33.079	7.184	
303	1305	B	1	2	19	20	1.69	1.69	1.105	30.950	13.338	
303	1305	B	1	2	24	25	1.74	1.74	1.1407	32.626	7.471	
303	1305	B	1	2	29	30	1.79	1.79	1.177	30.537	7.208	
303	1305	B	1	2	34	35	1.84	1.84	1.2142	32.893		
303	1305	B	1	2	39	40	1.89	1.89	1.2515	33.323		
303	1305	B	1	2	44	45	1.94	1.94	1.2887	32.461		
303	1305	B	1	2	49	50	1.99	1.99	1.3259	32.777		
303	1305	B	1	2	54	55	2.04	2.04	1.3632	31.502		
303	1305	B	1	2	59	60	2.09	2.09	1.4004	30.689		
303	1305	B	1	2	64	65	2.14	2.14	1.4382	30.162		

Leg	Site	H	Core	Section	Top(cm)	Bot(cm)	Depth(mbsf)	Depth(mcd)	Age (kyr)	%CaCO3	%SiO2	Sortable Silt
303	1305	B	1	2	69	70	2.19	2.19	1.4772	28.838		
303	1305	B	1	2	74	75	2.24	2.24	1.5161	27.985		
303	1305	B	1	2	79	80	2.29	2.29	1.555	29.802		
303	1305	B	1	2	84	85	2.34	2.34	1.594	29.973		
303	1305	B	1	2	89	90	2.39	2.39	1.6329	30.190		
303	1305	B	1	2	94	95	2.44	2.44	1.6718	29.996		
303	1305	B	1	2	99	100	2.49	2.49	1.7113	30.565		
303	1305	B	1	2	104	105	2.54	2.54	1.7521	31.336		
303	1305	B	1	2	109	110	2.59	2.59	1.7928	30.533		
303	1305	B	1	2	114	115	2.64	2.64	1.8336	33.068		
303	1305	B	1	2	119	120	2.69	2.69	1.8743	31.056		
303	1305	B	1	2	124	125	2.74	2.74	1.9151	29.381		
303	1305	B	1	2	129	130	2.79	2.79	1.9558	32.072		
303	1305	B	1	2	134	135	2.84	2.84	1.997	27.707		
303	1305	B	1	2	139	140	2.89	2.89	2.0397	32.076		
303	1305	B	1	2	144	145	2.94	2.94	2.0825	30.427		
303	1305	B	1	2	149	150	2.99	2.99	2.1252	30.241		
303	1305	B	1	3	4	5	3.04	3.04	2.1679	31.236		
303	1305	B	1	3	9	10	3.09	3.09	2.2106	32.017		
303	1305	B	1	3	14	15	3.14	3.14	2.2533	30.847		
303	1305	B	1	3	19	20	3.19	3.19	2.2963	32.323		
303	1305	B	1	3	24	25	3.24	3.24	2.3411	29.908		
303	1305	B	1	3	29	30	3.29	3.29	2.3859	31.236		
303	1305	B	1	3	34	35	3.34	3.34	2.4307	31.900		
303	1305	B	1	3	39	40	3.39	3.39	2.4755	26.907		
303	1305	B	1	3	44	45	3.44	3.44	2.5204	29.741		
303	1305	B	1	3	49	50	3.49	3.49	2.5652	27.879		
303	1305	B	1	3	54	55	3.54	3.54	2.6102	27.276		
303	1305	B	1	3	59	60	3.59	3.59	2.6572	25.473		
303	1305	B	1	3	64	65	3.64	3.64	2.7043	27.347		
303	1305	B	1	3	69	70	3.69	3.69	2.7514	26.448		
303	1305	B	1	3	74	75	3.74	3.74	2.7984	25.822		
303	1305	B	1	3	79	80	3.79	3.79	2.8455	25.027		
303	1305	B	1	3	84	85	3.84	3.84	2.8925	25.101		
303	1305	B	1	3	89	90	3.89	3.89	2.9396	24.656		
303	1305	B	1	3	94	95	3.94	3.94	2.9891	24.661		
303	1305	B	1	3	99	100	3.99	3.99	3.0386	26.991		
303	1305	B	1	3	104	105	4.04	4.04	3.0881	26.276		
303	1305	B	1	3	109	110	4.09	4.09	3.1376	26.411		
303	1305	B	1	3	114	115	4.14	4.14	3.1871	25.509		
303	1305	B	1	3	119	120	4.19	4.19	3.2366	23.894		
303	1305	B	1	3	124	125	4.24	4.24	3.2861	25.288		
303	1305	B	1	3	129	130	4.29	4.29	3.3381	24.515		
303	1305	B	1	3	134	135	4.34	4.34	3.3902	22.059		
303	1305	B	1	3	139	140	4.39	4.39	3.4423	22.501		
303	1305	B	1	3	144	145	4.44	4.44	3.4944	21.639		

Leg	Site	H	Core	Section	Top(cm)	Bot(cm)	Depth(mbsf)	Depth(mcd)	Age (kyr)	%CaCO3	%SiO2	Sortable Silt
303	1305	B	1	3	149	150	4.49	4.49	3.5465	21.976		
303	1305	B	1	4	4	5	4.54	4.54	3.5987	22.645		
303	1305	B	1	4	9	10	4.59	4.59	3.6508	23.748		
303	1305	B	1	4	14	15	4.64	4.64	3.7054	23.119		
303	1305	B	1	4	19	20	4.69	4.69	3.7603	24.920		
303	1305	B	1	4	24	25	4.74	4.74	3.8153	17.882		
303	1305	B	1	4	29	30	4.79	4.79	3.8703	17.810		
303	1305	B	1	4	34	35	4.84	4.84	3.9252	17.573		
303	1305	B	1	4	39	40	4.89	4.89	3.9802	15.519		
303	1305	B	1	4	44	45	4.94	4.94	4.0351	14.346		
303	1305	B	1	4	49	50	4.99	4.99	4.0926	15.614		
303	1305	B	1	4	54	55	5.04	5.04	4.1506	13.984		
303	1305	B	1	4	59	60	5.09	5.09	4.2086	11.111		
303	1305	B	1	4	64	65	5.14	5.14	4.2667	9.729		
303	1305	B	1	4	69	70	5.19	5.19	4.3247	9.091		
303	1305	B	1	4	74	75	5.24	5.24	4.3827	23.745		
303	1305	B	1	4	79	80	5.29	5.29	4.4408	25.420		
303	1305	B	1	4	84	85	5.34	5.34	4.5013	24.687		
303	1305	B	1	4	89	90	5.39	5.39	4.5626	23.508		
303	1305	B	1	4	94	95	5.44	5.44	4.624	26.145		
303	1305	B	1	4	99	100	5.49	5.49	4.6854	26.608	4.632	
303	1305	B	1	4	104	105	5.54	5.54	4.7468	28.430	4.832	
303	1305	B	1	4	109	110	5.59	5.59	4.8081	26.940	5.718	
303	1305	B	1	4	114	115	5.64	5.64	4.8695	23.486	4.070	
303	1305	B	1	4	119	120	5.69	5.69	4.9333	23.964	5.039	
303	1305	B	1	4	124	125	5.74	5.74	4.9983	20.514	5.088	
303	1305	B	1	4	129	130	5.79	5.79	5.0634	22.152	4.120	
303	1305	B	1	4	134	135	5.84	5.84	5.1284	22.680	3.895	
303	1305	B	1	4	139	140	5.89	5.89	5.1934	22.726	5.038	
303	1305	B	1	4	144	145	5.94	5.94	5.2584	21.137	5.041	
303	1305	B	1	4	149	150	5.99	5.99	5.3234	22.104	4.664	
303	1305	B	1	5	4	5	6.04	6.04	5.3908	23.494	5.229	
303	1305	B	1	5	9	10	6.09	6.09	5.4598	22.063	5.541	
303	1305	B	1	5	14	15	6.14	6.14	5.5288	19.854	5.124	
303	1305	B	1	5	19	20	6.19	6.19	5.5978	19.565	4.905	
303	1305	B	1	5	24	25	6.24	6.24	5.6668	20.006	5.281	
303	1305	B	1	5	29	30	6.29	6.29	5.7358	18.249	4.487	
303	1305	B	1	5	34	35	6.34	6.34	5.8048	18.835	3.817	
303	1305	B	1	5	39	40	6.39	6.39	5.876	17.625	4.592	
303	1305	B	1	5	44	45	6.44	6.44	5.9494	16.739	4.652	
303	1305	B	1	5	49	50	6.49	6.49	6.0227	18.333	4.943	
303	1305	B	1	5	54	55	6.54	6.54	6.0961	18.997	5.052	
303	1305	B	1	5	59	60	6.59	6.59	6.1694	17.583	5.092	
303	1305	B	1	5	64	65	6.64	6.64	6.2427	18.405	4.419	
303	1305	B	1	5	69	70	6.69	6.69	6.3161	17.031	3.766	
303	1305	B	1	5	74	75	6.74	6.74	6.3916	18.435	4.558	

Leg	Site	H	Core	Section	Top(cm)	Bot(cm)	Depth(mbsf)	Depth(mcd)	Age (kyr)	%CaCO3	%SiO2	Sortable Silt
303	1305	B	1	5	79	80	6.79	6.79	6.4697	16.937	3.854	
303	1305	B	1	5	84	85	6.84	6.84	6.5478	17.338	5.160	
303	1305	B	1	5	89	90	6.89	6.89	6.626	17.119	4.653	
303	1305	B	1	5	94	95	6.94	6.94	6.7041	17.565	4.295	
303	1305	B	1	5	99	100	6.99	6.99	6.7822	16.650	4.148	
303	1305	B	1	5	104	105	7.04	7.04	6.8603	15.980	4.507	
303	1305	B	1	5	109	110	7.09	7.09	6.9404	16.802	5.289	
303	1305	B	1	5	114	115	7.14	7.14	7.0238	15.107	3.640	
303	1305	B	1	5	119	120	7.19	7.19	7.1072	15.724	3.858	
303	1305	B	1	5	124	125	7.24	7.24	7.1906	13.054		
303	1305	B	1	5	129	130	7.29	7.29	7.2739	13.487		
303	1305	B	1	5	134	135	7.34	7.34	7.3573	13.951		
303	1305	B	1	5	139	140	7.39	7.39	7.4407	12.616		
303	1305	B	1	5	144	145	7.44	7.44	7.5259	10.810		
303	1305	B	1	5	149	150	7.49	7.49	7.6151	11.602		
303	1305	A	1	3	64	65	3.64	7.52	7.6686	12.105	2.401	19.61
303	1305	B	1	6	4	5	7.54	7.54	7.7043	12.843		
303	1305	A	1	3	69	70	3.69	7.57	7.7578	11.033	2.233	19.49
303	1305	A	1	3	74	75	3.74	7.62	7.8469	6.167	1.079	17.939
303	1305	A	1	3	79	80	3.79	7.67	7.9361	5.295	1.090	19.221
303	1305	A	1	3	84	85	3.84	7.72	8.0253	7.528	1.620	17.831
303	1305	A	1	3	89	90	3.89	7.77	8.1145	5.591	1.303	22.284
303	1305	A	1	3	94	95	3.94	7.82	8.2091	4.168	1.205	25.799
303	1305	A	1	3	99	100	3.99	7.87	8.3047	4.507	0.915	27.249
303	1305	A	1	3	104	105	4.04	7.92	8.4003	13.842	2.289	23.707
303	1305	A	1	3	109	110	4.09	7.97	8.4959	11.157	2.475	22.782
303	1305	A	1	3	114	115	4.14	8.02	8.5916	12.312	2.294	21.738
303	1305	A	1	3	119	120	4.19	8.07	8.6872	11.111	1.950	21.313
303	1305	A	1	3	124	125	4.24	8.12	8.7828	9.730	2.347	20.145
303	1305	A	1	3	129	130	4.29	8.17	8.8839	10.802	2.644	20.998
303	1305	A	1	3	134	135	4.34	8.22	8.9867	9.952	2.377	20.236
303	1305	A	1	3	139	140	4.39	8.27	9.0895	8.857	2.418	19.04
303	1305	A	1	3	144	145	4.44	8.32	9.1923	9.207	1.686	15.717
303	1305	A	1	3	149	150	4.49	8.37	9.295	7.124	1.611	15.832
303	1305	A	1	4	4	5	4.54	8.42	9.3978	5.232	1.261	18.225
303	1305	A	1	4	9	10	4.59	8.47	9.5006	11.059	2.364	19.275
303	1305	A	1	4	14	15	4.64	8.52	9.609	15.234	2.328	19.529
303	1305	A	1	4	19	20	4.69	8.57	9.7197	12.071	2.406	21.101
303	1305	A	1	4	24	25	4.74	8.62	9.8305	13.617	2.415	20.241
303	1305	A	1	4	29	30	4.79	8.67	9.9413	12.442	2.905	22.405
303	1305	A	1	4	34	35	4.84	8.72	10.052	14.210	2.643	23.587
303	1305	A	1	4	39	40	4.89	8.77	10.163	13.632	2.599	22.76
303	1305	A	1	4	44	45	4.94	8.82	10.274	11.894	1.717	17.534
303	1305	A	1	4	49	50	4.99	8.87	10.39	10.851	2.158	21.46
303	1305	A	1	4	54	55	5.04	8.92	10.51	11.152	2.783	22.421
303	1305	A	1	4	59	60	5.09	8.97	10.629	10.882	3.252	21.804

Leg	Site	H	Core	Section	Top(cm)	Bot(cm)	Depth(mbsf)	Depth(mcd)	Age (kyr)	%CaCO3	%SiO2	Sortable Silt
303	1305	A	1	4	64	65	5.14	9.02	10.749	9.885	1.968	20.709
303	1305	A	1	4	69	70	5.19	9.07	10.869	10.429	2.051	22.057
303	1305	A	1	4	74	75	5.24	9.12	10.989	9.294	2.258	20.675
303	1305	A	1	4	79	80	5.29	9.17	11.108	10.316	2.322	16.093
303	1305	A	1	4	84	85	5.34	9.22	11.234	11.017	2.113	23.215
303	1305	A	1	4	89	90	5.39	9.27	11.364	11.253	1.764	21.811
303	1305	A	1	4	94	95	5.44	9.32	11.493	11.188	2.320	22.622
303	1305	A	1	4	99	100	5.49	9.37	11.623	9.879	2.007	21.941
303	1305	A	1	4	104	105	5.54	9.42	11.753	10.846	2.054	21.751
303	1305	A	1	4	109	110	5.59	9.47	11.883	10.324	2.014	21.878
303	1305	A	1	4	114	115	5.64	9.52	12.013	7.267	1.785	18.977
303	1305	A	1	4	119	120	5.69	9.57	12.148	9.604	1.463	16.385
303	1305	A	1	4	124	125	5.74	9.62	12.289	12.642	3.014	22.349
303	1305	A	1	4	129	130	5.79	9.67	12.431	14.120	2.545	12.324
303	1305	A	1	4	134	135	5.84	9.72	12.572	15.275	2.514	21.46
303	1305	A	1	4	139	140	5.89	9.77	12.713	14.258	2.294	19.954
303	1305	A	1	4	144	145	5.94	9.82	12.854	20.382	3.468	
303	1305	A	1	4	149	150	5.99	9.87	12.996	16.574	2.452	19.863
303	1305	A	1	5	4	5	6.04	9.92	13.165	17.835	3.288	18.127
303	1305	A	1	5	9	10	6.09	9.97	13.372	16.188	2.252	16.54
303	1305	A	1	5	14	15	6.14	10.02	13.58	16.125	2.907	17.905
303	1305	A	1	5	19	20	6.19	10.07	13.787	16.667	2.312	18.672
303	1305	A	1	5	24	25	6.24	10.12	13.995	17.616	3.016	12.152
303	1305	A	1	5	29	30	6.29	10.17	14.202	17.514	3.137	15.745
303	1305	A	1	5	34	35	6.34	10.22	14.41	19.977	3.245	14.674
303	1305	A	1	5	39	40	6.39	10.27	15.006	18.119	3.567	19.845
303	1305	B	2	1	139	140	9.69	10.31	16.062	14.883		
303	1305	B	2	1	144	145	9.74	10.36	17.382	15.337		
303	1305	B	2	1	149	150	9.79	10.41	18.702	13.245		
303	1305	B	2	2	4	5	9.84	10.46	20.022	10.668		
303	1305	B	2	2	9	10	9.89	10.51	21.342	9.356		
303	1305	B	2	2	14	15	9.94	10.56	22.662	4.579		
303	1305	B	2	2	19	20	9.99	10.61	23.952	5.270		
303	1305	B	2	2	24	25	10.04	10.66	24.888	7.176		
303	1305	B	2	2	29	30	10.09	10.71	25.824	11.411		
303	1305	B	2	2	34	35	10.14	10.76	26.761	11.672		
303	1305	B	2	2	39	40	10.19	10.81	27.697	12.442		
303	1305	B	2	2	44	45	10.24	10.86	28.634	18.047		
303	1305	B	2	2	49	50	10.29	10.91	29.57	20.979		
303	1305	B	2	2	54	55	10.34	10.96	30.504	14.951		
303	1305	B	2	2	59	60	10.39	11.01	31.159	14.627		
303	1305	B	2	2	64	65	10.44	11.06	31.814	14.437		
303	1305	B	2	2	69	70	10.49	11.11	32.469	12.746		
303	1305	B	2	2	74	75	10.54	11.16	33.123	12.092		
303	1305	B	2	2	79	80	10.59	11.21	33.778	13.538		
303	1305	B	2	2	84	85	10.64	11.26	34.433	12.563		

Leg	Site	H	Core	Section	Top(cm)	Bot(cm)	Depth(mbsf)	Depth(mcd)	Age (kyr)	%CaCO3	%SiO2	Sortable Silt
303	1305	B	2	2	89	90	10.69	11.31	35.088	12.718		
303	1305	B	2	2	94	95	10.74	11.36	35.597	12.856		
303	1305	B	2	2	99	100	10.79	11.41	36.097	12.397		
303	1305	B	2	2	104	105	10.84	11.46	36.596	9.058		
303	1305	B	2	2	109	110	10.89	11.51	37.096	9.080		
303	1305	B	2	2	114	115	10.94	11.56	37.596	11.489		
303	1305	B	2	2	119	120	10.99	11.61	38.095	12.403		
303	1305	B	2	2	124	125	11.04	11.66	38.595	11.716		
303	1305	B	2	2	129	130	11.09	11.71	38.988	12.948		
303	1305	B	2	2	134	135	11.14	11.76	39.366	16.733		
303	1305	B	2	2	139	140	11.19	11.81	39.743	23.477		
303	1305	B	2	2	144	145	11.24	11.86	40.121	27.009		
303	1305	B	2	2	149	150	11.29	11.91	40.498	18.458		
303	1305	B	2	3	4	5	11.34	11.96	40.876	13.851		
303	1305	B	2	3	9	10	11.39	12.01	41.253	13.657		
303	1305	B	2	3	14	15	11.44	12.06	41.57	13.456		
303	1305	B	2	3	19	20	11.49	12.11	41.871	13.674		
303	1305	B	2	3	24	25	11.54	12.16	42.172	15.704		
303	1305	B	2	3	29	30	11.59	12.21	42.473	15.047		
303	1305	B	2	3	34	35	11.64	12.26	42.774	13.875		
303	1305	B	2	3	39	40	11.69	12.31	43.075	15.045		
303	1305	B	2	3	44	45	11.74	12.36	43.376	14.628		
303	1305	B	2	3	49	50	11.79	12.41	43.668	20.626		
303	1305	B	2	3	54	55	11.84	12.46	43.957	18.186		
303	1305	B	2	3	59	60	11.89	12.51	44.246	13.826		
303	1305	B	2	3	64	65	11.94	12.56	44.535	12.447		
303	1305	B	2	3	69	70	11.99	12.61	44.824	10.264		
303	1305	B	2	3	74	75	12.04	12.66	45.114	10.319		
303	1305	B	2	3	79	80	12.09	12.71	45.403	12.702		
303	1305	B	2	3	84	85	12.14	12.76	45.745	20.099		
303	1305	B	2	3	89	90	12.19	12.81	46.117	21.088		
303	1305	B	2	3	94	95	12.24	12.86	46.488	16.911		
303	1305	B	2	3	99	100	12.29	12.91	46.859	16.558		
303	1305	B	2	3	104	105	12.34	12.96	47.23	16.776		
303	1305	B	2	3	109	110	12.39	13.01	47.602	17.398		
303	1305	B	2	3	114	115	12.44	13.06	47.973	18.239		
303	1305	B	2	3	119	120	12.49	13.11	48.476	19.128		
303	1305	B	2	3	124	125	12.54	13.16	49.072	21.604		
303	1305	B	2	3	129	130	12.59	13.21	49.668	21.556		
303	1305	B	2	3	134	135	12.64	13.26	50.265	13.644		
303	1305	B	2	3	139	140	12.69	13.31	50.861	12.612		
303	1305	B	2	3	144	145	12.74	13.36	51.458	11.611		
303	1305	B	2	3	149	150	12.79	13.41	52.054	10.894		
303	1305	B	2	4	4	5	12.84	13.46	53.169	11.749		
303	1305	B	2	4	9	10	12.89	13.51	54.777	11.667		
303	1305	B	2	4	14	15	12.94	13.56	56.384	8.761		

Leg	Site	H	Core	Section	Top(cm)	Bot(cm)	Depth(mbsf)	Depth(mcd)	Age (kyr)	%CaCO3	%SiO2	Sortable Silt
303	1305	B	2	4	19	20	12.99	13.61	57.991	10.720		
303	1305	B	2	4	24	25	13.04	13.66	59.599	11.436		
303	1305	B	2	4	29	30	13.09	13.71	61.206	12.057		
303	1305	B	2	4	34	35	13.14	13.76	62.813	12.077		
303	1305	B	2	4	39	40	13.19	13.81	64.36	12.951		
303	1305	B	2	4	44	45	13.24	13.86	65.83	16.477		
303	1305	B	2	4	49	50	13.29	13.91	67.299	26.263		
303	1305	B	2	4	54	55	13.34	13.96	68.769	25.933		
303	1305	B	2	4	59	60	13.39	14.01	70.239	21.335		
303	1305	B	2	4	64	65	13.44	14.06	71.709	18.616		
303	1305	B	2	4	69	70	13.49	14.11	73.179	20.546		
303	1305	B	2	4	74	75	13.54	14.16	74.199	20.669		
303	1305	B	2	4	79	80	13.59	14.21	74.461	21.293		
303	1305	B	2	4	84	85	13.64	14.26	74.722	20.864		
303	1305	B	2	4	89	90	13.69	14.31	74.983	21.310		
303	1305	B	2	4	94	95	13.74	14.36	75.245	31.698		
303	1305	B	2	4	99	100	13.79	14.41	75.506	32.088		
303	1305	B	2	4	104	105	13.84	14.46	75.767	32.865		
303	1305	B	2	4	109	110	13.89	14.51	76.007	32.526		
303	1305	B	2	4	114	115	13.94	14.56	76.197	29.985		
303	1305	B	2	4	119	120	13.99	14.61	76.387	31.230		
303	1305	B	2	4	124	125	14.04	14.66	76.577	31.348		
303	1305	B	2	4	129	130	14.09	14.71	76.767	27.221		
303	1305	B	2	4	134	135	14.14	14.76	76.957	26.638		
303	1305	B	2	4	139	140	14.19	14.81	77.147	27.340		
303	1305	B	2	4	144	145	14.24	14.86	77.329	26.303		
303	1305	B	2	4	149	150	14.29	14.91	77.482	24.622		
303	1305	B	2	5	4	5	14.34	14.96	77.635	22.032		
303	1305	B	2	5	9	10	14.39	15.01	77.789	20.740		
303	1305	B	2	5	14	15	14.44	15.06	77.942	18.122		
303	1305	B	2	5	19	20	14.49	15.11	78.096	17.518		
303	1305	B	2	5	24	25	14.54	15.16	78.249	15.752		
303	1305	B	2	5	29	30	14.59	15.21	78.401	11.259		
303	1305	B	2	5	34	35	14.64	15.26	78.547	11.855		
303	1305	B	2	5	39	40	14.69	15.31	78.693	10.355		
303	1305	B	2	5	44	45	14.74	15.36	78.838	8.686		
303	1305	B	2	5	49	50	14.79	15.41	78.984	10.839		
303	1305	B	2	5	54	55	14.84	15.46	79.129	14.151		
303	1305	B	2	5	59	60	14.89	15.51	79.275	14.108		
303	1305	B	2	5	64	65	14.94	15.56	79.422	16.956		
303	1305	B	2	5	69	70	14.99	15.61	79.584	15.529		
303	1305	B	2	5	74	75	15.04	15.66	79.745	12.291		
303	1305	B	2	5	79	80	15.09	15.71	79.907	13.294		
303	1305	B	2	5	84	85	15.14	15.76	80.069	13.068		
303	1305	B	2	5	89	90	15.19	15.81	80.231	11.874		
303	1305	B	2	5	94	95	15.24	15.86	80.392	11.053		

Leg	Site	H	Core	Section	Top(cm)	Bot(cm)	Depth(mbsf)	Depth(mcd)	Age (kyr)	%CaCO3	%SiO2	Sortable Silt
303	1305	B	2	5	99	100	15.29	15.91	80.555	15.589		
303	1305	A	2	2	104	105	11.44	15.96	80.753	12.826	3.410	16.113
303	1305	A	2	2	109	110	11.49	16.01	80.951	16.290	2.846	17.544
303	1305	A	2	2	114	115	11.54	16.06	81.149	18.439	3.378	16.972
303	1305	A	2	2	119	120	11.59	16.11	81.347	14.304	2.585	18.284
303	1305	A	2	2	124	125	11.64	16.16	81.545	14.838	3.093	17.764
303	1305	A	2	2	129	130	11.69	16.21	81.743	12.267	1.944	17.391
303	1305	A	2	2	134	135	11.74	16.26	81.941	12.658	2.325	17.359
303	1305	A	2	2	139	140	11.79	16.31	82.19	13.662	2.956	18.198
303	1305	A	2	2	144	145	11.84	16.36	82.441	15.427	2.647	18.892
303	1305	A	2	2	149	150	11.89	16.41	82.692	15.713	2.438	12.26
303	1305	A	2	3	4	5	11.94	16.46	82.944	14.832	3.322	19.444
303	1305	A	2	3	9	10	11.99	16.51	83.195	12.414	2.766	18.324
303	1305	A	2	3	14	15	12.04	16.56	83.447	11.475	1.944	17.725
303	1305	A	2	3	19	20	12.09	16.61	83.698	12.629	2.531	17.563
303	1305	A	2	3	24	25	12.14	16.66	84.013	12.473	1.660	17.147
303	1305	A	2	3	29	30	12.19	16.71	84.338	15.026	2.348	17.774
303	1305	A	2	3	34	35	12.24	16.76	84.662	14.165	2.079	17.197
303	1305	A	2	3	39	40	12.29	16.81	84.986	10.886	1.605	16.115
303	1305	A	2	3	44	45	12.34	16.86	85.31	11.699	1.807	15.857
303	1305	A	2	3	49	50	12.39	16.91	85.634	13.975	2.005	15.394
303	1305	A	2	3	54	55	12.44	16.96	85.958	17.310	2.534	15.522
303	1305	A	2	3	59	60	12.49	17.01	86.431	16.570	2.045	15.024
303	1305	A	2	3	64	65	12.54	17.06	86.939	17.952	2.282	16.361
303	1305	A	2	3	69	70	12.59	17.11	87.447	21.226	2.883	12.076
303	1305	A	2	3	74	75	12.64	17.16	87.955	16.575	1.935	12.118
303	1305	A	2	3	79	80	12.69	17.21	88.463	15.464	2.293	12.111
303	1305	A	2	3	84	85	12.74	17.26	88.971	12.702	1.782	15.187
303	1305	A	2	3	89	90	12.79	17.31	89.479	12.773	1.357	12.107
303	1305	A	2	3	94	95	12.84	17.36	89.91	11.595	1.359	12.146
303	1305	A	2	3	99	100	12.89	17.41	90.313	12.670	1.328	14.753
303	1305	A	2	3	104	105	12.94	17.46	90.717	15.110	2.059	14.983
303	1305	A	2	3	109	110	12.99	17.51	91.12	14.537	1.888	16.042
303	1305	A	2	3	114	115	13.04	17.56	91.523	13.703	2.237	12.169
303	1305	A	2	3	119	120	13.09	17.61	91.927	13.464	2.806	16.482
303	1305	A	2	3	124	125	13.14	17.66	92.33	12.549	2.211	16.168
303	1305	A	2	3	129	130	13.19	17.71	92.604	14.080	2.156	16.768
303	1305	A	2	3	134	135	13.24	17.76	92.813	13.970	2.529	16.389
303	1305	A	2	3	139	140	13.29	17.81	93.023	14.170	2.169	18.604
303	1305	A	2	3	144	145	13.34	17.86	93.232	10.652	1.711	12.498
303	1305	A	2	3	149	150	13.39	17.91	93.441	10.660	1.783	
303	1305	A	2	4	4	5	13.44	17.96	93.65	12.350	2.326	
303	1305	A	2	4	9	10	13.49	18.01	93.859	10.687	2.480	
303	1305	A	2	4	14	15	13.54	18.06	94.044	9.913	1.942	
303	1305	A	2	4	19	20	13.59	18.11	94.211	10.348	2.059	
303	1305	A	2	4	24	25	13.64	18.16	94.379	10.123	2.239	

Leg	Site	H	Core	Section	Top(cm)	Bot(cm)	Depth(mbsf)	Depth(mcd)	Age (kyr)	%CaCO3	%SiO2	Sortable Silt
303	1305	A	2	4	29	30	13.69	18.21	94.546	9.474	2.008	
303	1305	A	2	4	34	35	13.74	18.26	94.714	10.456	2.511	
303	1305	A	2	4	39	40	13.79	18.31	94.882	12.045	2.983	
303	1305	A	2	4	44	45	13.84	18.36	95.049	12.750	2.434	
303	1305	A	2	4	49	50	13.89	18.41	95.199	10.258	2.494	
303	1305	A	2	4	54	55	13.94	18.46	95.332	9.006	1.587	
303	1305	A	2	4	59	60	13.99	18.51	95.466	10.036	1.961	
303	1305	A	2	4	64	65	14.04	18.56	95.599	11.358	2.227	
303	1305	A	2	4	69	70	14.09	18.61	95.733	11.847	2.001	
303	1305	A	2	4	74	75	14.14	18.66	95.866	12.451	2.708	
303	1305	A	2	4	79	80	14.19	18.71	96	13.022	2.623	
303	1305	A	2	4	84	85	14.24	18.76	96.121	11.513	1.627	
303	1305	A	2	4	89	90	14.29	18.81	96.227	10.925	2.302	
303	1305	A	2	4	94	95	14.34	18.86	96.333	8.897	1.872	
303	1305	A	2	4	99	100	14.39	18.91	96.439	7.718	7.816	
303	1305	A	2	4	104	105	14.44	18.96	96.545	8.167	1.990	
303	1305	A	2	4	109	110	14.49	19.01	96.651	6.829	1.627	
303	1305	A	2	4	114	115	14.54	19.06	96.758	7.679	1.714	
303	1305	A	2	4	119	120	14.59	19.11	96.856	8.003	1.946	
303	1305	A	2	4	124	125	14.64	19.16	96.941	7.760	1.958	
303	1305	A	2	4	129	130	14.69	19.21	97.026	8.378	1.934	
303	1305	A	2	4	134	135	14.74	19.26	97.111	8.911	1.957	
303	1305	A	2	4	139	140	14.79	19.31	97.196	9.735	2.249	
303	1305	A	2	4	144	145	14.84	19.36	97.281	10.574	2.487	
303	1305	A	2	4	149	150	14.89	19.41	97.366	9.466	1.826	
303	1305	A	2	5	4	5	14.94	19.46	97.447	10.763	2.594	
303	1305	A	2	5	9	10	14.99	19.51	97.517	9.054	2.056	
303	1305	A	2	5	14	15	15.04	19.56	97.587	8.303	2.342	
303	1305	A	2	5	19	20	15.09	19.61	97.657	8.576	2.141	
303	1305	A	2	5	24	25	15.14	19.66	97.727	8.671	2.076	
303	1305	A	2	5	29	30	15.19	19.71	97.797	8.827	2.746	
303	1305	A	2	5	34	35	15.24	19.76	97.867	7.991	2.455	
303	1305	A	2	5	39	40	15.29	19.81	97.935	8.719	2.634	
303	1305	A	2	5	44	45	15.34	19.86	97.995	8.396	2.183	
303	1305	A	2	5	49	50	15.39	19.91	98.055	8.726	2.971	
303	1305	A	2	5	54	55	15.44	19.96	98.116	8.132	2.424	
303	1305	A	2	5	59	60	15.49	20.01	98.176	9.420	3.451	
303	1305	A	2	5	64	65	15.54	20.06	98.236	9.606	2.689	
303	1305	A	2	5	69	70	15.59	20.11	98.296	13.492	3.301	
303	1305	A	2	5	74	75	15.64	20.16	98.356	13.545	3.729	
303	1305	A	2	5	79	80	15.69	20.21	98.412	9.728	2.525	
303	1305	A	2	5	84	85	15.74	20.26	98.467	10.376	2.849	
303	1305	A	2	5	89	90	15.79	20.31	98.523	7.849	2.483	
303	1305	A	2	5	94	95	15.84	20.36	98.579	8.315	2.821	
303	1305	A	2	5	99	100	15.89	20.41	98.634	7.085	2.610	
303	1305	A	2	5	104	105	15.94	20.46	98.69	7.195	2.836	

Leg	Site	H	Core	Section	Top(cm)	Bot(cm)	Depth(mbsf)	Depth(mcd)	Age (kyr)	%CaCO3	%SiO2	Sortable Silt
303	1305	A	2	5	109	110	15.99	20.51	98.746	7.535	2.781	
303	1305	A	2	5	114	115	16.04	20.56	98.802	6.817	2.593	
303	1305	A	2	5	119	120	16.09	20.61	98.857	7.072	2.247	
303	1305	A	2	5	124	125	16.14	20.66	98.913	7.835	2.762	
303	1305	A	2	5	129	130	16.19	20.71	98.969	7.583	2.503	
303	1305	A	2	5	134	135	16.24	20.76	99.025	8.152	2.538	
303	1305	A	2	5	139	140	16.29	20.81	99.08	8.974	2.744	
303	1305	A	2	5	144	145	16.34	20.86	99.136	9.011	3.137	
303	1305	A	2	5	149	150	16.39	20.91	99.196	7.427	2.403	
303	1305	A	2	6	4	5	16.44	20.96	99.257	7.331	1.991	
303	1305	A	2	6	9	10	16.49	21.01	99.317	7.389	2.579	
303	1305	A	2	6	14	15	16.54	21.06	99.377	7.542	2.774	
303	1305	A	2	6	19	20	16.59	21.11	99.437	6.786	2.589	
303	1305	A	2	6	24	25	16.64	21.16	99.498	7.182	2.453	
303	1305	A	2	6	29	30	16.69	21.21	99.558	7.935	2.832	
303	1305	A	2	6	34	35	16.74	21.26	99.626	9.589	3.182	
303	1305	A	2	6	39	40	16.79	21.31	99.695	8.861	3.103	
303	1305	A	2	6	44	45	16.84	21.36	99.764	9.944	2.633	
303	1305	A	2	6	49	50	16.89	21.41	99.833	10.471	3.142	
303	1305	A	2	6	54	55	16.94	21.46	99.902	9.210	2.908	
303	1305	A	2	6	59	60	16.99	21.51	99.971	6.727	1.851	19.688
303	1305	A	2	6	64	65	17.04	21.56	100.04	9.494	2.640	12.038
303	1305	A	2	6	69	70	17.09	21.61	100.12	7.927	2.117	17.931
303	1305	A	2	6	74	75	17.14	21.66	100.2	8.550	2.354	16.409
303	1305	A	2	6	79	80	17.19	21.71	100.28	7.098	1.804	15.611
303	1305	A	2	6	84	85	17.24	21.76	100.36	8.422	2.435	11.884
303	1305	A	2	6	89	90	17.29	21.81	100.44	8.157	2.153	12.021
303	1305	B	3	2	89	90	20.19	21.82	100.46			
303	1305	B	3	2	94	95	20.24	21.87	100.54			
303	1305	B	3	2	99	100	20.29	21.92	100.62			
303	1305	B	3	2	104	105	20.34	21.97	100.72			
303	1305	B	3	2	109	110	20.39	22.02	100.82			
303	1305	B	3	2	114	115	20.44	22.07	100.91			
303	1305	B	3	2	119	120	20.49	22.12	101.01			
303	1305	B	3	2	124	125	20.54	22.17	101.11			
303	1305	B	3	2	129	130	20.59	22.22	101.21			
303	1305	B	3	2	134	135	20.64	22.27	101.3			
303	1305	B	3	2	139	140	20.69	22.32	101.42			
303	1305	B	3	2	144	145	20.74	22.37	101.54			
303	1305	B	3	2	149	150	20.79	22.42	101.65			
303	1305	B	3	3	4	5	20.84	22.47	101.77			
303	1305	B	3	3	9	10	20.89	22.52	101.89			
303	1305	B	3	3	14	15	20.94	22.57	102			
303	1305	B	3	3	19	20	20.99	22.62	102.12			
303	1305	B	3	3	24	25	21.04	22.67	102.26			
303	1305	B	3	3	29	30	21.09	22.72	102.39			

Leg	Site	H	Core	Section	Top(cm)	Bot(cm)	Depth(mbsf)	Depth(mcd)	Age (kyr)	%CaCO3	%SiO2	Sortable Silt
303	1305	B	3	3	34	35	21.14	22.77	102.53			
303	1305	B	3	3	39	40	21.19	22.82	102.67			
303	1305	B	3	3	44	45	21.24	22.87	102.81			
303	1305	B	3	3	49	50	21.29	22.92	102.95			
303	1305	B	3	3	54	55	21.34	22.97	103.09			
303	1305	B	3	3	59	60	21.39	23.02	103.25			
303	1305	B	3	3	64	65	21.44	23.07	103.41			
303	1305	B	3	3	69	70	21.49	23.12	103.58			
303	1305	B	3	3	74	75	21.54	23.17	103.74			
303	1305	B	3	3	79	80	21.59	23.22	103.91			
303	1305	B	3	3	84	85	21.64	23.27	104.07			
303	1305	B	3	3	89	90	21.69	23.32	104.24			
303	1305	B	3	3	94	95	21.74	23.37	104.42			
303	1305	B	3	3	99	100	21.79	23.42	104.62			
303	1305	B	3	3	104	105	21.84	23.47	104.81			
303	1305	B	3	3	109	110	21.89	23.52	105			
303	1305	B	3	3	114	115	21.94	23.57	105.19			
303	1305	B	3	3	119	120	21.99	23.62	105.39			
303	1305	B	3	3	124	125	22.04	23.67	105.58			
303	1305	B	3	3	129	130	22.09	23.72	105.89			
303	1305	B	3	3	134	135	22.14	23.77	106.26			
303	1305	B	3	3	139	140	22.19	23.82	106.63			
303	1305	B	3	3	144	145	22.24	23.87	107.01			
303	1305	B	3	3	149	150	22.29	23.92	107.38			
303	1305	B	3	4	4	5	22.34	23.97	107.75			
303	1305	B	3	4	9	10	22.39	24.02	108.12			
303	1305	B	3	4	14	15	22.44	24.07	108.59			
303	1305	B	3	4	19	20	22.49	24.12	109.12			
303	1305	B	3	4	24	25	22.54	24.17	109.66			
303	1305	B	3	4	29	30	22.59	24.22	110.19			
303	1305	B	3	4	34	35	22.64	24.27	110.72			
303	1305	B	3	4	39	40	22.69	24.32	111.26			
303	1305	B	3	4	44	45	22.74	24.37	111.79			
303	1305	B	3	4	49	50	22.79	24.42	112.27			
303	1305	B	3	4	54	55	22.84	24.47	112.69			
303	1305	B	3	4	59	60	22.89	24.52	113.11			
303	1305	B	3	4	64	65	22.94	24.57	113.53			
303	1305	B	3	4	69	70	22.99	24.62	113.96			
303	1305	B	3	4	74	75	23.04	24.67	114.38			
303	1305	B	3	4	79	80	23.09	24.72	114.8			
303	1305	B	3	4	84	85	23.14	24.77	115.13			
303	1305	B	3	4	89	90	23.19	24.82	115.34			
303	1305	B	3	4	94	95	23.24	24.87	115.55			
303	1305	B	3	4	99	100	23.29	24.92	115.76			
303	1305	B	3	4	104	105	23.34	24.97	115.97			
303	1305	B	3	4	109	110	23.39	25.02	116.18			

Leg	Site	H	Core	Section	Top(cm)	Bot(cm)	Depth(mbsf)	Depth(mcd)	Age (kyr)	%CaCO3	%SiO2	Sortable Silt
303	1305	B	3	4	114	115	23.44	25.07	116.39			
303	1305	B	3	4	119	120	23.49	25.12	116.58			
303	1305	B	3	4	124	125	23.54	25.17	116.74			
303	1305	B	3	4	129	130	23.59	25.22	116.91			
303	1305	B	3	4	134	135	23.64	25.27	117.07			
303	1305	B	3	4	139	140	23.69	25.32	117.23			
303	1305	B	3	4	144	145	23.74	25.37	117.4			
303	1305	B	3	4	149	150	23.79	25.42	117.56			
303	1305	B	3	5	4	5	23.84	25.47	117.72			
303	1305	B	3	5	9	10	23.89	25.52	117.85			
303	1305	B	3	5	14	15	23.94	25.57	117.98			
303	1305	B	3	5	19	20	23.99	25.62	118.12			
303	1305	B	3	5	24	25	24.04	25.67	118.25			
303	1305	B	3	5	29	30	24.09	25.72	118.39			
303	1305	A	3	2	39	40	20.29	25.8	118.6	30.590	6.211	23.198
303	1305	A	3	2	44	45	20.34	25.85	118.72	28.096	4.964	22.359
303	1305	A	3	2	49	50	20.39	25.9	118.84	23.694	5.572	21.618
303	1305	A	3	2	54	55	20.44	25.95	118.95	17.151	3.797	20.304
303	1305	A	3	2	59	60	20.49	26	119.07	31.100	6.623	22.013
303	1305	A	3	2	64	65	20.54	26.05	119.18	30.404	6.104	23.1
303	1305	A	3	2	69	70	20.59	26.1	119.3	31.189	6.184	22.077
303	1305	A	3	2	74	75	20.64	26.15	119.41	31.229	7.390	10.385
303	1305	A	3	2	79	80	20.69	26.2	119.52	28.838	5.742	19.446
303	1305	A	3	2	84	85	20.74	26.25	119.62	28.208	6.121	22.883
303	1305	A	3	2	89	90	20.79	26.3	119.72	26.195	5.842	21.204
303	1305	A	3	2	94	95	20.84	26.35	119.83	26.667	5.598	23.99
303	1305	A	3	2	99	100	20.89	26.4	119.93	23.956	5.815	23.986
303	1305	A	3	2	104	105	20.94	26.45	120.03	25.182	5.774	22.585
303	1305	A	3	2	109	110	20.99	26.5	120.13	25.342	5.553	18.796
303	1305	A	3	2	114	115	21.04	26.55	120.23	22.919	6.342	22.132
303	1305	A	3	2	119	120	21.09	26.6	120.33	24.123	6.305	20.198
303	1305	A	3	2	124	125	21.14	26.65	120.42	19.926	5.168	22.109
303	1305	A	3	2	129	130	21.19	26.7	120.51	21.010	4.527	21.51
303	1305	A	3	2	134	135	21.24	26.75	120.61	19.660	4.560	23.517
303	1305	A	3	2	139	140	21.29	26.8	120.7	20.408	4.980	
303	1305	A	3	2	144	145	21.34	26.85	120.8	18.772	4.259	10.142
303	1305	A	3	2	149	150	21.39	26.9	120.89	19.497	4.824	20.379
303	1305	A	3	3	4	5	21.44	26.95	120.98	14.809	3.614	19.429
303	1305	A	3	3	9	10	21.49	27	121.07	11.039	2.807	17.625
303	1305	A	3	3	14	15	21.54	27.05	121.16	9.181	2.455	16.871
303	1305	A	3	3	19	20	21.59	27.1	121.25	25.206	5.551	20.555
303	1305	A	3	3	24	25	21.64	27.15	121.34	22.529	5.545	12.53
303	1305	A	3	3	29	30	21.69	27.2	121.43	20.897	4.818	22.218
303	1305	A	3	3	34	35	21.74	27.25	121.51	21.051	5.027	21.407
303	1305	A	3	3	39	40	21.79	27.3	121.6	18.006	5.209	20.219
303	1305	A	3	3	44	45	21.84	27.35	121.69	19.763	3.948	21.013

Leg	Site	H	Core	Section	Top(cm)	Bot(cm)	Depth(mbsf)	Depth(mcd)	Age (kyr)	%CaCO3	%SiO2	Sortable Silt
303	1305	A	3	3	49	50	21.89	27.4	121.78	14.631	3.841	19.797
303	1305	A	3	3	54	55	21.94	27.45	121.86	10.676	2.970	19.728
303	1305	A	3	3	59	60	21.99	27.5	121.95	22.419	5.261	22.176
303	1305	A	3	3	64	65	22.04	27.55	122.04	19.435	5.208	23.303
303	1305	A	3	3	69	70	22.09	27.6	122.13	20.739	5.193	21.986
303	1305	A	3	3	74	75	22.14	27.65	122.21	25.030	5.680	24.592
303	1305	A	3	3	79	80	22.19	27.7	122.3	24.919	5.306	20.251
303	1305	A	3	3	84	85	22.24	27.75	122.39	23.692	6.249	12.132
303	1305	A	3	3	89	90	22.29	27.8	122.48	21.094	5.599	24.164
303	1305	A	3	3	94	95	22.34	27.85	122.56	22.317	6.036	24.967
303	1305	A	3	3	99	100	22.39	27.9	122.65	20.610	5.041	23.469
303	1305	A	3	3	104	105	22.44	27.95	122.74	18.999	4.412	26.736
303	1305	A	3	3	109	110	22.49	28	122.83	17.713	4.083	21.311
303	1305	A	3	3	114	115	22.54	28.05	122.92	17.364	4.716	25.105
303	1305	A	3	3	119	120	22.59	28.1	123.01	16.616	3.079	29.194
303	1305	A	3	3	124	125	22.64	28.15	123.09	17.258	4.514	12.535
303	1305	A	3	3	129	130	22.69	28.2	123.18	16.007	4.638	25.441
303	1305	A	3	3	134	135	22.74	28.25	123.27	15.262	4.748	24.71
303	1305	A	3	3	139	140	22.79	28.3	123.36	18.241	4.305	12.581
303	1305	A	3	3	144	145	22.84	28.35	123.45	13.777	3.296	6.249
303	1305	A	3	3	149	150	22.89	28.4	123.54	14.539	3.610	25.656
303	1305	A	3	4	4	5	22.94	28.45	123.63	13.819	3.487	23.391
303	1305	A	3	4	9	10	22.99	28.5	123.73	14.200	3.769	23.004
303	1305	A	3	4	14	15	23.04	28.55	123.82	13.921	3.893	26.464
303	1305	A	3	4	19	20	23.09	28.6	123.91	11.791	3.423	23.711
303	1305	A	3	4	24	25	23.14	28.65	124	11.888	3.325	25.715
303	1305	A	3	4	29	30	23.19	28.7	124.09	9.551	3.529	22.513
303	1305	A	3	4	34	35	23.24	28.75	124.19	12.652	3.502	25.149
303	1305	A	3	4	39	40	23.29	28.8	124.28	10.206	3.257	24.264
303	1305	A	3	4	44	45	23.34	28.85	124.38	10.402	2.979	22.855
303	1305	A	3	4	49	50	23.39	28.9	124.47	10.241	3.392	22.978
303	1305	A	3	4	54	55	23.44	28.95	124.57	8.032	3.370	23.557
303	1305	A	3	4	59	60	23.49	29	124.66	10.331	3.624	23.391
303	1305	A	3	4	64	65	23.54	29.05	124.76	8.975	2.875	24.408
303	1305	A	3	4	69	70	23.59	29.1	124.86	8.787	2.798	14.334
303	1305	A	3	4	74	75	23.64	29.15	124.96	10.745	3.389	23.491
303	1305	A	3	4	79	80	23.69	29.2	125.06	10.022	3.395	23.3
303	1305	A	3	4	84	85	23.74	29.25	125.16	10.188	3.080	22.493
303	1305	A	3	4	89	90	23.79	29.3	125.26	9.532	2.955	22.979
303	1305	A	3	4	94	95	23.84	29.35	125.35	11.528	3.532	23.198
303	1305	A	3	4	99	100	23.89	29.4	125.46	11.601	3.013	20.956
303	1305	A	3	4	104	105	23.94	29.45	125.56	10.499	2.876	23.168
303	1305	A	3	4	109	110	23.99	29.5	125.67	11.771	3.263	22.299
303	1305	A	3	4	114	115	24.04	29.55	125.77	10.977	3.147	21.69
303	1305	A	3	4	119	120	24.09	29.6	125.87	12.804	2.993	20.631
303	1305	A	3	4	124	125	24.14	29.65	125.98	13.293	3.804	20.576

Leg	Site	H	Core	Section	Top(cm)	Bot(cm)	Depth(mbsf)	Depth(mcd)	Age (kyr)	%CaCO3	%SiO2	Sortable Silt
303	1305	A	3	4	129	130	24.19	29.7	126.08	14.649	4.376	21.561
303	1305	A	3	4	134	135	24.24	29.75	126.19	18.468	4.801	18.435
303	1305	A	3	4	139	140	24.29	29.8	126.3	19.477	5.095	11.255
303	1305	A	3	4	144	145	24.34	29.85	126.41	30.177	7.378	26.884
303	1305	A	3	4	149	150	24.39	29.9	126.52	34.528	9.645	24.64
303	1305	A	3	5	4	5	24.44	29.95	126.63	26.748	6.361	22.486
303	1305	A	3	5	9	10	24.49	30	126.74	9.477	3.084	22.803
303	1305	A	3	5	14	15	24.54	30.05	126.84	9.787	3.000	22.845
303	1305	A	3	5	19	20	24.59	30.1	126.96	8.844	3.126	22.286
303	1305	A	3	5	24	25	24.64	30.15	127.07	8.746	3.258	20.638
303	1305	A	3	5	29	30	24.69	30.2	127.19	9.408	3.136	21.336
303	1305	A	3	5	34	35	24.74	30.25	127.3	9.380	3.040	20.738
303	1305	A	3	5	39	40	24.79	30.3	127.42	10.021	2.633	20.176
303	1305	A	3	5	44	45	24.84	30.35	127.53	9.342	3.156	19.563
303	1305	A	3	5	49	50	24.89	30.4	127.65	7.166	2.615	17.023
303	1305	A	3	5	54	55	24.94	30.45	127.77	10.149	3.080	18.724
303	1305	A	3	5	59	60	24.99	30.5	127.89	9.675	3.606	18.951
303	1305	A	3	5	64	65	25.04	30.55	128.01	13.241	3.759	21.128
303	1305	A	3	5	69	70	25.09	30.6	128.13	9.241	3.275	21.442
303	1305	A	3	5	74	75	25.14	30.65	128.25	10.000	3.379	22.203
303	1305	A	3	5	79	80	25.19	30.7	128.37	8.289	2.892	22.798
303	1305	A	3	5	84	85	25.24	30.75	128.49	8.431	2.951	21.588
303	1305	A	3	5	89	90	25.29	30.8	128.62	5.330	2.396	22.76
303	1305	A	3	5	94	95	25.34	30.85	128.75	3.113	1.498	18.047
303	1305	A	3	5	99	100	25.39	30.9	128.88	4.162	1.649	17.12
303	1305	A	3	5	104	105	25.44	30.95	129	4.103	1.575	20.054
303	1305	A	3	5	109	110	25.49	31	129.13	8.266	2.900	19.371
303	1305	A	3	5	114	115	25.54	31.05	129.26	5.849	2.599	16.495
303	1305	A	3	5	119	120	25.59	31.1	129.39	7.565	3.040	20.047
303	1305	A	3	5	124	125	25.64	31.15	129.52	5.987	2.708	21.961
303	1305	A	3	5	129	130	25.69	31.2	129.65	4.742	2.958	18.364
303	1305	A	3	5	134	135	25.74	31.25	129.79	6.254	3.310	20.584
303	1305	A	3	5	139	140	25.79	31.3	129.92	7.472	3.093	20.274
303	1305	A	3	5	144	145	25.84	31.35	130.06	6.202	2.910	
303	1305	A	3	5	149	150	25.89	31.4	130.19	3.043	2.067	
303	1305	A	3	6	4	5	25.94	31.45	130.32	3.419	1.829	23.082
303	1305	A	3	6	9	10	25.99	31.5	130.46	3.392	1.522	19.362
303	1305	A	3	6	14	15	26.04	31.55	130.6	9.453	3.778	18.817
303	1305	A	3	6	19	20	26.09	31.6	130.75	8.980	3.775	18.174
303	1305	A	3	6	24	25	26.14	31.65	130.89	4.278	2.443	15.43
303	1305	A	3	6	29	30	26.19	31.7	131.03	4.598	2.092	14.167
303	1305	A	3	6	34	35	26.24	31.75	131.17	4.248	1.904	18.552
303	1305	A	3	6	39	40	26.29	31.8	131.31	19.696	5.975	18.753
303	1305	A	3	6	44	45	26.34	31.85	131.49	13.495	3.444	
303	1305	A	3	6	49	50	26.39	31.9	131.69	9.002	3.185	
303	1305	A	3	6	54	55	26.44	31.95	131.89	8.274	3.096	

Leg	Site	H	Core	Section	Top(cm)	Bot(cm)	Depth(mbsf)	Depth(mcd)	Age (kyr)	%CaCO3	%SiO2	Sortable Silt
303	1305	A	3	6	59	60	26.49	32	132.09	8.267	3.390	
303	1305	A	3	6	64	65	26.54	32.05	132.29	9.026	2.830	
303	1305	A	3	6	69	70	26.59	32.1	132.49	13.636	4.367	
303	1305	A	3	6	74	75	26.64	32.15	132.7	11.767	3.206	
303	1305	A	3	6	79	80	26.69	32.2	133	15.065	3.667	
303	1305	A	3	6	84	85	26.74	32.25	133.38	15.644		
303	1305	A	3	6	89	90	26.79	32.3	133.76	11.937		
303	1305	A	3	6	94	95	26.84	32.35	134.15	14.508		
303	1305	A	3	6	99	100	26.89	32.4	134.53	11.789		17.852
303	1305	A	3	6	104	105	26.94	32.45	134.91	12.372		17.562
303	1305	A	3	6	109	110	26.99	32.5	135.29	9.778		18.399
303	1305	A	3	6	114	115	27.04	32.55	135.76	7.746		18.319
303	1305	A	3	6	119	120	27.09	32.6	136.33	3.216		17.457
303	1305	A	3	6	124	125	27.14	32.65	136.9	3.410		12.088
303	1305	A	3	6	129	130	27.19	32.7	137.47	3.343		12.122
303	1305	A	3	6	134	135	27.24	32.75	138.04	3.945		12.091

Appendix C

Depth(mcd)	Age (ka)	Sed rate	O18 PDB	o18 rep1	o18 rep2	Sortable Silt	Depth(mcd)	%CaCO3	%SiO2
0.01	4.68	9.35	2.58			11.91	0.01	36.03	1.84
0.06	5.22	9.36	2.78			26.65	0.06	9.88	4.68
0.11	5.75	9.36				26.92	0.11	13.33	6.88
0.16	6.29	9.35				26.08	0.16	11.35	6.11
0.21	6.82	9.36				24.72	0.21	11.55	4.70
0.26	7.35	9.36				21.99	0.26	11.36	4.34
0.31	7.89	9.35	2.67			22.26	0.31	11.53	4.00
0.36	8.42	9.36				23.63	0.36	9.14	4.02
0.41	8.96	8.81	2.68			22.83	0.41	10.15	4.34
0.46	9.53	8.39	2.88			21.20	0.46	9.29	4.19
0.51	10.12	8.39	2.69			22.66	0.51	8.82	3.32
0.56	10.72	8.39	2.94				0.56		
0.61	11.31	8.39	3.82				0.61		
0.66	11.91	8.39	3.15	2.96	3.60		0.66		
0.71	12.51	8.40	3.70	3.52	3.45		0.71		
0.76	13.10	7.20	3.63	3.75	3.47		0.76		
0.81	13.79	7.09	3.55	3.69	3.40	19.80	0.81	7.92	4.50
0.86	14.50	7.08	3.65	4.14	3.60	20.28	0.86	8.97	3.43
0.91	15.21	7.08	3.59	3.55	3.34	19.80	0.91	10.68	3.13
0.96	15.91	7.09	3.54	3.48	3.82	20.43	0.96	11.32	1.76
1.01	16.62	7.08	4.12	4.43		20.15	1.01	10.95	1.36
1.06	17.32	7.63	4.74	4.66		20.58	1.06	9.58	0.82
1.11	17.98	10.35	4.74	4.66		25.15	1.11	9.74	0.66
1.16	18.46	10.33	4.80	4.60		21.53	1.16	9.00	1.00
1.21	18.94	10.35	4.69	4.59		21.65	1.21	7.45	0.09
1.26	19.43	10.33	4.73			20.96	1.26	8.07	0.53
1.31	19.91	10.35	4.66			22.41	1.31	8.17	0.83
1.36	20.39	10.33	4.74	4.66		20.26	1.36	7.74	1.70
1.41	20.88	17.09	4.75	4.66		19.77	1.41	6.71	0.62
1.51	21.46	20.75	4.74	4.64		18.61	1.51	5.82	1.70
1.56	21.70	20.75	4.70	4.67		20.70	1.56	5.88	0.53
1.61	21.95	20.75	4.63	4.55		20.45	1.61	6.68	0.90
1.66	22.19	20.83	4.86	4.60		20.96	1.66	5.39	0.29
1.71	22.43	20.75	3.58	4.15		19.83	1.71	5.72	1.40
1.76	22.67	44.25	2.64	2.50		21.73	1.76	5.45	2.25
1.81	22.78	49.50	3.29	2.22		19.68	1.81	4.93	0.86
1.86	22.88	49.50	3.10	2.57		19.53	1.86	5.39	1.95
1.91	22.98	49.50	4.02	2.99		16.63	1.91	6.11	1.49
1.96	23.08	49.02	4.13	4.44		17.19	1.96	6.67	0.84
2.01	23.19	49.50	4.24	4.55		17.23	2.01	6.69	1.20
2.06	23.29	38.46	3.24	3.24		12.20	2.06	6.38	0.46
2.11	23.42	23.58	3.34	4.13		17.93	2.11	7.04	1.40
2.16	23.63	23.70	3.61	4.31		18.14	2.16	7.82	2.87

Depth(mcd)	Age (ka)	Sed rate	O18 PDB	o18 rep1	o18 rep2	Sortable Silt	Depth(mcd)	%CaCO3	%SiO2
2.21	23.84	23.58	4.24	4.29		17.19	2.21	6.44	2.31
2.26	24.05	23.58	3.87	3.65		15.85	2.26	6.66	0.48
2.31	24.26	23.58	3.78	3.32		16.81	2.31	7.67	1.71
2.36	24.48	23.58	4.65	4.64		19.88	2.36	7.14	1.20
2.41	24.69	10.96	4.53	4.56		19.07	2.41	6.68	3.06
2.46	25.14	8.10	4.45	4.45		18.05	2.46	6.80	1.39
2.51	25.76	8.12	4.45			18.83	2.51	8.46	1.84
2.56	26.38	8.10	4.74	4.60		17.26	2.56	11.52	2.23
2.61	26.99	8.10	4.70	4.49		21.39	2.61	9.38	1.64
2.66	27.61	8.10	4.29			15.45	2.66	8.16	5.51
2.71	28.23	8.12	4.05			12.34	2.71	7.93	6.07
2.76	28.84	19.23	3.76	4.28		12.07	2.76	7.59	4.18
2.80	29.05	21.28	2.77			16.60	2.80	7.81	4.95
2.81	29.10	21.28	2.82				2.86	7.23	3.25
2.86	29.33	21.28	2.58	4.09		12.46	2.91	7.00	2.08
2.91	29.57	21.28	3.94			17.21	2.96	7.44	3.03
2.96	29.80	21.37	4.39	4.09		16.61	3.01	7.73	2.72
3.01	30.04	21.28	4.07			17.19	3.06	7.96	2.74
3.02	30.08	21.28	3.92				3.11	6.69	3.80
3.06	30.27	23.70	4.51	4.32		15.76	3.16	6.86	3.59
3.11	30.48	32.89	3.69			12.01	3.21	6.83	4.21
3.16	30.64	32.89	4.31			15.80	3.26	7.04	3.34
3.21	30.79	32.68	3.55	2.44		12.32	3.31	7.45	2.91
3.26	30.94	32.89	3.62	3.22		17.35	3.36	7.69	1.66
3.31	31.09	32.89	4.27	4.01		16.62	3.41	6.30	2.96
3.36	31.24	32.89	4.28	4.02		12.17	3.46	5.84	3.09
3.41	31.40	40.00	4.31	4.07		17.81	3.51	5.54	3.10
3.46	31.52	45.87	4.32	4.02		18.11	3.56	5.70	4.35
3.51	31.63	45.87	4.15	4.02		17.38	3.61	6.15	3.11
3.56	31.74	45.87	3.81			16.74	3.66	5.53	2.25
3.61	31.85	45.87	4.14			17.36	3.71	7.32	3.17
3.66	31.96	45.87	4.47			11.84	3.76	7.98	2.72
3.71	32.07	45.87	4.27			16.74	3.81	8.21	3.32
3.76	32.18	56.82	3.76			12.40	3.86	6.85	3.32
3.81	32.26	56.18	4.36			18.53	3.91	7.00	1.56
3.86	32.35	56.82	3.94			17.74	3.96	7.77	2.56
3.91	32.44	56.82	4.06			22.22	4.01	7.01	3.13
3.96	32.53	56.82	4.18			20.04	4.06	5.47	2.17
4.01	32.62	56.82	4.24			17.45	4.11	5.03	2.88
4.06	32.70	58.82	4.05			12.07	4.16	6.12	3.19
4.11	32.79	61.73	4.45			17.71	4.21	6.59	3.31
4.16	32.87	61.73	4.31			18.37	4.26	5.98	3.12
4.21	32.95	62.50	4.46			17.47	4.31	6.60	2.33
4.26	33.03	61.73				12.42	4.36	6.30	2.26
4.31	33.11	61.73	4.22			18.56	4.41	6.04	0.86

Depth(mcd)	Age (ka)	Sed rate	O18 PDB	o18 rep1	o18 rep2	Sortable Silt	Depth(mcd)	%CaCO3	%SiO2
4.36	33.19	62.50	4.14			21.00	4.46	5.22	1.68
4.41	33.27	60.98	4.26			23.50	4.51	5.92	2.53
4.46	33.36	61.73	3.95			21.30	4.56	6.97	2.25
4.51	33.44	60.98	3.95			21.59	4.61	6.88	1.46
4.56	33.52	60.98	4.07			20.97	4.66	6.41	-17.66
4.61	33.60	60.98	4.34			19.54	4.71	6.26	2.47
4.66	33.68	60.98	4.46			20.24	4.76	5.61	2.51
4.71	33.76	60.98	4.17			18.73	4.81	5.64	2.24
4.76	33.85	56.18	4.12			18.29	4.86	6.16	1.77
4.81	33.94	56.18	4.30			19.21	4.91	5.71	1.35
4.86	34.02	56.18	4.23			19.99	4.96	5.95	1.19
4.91	34.11	56.18	4.19			21.27	5.01	4.91	1.89
4.96	34.20	56.18	4.02			22.11	5.06	4.55	1.64
5.01	34.29	56.18	4.34			21.31	5.11	5.88	2.29
5.06	34.38	54.35	4.26			19.56	5.16	5.61	2.17
5.11	34.47	50.00				21.03	5.21	5.44	2.05
5.16	34.57	49.50				19.26	5.26	5.11	1.50
5.21	34.67	50.00				18.60	5.31	4.77	2.77
5.26	34.77	50.00	4.38			19.78	5.36	5.34	3.27
5.31	34.87	50.00	4.53			19.67	5.41	4.93	2.07
5.36	34.97	50.00	4.24			18.49	5.46	4.46	2.33
5.41	35.07	45.45	4.25			20.13	5.51	4.77	1.58
5.46	35.18	43.86	4.08			20.04	5.56	4.88	2.26
5.51	35.30	43.86	4.28			19.58	5.61	4.64	2.78
5.56	35.41	43.86				12.48	5.66	5.40	2.39
5.61	35.53	43.96				21.49	5.71	5.37	2.05
5.65	35.62	43.48	3.53				5.76	5.53	1.00
5.66	35.64	43.48				12.42	5.81	5.73	4.62
5.70	35.73	45.45	4.10				5.86	24.95	2.52
5.71	35.75	43.48				12.36	5.90	7.78	1.83
5.75	35.85	43.48	4.03				5.95	8.10	1.80
5.76	35.87	38.46				19.28	6.00	9.52	1.62
5.80	35.97	38.46	3.94				6.05	10.06	2.07
5.81	36.00	38.10	4.23			18.71	6.10	7.14	1.77
5.85	36.10	38.46	3.00	3.34			6.15	6.32	2.84
5.86	36.13	38.46	4.25			17.85	6.20	6.37	1.17
5.90	36.23	38.46	3.83			16.44	6.25	7.53	1.39
5.91	36.26	38.46	4.18				6.30	6.67	1.57
5.95	36.36	38.46	3.66			17.23	6.35	6.55	1.31
5.96	36.39	38.10	4.36				6.40	5.48	1.55
6.00	36.49	38.46	3.74			16.58	6.45	5.81	2.41
6.05	36.62	37.31	4.05			15.81	6.50	5.97	2.48
6.10	36.76	33.78	2.99	4.04		14.16	6.55	5.83	0.92
6.15	36.91	33.78	4.12	3.83		15.95	6.60	7.83	0.99
6.20	37.05	33.78	3.53	4.25		14.75	6.65	6.37	0.62

Depth(mcd)	Age (ka)	Sed rate	O18 PDB	o18 rep1	o18 rep2	Sortable Silt	Depth(mcd)	%CaCO3	%SiO2
6.25	37.20	33.78	2.94	3.27		14.35	6.70	10.67	1.82
6.30	37.35	33.78	3.60			12.13	6.75	11.51	0.50
6.35	37.50	33.56	3.94			21.49	6.80	7.04	1.12
6.40	37.65	31.65	4.03			22.30	6.85	7.23	0.96
6.45	37.81	29.94	4.04			21.67	6.90	8.08	0.48
6.50	37.97	29.94	4.13			22.23	6.95	8.94	0.18
6.55	38.14	29.94	4.12			19.75	7.00	7.74	0.33
6.60	38.31	29.76	4.00			20.04	7.05	6.12	0.88
6.65	38.47	29.94	3.82			20.82	7.10	5.83	1.39
6.70	38.64	29.94	3.99			20.55	7.15	6.99	0.52
6.75	38.81	26.74	4.32			23.03	7.20	6.60	0.49
6.80	39.00	26.46	4.31			19.01	7.25	6.01	0.78
6.85	39.18	26.32	4.13			17.11	7.30	6.84	1.11
6.90	39.37	26.32	4.21			18.56	7.35	8.53	0.77
6.95	39.56	26.46	4.38			19.09	7.40	7.75	2.09
7.00	39.75	26.32	4.22			19.37	7.45	7.37	1.69
7.05	39.94	20.41	4.37			20.17	7.50	7.08	1.81
7.10	40.19	11.16	4.08			18.67	7.55	7.66	2.24
7.15	40.64	11.16	4.17			19.61	7.60	5.47	1.54
7.20	41.08	11.16	4.47			18.65	7.65	5.70	0.86
7.25	41.53	11.16	4.53			19.83	7.70	5.50	0.93
7.30	41.98	11.16	4.25			19.66	7.75	5.36	0.98
7.35	42.43	11.16	4.25			18.77	7.80	7.10	0.86
7.40	42.88	10.48	4.45			12.00	7.85	6.60	2.22
7.45	43.35	9.96	4.21			18.42	7.90	6.92	1.56
7.50	43.86	9.98	4.12			18.12	7.95	8.06	1.33
7.55	44.36	9.96	4.51			18.51	8.00	8.15	2.02
7.60	44.86	9.98	4.71			19.05	8.05	8.63	1.99
7.65	45.36	9.96	4.44			21.38	8.10	7.80	4.40
7.70	45.86	9.98	4.17			20.47	8.15	8.06	1.53
7.75	46.36	10.06	4.26			21.64	8.20	7.29	1.53
7.80	46.86	10.10	4.11			19.93	8.25	7.96	2.62
7.85	47.35	10.08	4.19			19.65	8.30	6.24	0.36
7.90	47.85	10.08	4.28			19.07	8.35	6.04	1.30
7.95	48.35	10.08	4.27			18.18	8.40	19.81	
8.00	48.84	10.10	4.38			16.67	8.45	7.77	3.42
8.05	49.34	10.14	4.43			17.76	8.50	10.13	1.62
8.10	49.83	10.33	4.07				8.55	9.81	2.32
8.15	50.31	10.33	4.13				8.60	11.93	1.04
8.20	50.80	10.35	4.23			19.50	8.65	10.65	0.96
8.25	51.28	10.33	4.44			22.40	8.70	8.58	1.35
8.30	51.77	10.33	4.34			22.05	8.75	5.80	1.38
8.35	52.25	10.33	3.70			23.07	8.80	5.10	1.22
8.40	52.73	10.53	3.91			21.30	8.85	5.57	1.13
8.45	53.21	10.64	4.07			20.62	8.90	4.89	1.33

Depth(mcd)	Age (ka)	Sed rate	O18 PDB	o18 rep1	o18 rep2	Sortable Silt	Depth(mcd)	%CaCO3	%SiO2
8.50	53.68	10.62	3.75			20.97	8.95	7.38	1.43
8.55	54.15	10.64	3.63			20.97	9.00	6.41	1.36
8.60	54.62	10.64	3.77			19.19	9.05	8.00	1.91
8.65	55.09	10.64	4.16			20.16	9.10	7.50	2.22
8.70	55.56	10.64	4.21			17.28	9.15	6.46	1.53
8.75	56.03	10.99	3.83				9.20	8.18	1.56
8.80	56.48	11.01	4.27			18.39	9.25	7.34	7.55
8.85	56.94	11.01	4.22			20.14	9.30	6.76	6.58
8.90	57.39	11.01	4.00			20.19	9.33	7.00	
8.95	57.85	11.01	3.90			19.80	9.38	8.42	
9.00	58.30	11.01	3.91			19.67	9.43	8.45	
9.05	58.75	11.09	4.45			19.85	9.48	4.00	
9.10	59.21	11.36	4.31			20.41	9.53	6.94	
9.15	59.65	11.36				18.72	9.58	4.85	
9.20	60.09	11.36	4.16			18.91	9.63	12.81	
9.25	60.53	11.39				20.42	9.68	5.71	
9.30	60.96	11.36				19.54	9.73	7.33	
9.33	61.23	11.36				18.82	9.78	9.26	
9.35	61.40	11.36	4.47				9.83	11.04	
9.38	61.67	11.36				18.14	9.88	9.21	
9.40	61.84	11.36	4.38				9.93	5.65	
9.43	62.11	11.43				12.26	9.98	13.22	
9.45	62.28	11.45	4.17				10.03	8.19	
9.48	62.55	11.43				18.95	10.08	29.68	
9.50	62.72	11.45	4.41				10.13	8.78	
9.53	62.98	11.43				18.78	10.18	17.86	
9.55	63.16	11.41	4.30				10.23	15.29	
9.58	63.42	11.44				12.09	10.28	13.98	
9.63	63.86	11.44				17.99	10.33	11.01	
9.68	64.29	11.44				18.18	10.38	9.59	
9.73	64.73	11.42				17.77	10.43	8.91	
9.78	65.17	11.39				17.06	10.48	24.33	
9.83	65.61	11.42				17.35	10.53	19.46	
9.88	66.05	11.39				17.31	10.58	6.41	
9.93	66.49	11.39	4.18			11.99	10.63	22.27	
9.98	66.92	11.42	4.07			18.54	10.68	14.43	
10.03	67.36	11.39	4.14			17.46	10.73	45.24	
10.08	67.80	11.34	4.21			16.76	10.78	23.27	
10.13	68.24	11.34	4.10			17.68	10.83	20.35	
10.18	68.68	11.31	4.27			17.93	10.88	8.45	
10.23	69.13	11.34	4.37			12.24	10.93	9.51	
10.28	69.57	11.34	4.26			12.29	10.98	9.71	
10.33	70.01	11.31	4.26			19.09	11.03	12.37	
10.38	70.45	11.31	4.27			17.93	11.08	14.83	
10.43	70.89	11.26	4.24			13.74	11.13	5.62	

Depth(mcd)	Age (ka)	Sed rate	O18 PDB	o18 rep1	o18 rep2	Sortable Silt	Depth(mcd)	%CaCO3	%SiO2
10.48	71.34	11.24	4.29			12.25	11.18	9.63	
10.53	71.78	11.24	4.22			12.25	11.23	15.17	
10.58	72.23	11.24	4.14			16.15	11.28	15.92	
10.63	72.67	11.26	3.80			12.23	11.33	7.21	
10.68	73.11	11.24	3.79			19.86	11.38	32.37	
10.73	73.56	11.19	4.14			19.98	11.43	10.18	
10.78	74.01	11.16	3.73			11.88	11.48	10.27	6.68
10.83	74.45	11.16	3.63			11.87	11.53	9.29	5.19
10.88	74.90	11.16	3.73			12.32	11.58	11.89	5.26
10.93	75.35	11.14	3.96			12.33	11.63	10.36	8.02
10.98	75.80	11.16	3.65			21.88	11.68	9.06	10.92
11.03	76.25	11.16	3.65			21.24	11.73	8.19	11.42
11.08	76.70	11.09	3.58			12.31	11.78	8.91	4.79
11.13	77.15	11.06	3.86			21.36	11.83	9.49	4.85
11.18	77.60	11.09	3.54			21.36	11.88	3.65	8.04
11.23	78.05	11.06	3.69			21.75	11.93	6.31	2.86
11.28	78.50	11.09	3.74			12.32	11.98	8.13	4.46
11.33	78.95	11.06	3.52			20.17	12.03	7.83	4.92
11.38	79.40	11.06	3.57			12.03	12.08	7.89	4.21
11.43	79.86	11.01	3.45			20.09	12.13	8.48	5.42
11.48	80.31	10.99	3.86			17.66	12.18	7.61	4.79
11.53	80.77	10.99	3.53			18.61	12.23	7.52	5.45
11.58	81.22	11.01	3.54			20.39	12.28	52.31	6.06
11.63	81.67	10.99	3.76			27.86	12.33	8.05	5.56
11.68	82.13	11.01	3.63			24.86	12.38	7.47	8.04
11.73	82.58	11.49	3.37			22.89	12.43	7.28	4.90
11.78	83.02	11.82	3.86			18.79	12.48	5.92	6.91
11.83	83.44	11.85	4.26			21.32	12.53	7.09	3.98
11.88	83.86	11.82	3.66			21.53	12.58	6.32	4.58
11.93	84.29	11.85	3.99			19.90	12.63	6.79	
11.98	84.71	11.82	3.94			20.07	12.68	6.06	
12.03	85.13	11.82	3.68			22.71	12.73	7.18	
12.08	85.55	32.68	3.80			20.03	12.78	6.61	
12.13	85.71	35.21	4.07			19.80	12.83	7.49	
12.18	85.85	34.97	4.05			12.11	12.88	7.56	
12.23	85.99	34.97	4.19			17.28	12.93	7.80	
12.28	86.14	34.97	4.02			16.75	12.98	7.50	
12.33	86.28	34.97	4.28			19.97	13.03	9.28	
12.38	86.42	36.76	3.83			18.18	13.08	8.29	
12.43	86.56	42.02	4.12			18.61	13.13	8.40	
12.48	86.68	41.67	3.75			17.74	13.18	7.73	
12.53	86.80	41.67	4.06			18.49	13.23	7.70	
12.58	86.92	41.67	3.86			17.21	13.28	9.55	
12.63	87.04	41.67	3.88			12.27	13.33	6.44	
12.68	87.16	42.02	3.87			17.51	13.38	7.95	

Depth(mcd)	Age (ka)	Sed rate	O18 PDB	o18 rep1	o18 rep2	Sortable Silt	Depth(mcd)	%CaCO3	%SiO2
12.73	87.28	45.45	4.02			18.59	13.43	7.91	
12.78	87.39	48.08	3.77			17.54	13.48	7.30	
12.83	87.49	48.08	3.24			17.73	13.53	8.67	
12.88	87.59	48.08	4.03			16.83	13.58	6.98	
12.93	87.70	48.08	3.87			18.01	13.63	7.77	
12.98	87.80	47.62	4.04			17.40	13.68	5.69	
13.03	87.91	48.08	3.89			17.69	13.73	11.15	
13.08	88.01	52.63	3.65			17.31	13.78	10.59	
13.13	88.11	52.08	3.89			18.08	13.83	9.95	
13.18	88.20	52.08	3.80			18.58	13.88	9.90	
13.23	88.30	52.63	3.87			20.37	13.93	11.32	
13.28	88.39	52.08	3.93			20.68	13.98	7.53	
13.33	88.49	52.63	4.11			19.35	14.03	9.79	
13.38	88.58	52.63	3.85			20.31	14.08	9.67	
13.43	88.68	52.63	3.60			20.97	14.13	10.32	
13.48	88.77	53.19	2.95			21.26	14.18	10.61	
13.53	88.87	53.19	3.50			22.57	14.23	12.91	
13.58	88.96	53.19	3.62			21.18	14.28	12.78	
13.63	89.06	53.19	3.14			21.42	14.33	11.36	
13.68	89.15	53.19	2.98			20.21	14.38	12.06	
13.73	89.24	51.02	2.86			25.15	14.43	11.71	
13.78	89.34	50.00	4.16			20.35	14.48	10.74	
13.83	89.44	50.51	4.37			21.65	14.53	12.31	
13.88	89.54	50.00	3.80			23.71	14.58	12.37	
13.93	89.64	50.51	3.76			23.59	14.62	12.82	
13.98	89.74	50.00	3.36			20.76	14.67	12.01	
14.03	89.84	50.00	3.90			22.93	14.72	10.92	
14.08	89.94	45.05	3.97			20.30	14.77	12.81	
14.13	90.05	44.64	4.12			22.85	14.78	12.94	4.82
14.18	90.16	44.64	4.17			23.28	14.83	15.05	6.44
14.23	90.27	45.05	4.25			21.39	14.88	16.07	5.49
14.28	90.39	44.64	4.44			19.84	14.93	18.04	6.33
14.33	90.50	44.64	4.50			20.23	14.98	20.19	6.76
14.38	90.61	42.37	4.36			22.88	15.03	17.28	5.85
14.43	90.73	38.46	4.42			24.44	15.08	17.34	6.38
14.48	90.86	38.17	4.27			19.39	15.13	16.46	6.64
14.53	90.99	38.46	3.20			19.62	15.18	15.39	5.65
14.58	91.12	38.46	4.24			18.92	15.23	14.81	6.36
14.62	91.22	38.46	4.20			18.13	15.28	15.64	5.74
14.63	91.25	38.10	4.46				15.33	20.68	8.57
14.67	91.35	38.46				20.34	15.38	14.06	5.26
14.68	91.38	38.46	4.24				15.43	14.90	5.96
14.72	91.48	38.46				17.00	15.48	16.91	4.28
14.73	91.51	30.30	4.17				15.53	21.16	4.78
14.77	91.64	27.03				22.70	15.58	24.39	5.06

Depth(mcd)	Age (ka)	Sed rate	O18 PDB	o18 rep1	o18 rep2	Sortable Silt	Depth(mcd)	%CaCO3	%SiO2
14.78	91.68	27.03	3.75			12.13	15.63	19.54	5.04
14.83	91.86	27.03	4.06			12.36	15.68	18.17	5.46
14.88	92.05	27.03	4.07			11.91	15.73	15.61	5.22
14.93	92.23	27.03	3.94			11.89	15.78	12.61	4.74
14.98	92.42	27.03	3.81			15.81	15.83	14.61	7.18
15.03	92.60	25.25	4.12			18.24	15.88	19.12	7.37
15.08	92.80	12.02	3.83			12.37	15.98	14.38	6.34
15.13	93.22	12.02	3.66			12.04	16.03	12.69	7.04
15.18	93.63	12.02	3.43			18.39	16.08	13.18	6.74
15.23	94.05	12.02	3.59			12.37	16.13	15.31	8.68
15.28	94.47	11.99	3.45			20.24	16.18	13.48	7.41
15.33	94.88	12.02	3.55			12.35	16.23	15.16	5.88
15.38	95.30	10.64				11.69	16.28	16.26	6.84
15.43	95.77	9.07	4.14			12.32	16.33	14.60	4.45
15.48	96.32	9.07	3.83			12.07	16.38	15.74	5.82
15.53	96.87	9.06	3.86			11.92	16.43	11.27	4.94
15.58	97.42	9.07	3.75			21.18	16.48	14.93	7.97
15.63	97.97	9.07	3.68			19.93	16.53	10.33	7.27
15.68	98.52	9.06	3.41			21.90	16.58	10.34	7.98
15.73	99.08	9.24	3.46			12.09	16.63	9.92	8.13
15.78	99.62	9.38	3.61			12.35	16.68	11.63	7.01
15.83	100.15	9.26	3.93			12.06	16.73	10.92	8.58
15.88	100.69	9.26	3.88			11.88	16.78	11.49	6.07
15.98	101.77	9.26	3.93			12.27	16.83	12.48	7.67
16.03	102.31	9.62				12.16	16.88	12.03	7.84
16.08	102.83	13.16				18.28	16.93	13.34	6.53
16.13	103.21	13.16				11.71	16.98	12.81	6.60
16.18	103.59	13.16				17.91	17.03	13.81	6.70
16.23	103.97	13.16				17.21	17.08	14.10	5.67
16.28	104.35	13.51	3.69			18.26	17.13	14.58	4.81
16.33	104.72	13.16	3.93			18.58	17.18	13.67	5.58
16.38	105.10	17.24	3.59			17.53	17.23	10.30	7.03
16.43	105.39	29.41	3.67			17.75	17.28	11.56	6.04
16.48	105.56	29.41	3.75			22.32	17.33	12.34	7.35
16.53	105.73	29.41	3.92			20.63	17.38	12.01	5.28
16.58	105.90	29.41	4.14			19.20	17.43	13.78	6.52
16.63	106.07	29.41				12.16	17.48	13.86	4.37
16.68	106.24	29.41	4.01			16.06	17.53	11.36	5.96
16.73	106.41	35.71	3.83			18.77	17.58	12.70	5.06
16.78	106.55	35.71	3.74			21.39	17.63	12.74	5.79
16.83	106.69	38.46	3.74			19.49	17.68	14.34	5.20
16.88	106.82	35.71	3.78			18.83	17.73	9.41	4.68
16.93	106.96	35.71	3.71			22.01	17.78	8.82	4.20
16.98	107.10	38.46	3.76			19.49	17.83	10.54	4.26
17.03	107.23	35.71	3.64			22.98	17.88	9.40	4.85

Depth(mcd)	Age (ka)	Sed rate	O18 PDB	o18 rep1	o18 rep2	Sortable Silt	Depth(mcd)	%CaCO3	%SiO2
17.08	107.37	45.45	3.63			11.90	17.93	14.89	3.12
17.13	107.48	41.67	3.62			11.69	17.98	7.90	4.33
17.18	107.60	41.67	3.53			11.94	18.03	8.07	5.34
17.23	107.72	41.67	3.31			19.20	18.08	8.60	4.64
17.28	107.84	45.45	3.28			19.60	18.13	8.25	5.74
17.33	107.95	41.67	3.33			15.29	18.18	8.42	5.42
17.38	108.07	45.45	3.23			18.09	18.23	8.68	4.79
17.43	108.18	45.45	3.54			17.85	18.28	8.20	5.48
17.48	108.29	50.00	4.10			18.79	18.33	7.79	5.34
17.53	108.39	50.00	3.53			17.65	18.38	7.79	4.64
17.58	108.49	50.00	4.27			18.20	18.43	9.79	5.71
17.63	108.59	50.00	4.26			18.50	18.48	10.62	5.57
17.68	108.69	45.45	3.95			12.17	18.53	9.02	5.37
17.73	108.80	55.56	4.00			17.61	18.58	12.05	6.25
17.78	108.89	55.56	3.97			11.68	18.63	9.52	5.14
17.83	108.98	55.56	3.83			20.65	18.68	8.97	4.35
17.88	109.07	55.56	3.64			12.35	18.73	10.36	5.02
17.93	109.16	55.56	3.79			20.78	18.78	8.70	4.11
17.98	109.25	55.56	4.02			21.10	18.83	9.59	4.97
18.03	109.34	55.56	3.67			20.53	18.88	8.56	4.68
18.08	109.43	62.50	4.02			11.90	18.93	8.56	5.58
18.13	109.51	55.56	4.01			21.57	18.98	9.92	5.84
18.18	109.60	62.50	3.99			22.01	19.03	6.70	5.67
18.23	109.68	62.50	3.91			12.26	19.08	8.53	7.26
18.28	109.76	62.50	3.60			12.35	19.13	10.57	6.26
18.33	109.84	62.50	3.76			12.32	19.18	9.76	5.01
18.38	109.92	62.50	3.88			20.50	19.23	9.66	5.38
18.43	110.00	62.50	3.87			20.72	19.28	9.42	9.84
18.48	110.08	62.50	3.78			18.84	19.33	9.85	5.88
18.53	110.16	62.50	3.84			18.73	19.38	10.67	6.15
18.58	110.24	71.43	3.67			12.03	19.43	9.35	7.44
18.63	110.31	62.50	3.78			11.60	19.48	10.64	6.62
18.68	110.39	62.50	3.72			22.05	19.53	12.55	6.78
18.73	110.47	62.50	3.81			12.33	19.58	10.85	9.16
18.78	110.55	71.43	3.91			23.15	19.63	12.86	6.87
18.83	110.62	62.50	3.48			12.39	19.68	8.11	8.47
18.88	110.70	62.50	3.69			12.41	19.73	8.24	6.32
18.93	110.78	71.43	3.41			23.14	19.78	7.57	7.16
18.98	110.85	62.50	3.66			12.06	19.83	10.56	6.48
19.03	110.93	62.50	3.84			21.19	19.88	9.46	6.26
19.08	111.01	62.50	3.80			20.65	19.93	9.29	6.19
19.13	111.09	62.50	3.85			12.02	19.98	9.43	7.16
19.18	111.17	62.50	3.84			23.42	20.03	9.98	7.86
19.23	111.25	62.50	3.64				20.08	11.21	5.81
19.28	111.33	62.50	3.54			22.17	20.13	12.07	5.69

Depth(mcd)	Age (ka)	Sed rate	O18 PDB	o18 rep1	o18 rep2	Sortable Silt	Depth(mcd)	%CaCO3	%SiO2
19.33	111.41	62.50	3.63			11.91	20.18	7.66	6.14
19.38	111.49	62.50	3.47			12.37	20.23	6.22	5.64
19.43	111.57	55.56	3.52			20.66	20.28	6.22	7.32
19.48	111.66	55.56	3.34			18.80	20.33	7.21	7.79
19.53	111.75	55.56	3.48			17.96	20.38	6.62	6.60
19.58	111.84	62.50	3.50			17.70	20.43	7.41	7.74
19.63	111.92	55.56	3.70			18.79	20.48	9.78	5.22
19.68	112.01	55.56	3.58			19.36	20.53	10.80	4.48
19.73	112.10	50.00	3.60			22.10	20.57	11.71	3.43
19.78	112.20	50.00	3.57			12.36	20.62	12.06	4.51
19.83	112.30	50.00	3.70			22.07	20.67	10.32	3.79
19.88	112.40	50.00	3.65			20.25	20.72	8.79	4.54
19.93	112.50	55.56	3.66			12.48	20.77	8.58	4.66
19.98	112.59	50.00	3.56		3.69	23.15	20.82	7.60	5.27
20.03	112.69	45.45	3.66			21.31	20.87	7.61	3.77
20.08	112.80	45.45	3.65			19.06	20.92	7.99	3.57
20.13	112.91	41.67	3.58			20.10	20.97	9.71	5.52
20.18	113.03	45.45	3.83				21.02	10.93	3.89
20.23	113.14	41.67	3.54			18.64	21.07	20.71	6.60
20.28	113.26	44.44	3.97			12.31	21.12	39.24	2.76
20.32	113.35	33.33	3.80				21.17	10.70	5.71
20.33	113.38	44.44	4.19			16.97	21.22	6.56	9.55
20.37	113.47	50.00	3.90				21.27	17.30	2.27
20.38	113.49	40.00	4.09			18.38	21.32	15.51	2.84
20.42	113.59	35.71	2.78				21.37	16.17	2.05
20.47	113.73	36.36	3.93				21.42	14.07	3.90
20.43	113.62	35.71	3.77			18.61	21.47	11.71	3.50
20.48	113.76	36.36	3.85			18.35	21.52	11.51	3.45
20.52	113.87	50.00	3.79				21.57	14.55	2.60
20.53	113.89	36.36	3.85			22.85	21.62	10.28	2.10
20.57	114.00	33.33	3.74			21.32	21.67	12.03	2.99
20.58	114.03	36.36	3.69				21.72	12.18	3.12
20.62	114.14	35.71	3.75			21.91	21.77	7.63	4.24
20.67	114.28	38.46	2.88			21.82	21.82	5.96	1.43
20.72	114.41	33.33	3.59			21.24	21.87	4.98	0.77
20.73	114.44	23.53	3.32				21.92	5.29	2.46
20.77	114.61	22.73	3.55			20.32	21.97	4.98	0.53
20.82	114.83	21.74	4.14			21.18	22.02	4.89	1.26
20.87	115.06	22.73	3.22			20.57	22.07	5.84	1.46
20.92	115.28	22.73	3.26			20.48	22.12	4.89	1.99
20.97	115.50	22.73	3.68			19.99	22.17	5.31	3.19
21.02	115.72	19.23	3.41			12.28	22.22	5.96	3.38
21.07	115.98	4.03	2.88			12.44	22.27	5.84	1.83
21.12	117.22	4.03	2.58			12.35	22.32	4.39	1.11
21.17	118.46	4.07	2.76			24.14	22.37	3.87	1.37

Depth(mcd)	Age (ka)	Sed rate	O18 PDB	o18 rep1	o18 rep2	Sortable Silt	Depth(mcd)	%CaCO3	%SiO2
21.22	119.69	4.03	2.73			23.53	22.42	4.77	2.08
21.27	120.93	4.07	2.50			22.90	22.47	5.37	1.16
21.32	122.16	4.03	2.88			12.34	22.52	5.54	0.75
21.37	123.40	4.27	3.36			20.91	22.57	5.50	1.08
21.42	124.57	4.59	2.76			12.32	22.62	5.09	1.55
21.47	125.66	4.63	2.78			12.40	22.67	4.58	2.48
21.52	126.74	4.59	2.13			23.03	22.72	4.54	0.65
21.57	127.83	4.63	2.80			21.21	22.77	5.56	0.77
21.62	128.91	4.59	3.77			21.29	22.82	5.65	1.71
21.67	130.00	4.63	3.85			19.13	22.87	5.62	0.42
21.72	131.08	6.58	4.03			21.08	22.92	5.07	2.07
21.77	131.84	7.94	3.88			19.90	22.97	4.13	1.83
21.82	132.47	7.94	2.70			22.41	23.02	5.40	2.10
21.87	133.10	7.81	2.38			24.39	23.07	5.26	2.30
21.92	133.74	7.94	4.65			19.36	23.12	4.66	1.16
21.97	134.37	7.94	4.78			21.70	23.17	5.59	1.71
22.02	135.00	7.94	4.63			21.12	23.22	4.19	3.03
22.07	135.63	8.62	3.28			20.43	23.27	6.28	3.95
22.12	136.21	8.62	4.67			20.09	23.32	5.20	2.21
22.17	136.79	8.62	4.56			12.47	23.37	4.87	2.61
22.22	137.37	8.47	4.54			18.38	23.42	4.22	0.78
22.27	137.96	8.62	4.49			19.63	23.47	4.31	1.37
22.32	138.54	8.62	4.50			19.83	23.52	4.61	1.85
22.37	139.12	8.93	3.58			22.39	23.57	5.24	2.15
22.42	139.68	9.43	3.62			21.21	23.62	5.39	2.40
22.47	140.21	9.26	4.52			24.50	23.67	6.03	4.25
22.52	140.75	9.26	4.41			22.31	23.72	6.94	5.27
22.57	141.29	9.43	4.45			22.54	23.77	6.72	1.65
22.62	141.82	9.26	4.45			22.42	23.82	6.98	0.95
22.67	142.36	9.43	3.92			21.02	23.87	6.65	1.84
22.72	142.89	9.80	4.22			22.76	23.92	6.37	1.13
22.77	143.40	10.20	4.46			22.68	23.97	7.18	4.09
22.82	143.89	10.00	4.25			20.89	24.02	9.37	4.48
22.87	144.39	10.20	4.52			23.34	24.07	6.39	3.06
22.92	144.88	10.00	4.59			22.24	24.12	6.44	2.39
22.97	145.38	10.20	4.34			21.77	24.17	5.55	2.34
23.02	145.87	10.00	4.30			20.43	24.22	5.06	2.16
23.07	146.37	10.87	4.40			19.39	24.27	6.34	3.48
23.12	146.83	10.87	4.57			19.01	24.32	5.76	1.91
23.17	147.29	10.87	4.47			18.44	24.37	5.86	1.17
23.22	147.75	10.87	4.06			17.56	24.42	5.75	0.98
23.27	148.21	11.11	4.32			17.71	24.47	6.54	1.55
23.32	148.66	10.87	4.19			19.48	24.52	5.05	2.26
23.37	149.12	11.11	4.33			20.01	24.57	5.20	2.16
23.42	149.57	11.63	4.21			20.40	24.62	6.01	1.70

Depth(mcd)	Age (ka)	Sed rate	O18 PDB	o18 rep1	o18 rep2	Sortable Silt	Depth(mcd)	%CaCO3	%SiO2
23.47	150.00	11.63	4.14			21.60	24.67	6.05	1.63
23.52	150.43	11.90	4.28			21.41	24.72	5.32	1.87
23.57	150.85	11.63	4.38			21.26	24.77	5.38	1.48
23.62	151.28	11.63	4.51			21.00	24.82	4.90	3.96
23.67	151.71	11.63	4.25			18.96	24.87	4.66	2.62
23.72	152.14	12.50	4.32			19.13	24.92	4.49	0.80
23.77	152.54	12.50	4.23			18.51	24.97	4.75	2.28
23.82	152.94	12.50	4.65			18.36	25.02	6.92	1.25
23.87	153.34	12.50	4.72			18.56	25.07	6.43	0.26
23.92	153.74	12.50	4.68			18.40	25.12	6.96	1.90
23.97	154.14	12.82	4.52			18.88	25.17	4.74	3.65
24.02	154.53	12.50	4.41			17.18	25.22	5.17	3.49
24.07	154.93	13.51	4.22			18.65	25.27	5.10	1.93
24.12	155.30	13.16	4.31			19.30	25.32	5.81	2.88
24.17	155.68	13.51	4.46			17.37	25.37	4.41	1.09
24.22	156.05	13.51	3.65			19.08	25.42	6.40	1.52
24.27	156.42	13.51	3.80			21.46	25.47		
24.32	156.79	13.16	4.18			19.79	25.52		
24.37	157.17	13.89	3.98			18.72	25.57		
24.42	157.53	14.29	4.51			21.04	25.62		
24.47	157.88	14.29	4.10				25.67		
24.52	158.23	14.29	4.40			19.23	25.72		
24.57	158.58	14.71	4.30			19.79	25.77		
24.62	158.92	14.29	4.07			20.25	25.82		
24.67	159.27	14.29	4.15			18.49	25.87		
24.72	159.62	14.71	4.23			17.21	25.92		
24.77	159.96	15.63	4.36			18.69	25.97		
24.82	160.28	15.15	3.98			18.85	26.00		
24.87	160.61	15.15	4.00			18.38	26.05		
24.92	160.94	15.15	4.29			19.57	26.10		
24.97	161.27	15.63	4.18			16.20	26.15		
25.02	161.59	15.48	4.14			19.87	26.20		

Samuel Straker Henderson

Curriculum Vitae

Job Title Senior Petroleum Geologist, ExxonMobil Exploration Company

Education *Rutgers University*, New Brunswick, NJ
 Ph.D., Geological Sciences. 2006-2009
 M.Sc. Geological Sciences. 2002-2006

Vanderbilt University, Nashville, TN
 BS, Engineering Science, 1996-2002
 BS, Geology, 1996-2002

Professional Experience

August 2003-Present Teaching Assistant, Rutgers University

May 2003-Present Field Technician, GHR Consulting, Horsham, PA

June 2002-Present Graduate Research Assistant, Rutgers University

25 Sept. – 11 Nov. 2004 Shipboard Scientist, IODP Expedition 303

Summer 2004 Laboratory Technician, LDEO Borehole research group

1 August- 9 September 2002 Watchstander, KN166-14 Cruise, Gardar, Eirik Drifts

September 2001- May 2002 Undergraduate Researcher, Vanderbilt University